

INVESTIGATION OF HEAT TRANSFER AND ENTROPY PRODUCTION OF
HIGH TEMPERATURE MOLTEN CHLORIDE SALTS CIRCULATION IN
CONCENTRATING SOLAR POWER SYSTEMS

by

Ye Zhang

Copyright © Ye Zhang 2022

A Dissertation Submitted to the Faculty of the

DEPARTMENT OF AEROSPACE AND MECHANICAL ENGINEERING

In Partial Fulfillment of the Requirements

For the Degree of

DOCTOR OF PHILOSOPHY

In the Graduate College

THE UNIVERSITY OF ARIZONA

2022

THE UNIVERSITY OF ARIZONA
GRADUATE COLLEGE

As members of the Dissertation Committee, we certify that we have read the dissertation prepared by: Ye Zhang
titled: Investigation of Heat Transfer and Entropy Production of High Temperature Molten Chloride Salts Circulation in Concentrating Solar Power systems
and recommend that it be accepted as fulfilling the dissertation requirement for the Degree of Doctor of Philosophy.

Peiwen Li

Peiwen Li

Date: Apr 27, 2022

Qing Hao

Qing Hao

Date: May 1, 2022

Yitshak Zohar

Yitshak Zohar

Date: Apr 27, 2022

Carlos Alsua

Carlos Alsua

Date: Apr 27, 2022

Final approval and acceptance of this dissertation is contingent upon the candidate's submission of the final copies of the dissertation to the Graduate College.

I hereby certify that I have read this dissertation prepared under my direction and recommend that it be accepted as fulfilling the dissertation requirement.

Peiwen Li

Peiwen Li

Date: Apr 27, 2022

Department of Aerospace and Mechanical Engr.

ARIZONA

ACKNOWLEDGEMENT

I would like to express my deepest gratitude to people who have supported me financially, physically, and mentally in the long journey of my Ph.D. life. I have gained lots of knowledge and skills, built friendships with wonderful people, and become more mature in life.

First and foremost, my supreme gratitude is given to my academic advisor, Dr. Peiwen Li for training me and supporting me throughout my Ph.D. career. I am so fortunate to have had him as my advisor and followed his sagacious advice, patient instructions to complete my work. In the times when I feel deeply stressed, Dr. Li has always been supportive and encouraging to give me a lot of confidence to eventually accomplish the goals in research and study. I have learned so much from him not only about being a critical researcher, but also being a responsible person.

I also thank my minor advisor Dr. Carlos J. Alsua, and my committee members Dr. Yitshak Zohar, and Dr. Qing Hao. I have developed my professional knowledge from their courses and learned much from their academic and career comments and advice. Thank you for being my committee members. I am forever grateful for the time, patience, and support.

I'm also grateful to all the staff members in AME department for their support during these years, special thanks are due to Jini Kandyil, Nancy Preble, Liza Soto, Blondelle Arnold, Renee Meyerhofer, Chris Duggan, Joseph Hartley, and Dale Drew. Without their help, it would be extremely difficult for me to make progress in research projects.

I would like to thank all my previous and current fellow lab members for their constant support and help. Particularly I would like to thank Xiaoxin Wang, Shuyang Zhang, Ben Xu, Fouad Haddad, Qichao Hu, Xiankun Xu, and Xinhai Xu. I really enjoyed working with them and

learning from each other. Without their help, my Ph.D. study would never be so splendid and passionate.

I continue to thank all my dear friends, Robert Worner, Gewen Tang and his parents, Yue Xiao, Monica Zhao, Joyce Chen, Travis Shi, Chuhan Zhou, Hao Wu, Kenny Hao, and all those who have shown in my life. The days with them are unforgettable and always valuable for me. Thank you for adding so much fun to my life out of research.

Finally, I would like to specially thank my father Guiming Zhang, mother Yuying Wu, and my wife Ines Zhang for being endlessly supportive to my decision. Without their support, this dissertation would never be finished successfully. Their faith and love are the most important things that give me motivations to move onward and upward.

Table of Contents

LIST OF FIGURES	8
LIST OF TABLES	10
<i>ABSTRACT</i>	11
CHAPTER 1 INTRODUCTION.....	14
1.1 Background.....	14
1.2 Concentrating Solar Power (CSP) Technology	16
1.3 Thermal Energy Storage (TES) for CSP Systems	22
1.4 Development of Liquid Heat Transfer Fluid	23
1.4.1 Thermal oil.....	25
1.4.2 Molten salt	26
1.4.2.1 Nitrate/nitrite molten salts.....	26
1.4.2.2 Chlorides molten salts.....	28
1.4.3 Liquid metals	29
1.5 Gaps in the literature.....	31
1.6 Objectives of this work.....	33
CHAPTER 2 EXPERIMENTAL STUDY ON HEAT TRANSFER PERFORMANCE OF HIGH TEMPERATURE MOLTEN CHLORIDE SALTS IN CSP SYSTEMS.....	34
2.1 Introduction.....	34
2.2 Molten Salt Convective Heat Transfer Experimental Setup and Data Reduction	37
2.2.1 Molten salt flow loop.....	37
2.2.2 Detail of test section.....	40

2.2.3 Procedures of a test and operation	41
2.2.4 Data reduction and uncertainty analysis	43
2.3 Results and Discussions.....	45
2.4 Conclusions.....	50

**CHAPTER 3 ANALYSIS OF THE HEAT TRANSFER AND CRITERION OF
FREEZING OF MOLTEN SALT STARTUP FLOW IN RELATIVELY COLD PIPES**
..... 51

3.1 Introduction.....	51
3.2 Physical Model and Mathematical Description	52
3.2.1 Transient heat transfer between hot fluid and cold pipe being viewed as energy storage process.....	54
3.2.2 Fluid energy balance equation	56
3.2.3 Energy balance equation for the cold pipe wall.....	58
3.2.4 Numerical solution using method of characteristics	59
3.3 Results and Discussion	63
3.3.1 Effect of fluid velocity to the critical length	64
3.3.2 Effect of pipe diameter to the critical length.....	65
3.3.3 Effect of pipe wall thickness to the critical length.....	66
3.3.4 Effect of pipe wall temperature to the critical length.....	67
3.4 Conclusions.....	68

**CHAPTER 4 MODELING AND ANALYSIS OF ENTROPY PRODUCTION IN CSP
SYSTEMS FOR EVALUATION OF HTFS**

4.1 Introduction.....	70
4.2 Analysis of Entropy Production in Heat Transfer System in a CSP Plant.....	72

4.2.1 Entropy production rate in heat transfer processes	79
4.2.1.1 Heat transfer due to turbulent flow	79
4.2.1.2 Heat transfer due to laminar flow	81
4.2.2 Entropy production rate due to pressure losses.....	81
4.2.2.1 Flow with $2300 \leq Re \leq 2 \times 10^4$	82
4.2.2.2 Flow with $Re \geq 2 \times 10^4$	83
4.2.2.3 With laminar flow in heat exchangers and circulation pipes.....	84
4.2.2.4 Different Reynolds numbers in different devices	85
4.3 Discussion and Evaluation of Several Heat Transfer Fluids	85
4.3.1 Applications of the analysis for various heat transport systems	85
4.3.2 Cluster of properties contributing to entropy production.....	86
4.3.3 Examples of entropy production rate due to different HTFs for heat transport tasks..	88
4.3.4 The Carnot efficiency of the power system using the heat transported from solar collector.....	98
4.4 Conclusions.....	99
CHAPTER 5 CONCLUDING REMARKS AND FUTURE WORK	102
5.1 Concluding Remarks.....	102
5.2 Future Work	104
APPENDIX PAPERS REFERRED TO IN THIS DISSERTATION	105
REFERENCES.....	107

LIST OF FIGURES

<i>Fig. 1 Number of CSP technology-related patents</i>	18
<i>Fig. 2 Conceptual diagram for common CSP technology</i>	119
<i>Fig. 3 Operating temperature range for different liquid HTFs</i>	30
<i>Fig. 4 The chloride molten salt flow loop for the experiments</i>	38
<i>Fig. 5 The allocation of thermocouples for temperature and heat flux measurement at test section</i>	41
<i>Fig. 6 Salt melting and purification in salt processing tank</i>	42
<i>Fig. 7 Heat balance in the tests. Heat flux $q_{in}=7743\text{W/m}^2$, and temperatures ranged from 400°C to 600°C</i>	48
<i>Fig. 8 Experimental data of heat transfer coefficient and predictions using empirical correlations. Heat flux $q_{in}=7743\text{W/m}^2$ for the tests</i>	49
<i>Fig. 9 The agreement of all the tested Nu number between experimental data and predictions by Gnielinski correlation. Temperatures of tests ranged from 400°C to 600°C.....</i>	49
<i>Fig. 10 Similarity of structure of hot fluid flowing through packed solid material which can be viewed as a porous material</i>	54
<i>Fig. 11 Model used to analyze the heat transfer between hot fluid flowing through packed solid material</i>	55
<i>Fig. 12 Interception points of characteristics of Eq. (7) and (11)</i>	62
<i>Fig. 13 Variation of the critical length of pipe due to different flow velocity. $T_h=450^\circ\text{C}$, pipe wall thickness=2mm</i>	65
<i>Fig. 14 Variation of the critical length of pipe due to different diameter of the pipe. $T_h=450^\circ\text{C}$, pipe wall thickness=2mm</i>	66

Fig. 15 Variation of the critical length of pipe due to different pipe wall thickness. $T_h=450\text{ }^\circ\text{C}$, $T_l=350\text{ }^\circ\text{C}$, $D_o=0.0254\text{ m}$ 67

Fig. 16 The variation of critical length of pipe due to different pipe wall temperature. $T_h=450\text{ }^\circ\text{C}$, $D_o=0.0127\text{ m}$, pipe wall thickness= 1.0mm 68

Fig. 17 Flow loop that a HTF is used to transfer heat from solar collectors to the power plant 74

Fig. 18 The entropy production rate of a system using different HTFs at different operating temperatures for the task of transmitting 50 MW_{th} heat 93

Fig. 19 The entropy production rates from different THFs at different operating temperatures for the task of transferring heat from 100 MW_{th} to 600 MW_{th} . Results are based on Gnielinski equation for Nu of all fluids except for LEB that used equation in Table 6; and Petukhov equation was used for Darcy friction factor. 98

Fig. 20 The resulted Carnot efficiencies of the system using different HTFs at different operating temperatures for the tasks of transferring heat. Results are based on Gnielinski equation for Nu of all fluids except for LEB that used equation in Table 6; and Petukhov equation was used for Darcy friction factor. 99

LIST OF TABLES

<i>Table 1 Specific of instruments used in the high temperature molten salt loop</i>	<i>39</i>
<i>Table 2 Key properties of molten salt fluid and metal pipe</i>	<i>63</i>
<i>Table 3 Clusters of properties contributing entropy production in the system</i>	<i>87</i>
<i>Table 4 Properties of HTFs at average temperature of 200 °C and the results of entropy production rate.....</i>	<i>91</i>
<i>Table 5 Properties of HTFs at average temperature of 340 °C and the results of entropy production rate.....</i>	<i>91</i>
<i>Table 6 Properties of HTFs at average temperature of 450 °C and the results of entropy production rate.....</i>	<i>92</i>
<i>Table 7 Properties of HTFs at average temperature of 700 °C and the results of entropy production rate.....</i>	<i>92</i>
<i>Table 8 Summary of correlations for thermophysical properties of molten LBE.....</i>	<i>93</i>
<i>Table 9 Parameters in the analysis for different average fluid temperatures and several heat transfer tasks.....</i>	<i>94</i>

ABSTRACT

The global warming and worsening environment on the earth has been a great concern to human society in the last two decades. The major solution to the problem is to use clean and renewable energies for electricity generation, thus reducing the use of fossil fuels and cutting emission of CO₂. One of the most feasible approaches for accomplishing the goal is to significantly increase the harvest and utilization of solar energy, using Concentrating Solar Power (CSP) technology combined with Thermal Energy Storage (TES) systems.

Heat transfer fluids (HTFs) are used in CSP plants to receive heat from solar concentrator and then transfer it to heat exchanger, power turbine, or thermal storage system. To achieve higher energy efficiency from the CSP systems, the development of a new generation HTF to approach a higher temperature limit by using eutectic high temperature molten chloride salts is sponsored by the U.S. Department of Energy.

The first part of this dissertation is the experimental study of the convective heat transfer of the molten salt at high temperatures. For the first time, a circulation system and instrumentation of flow and heat transfer was designed and constructed to measure the heat transfer coefficient of the . Experimental measurement of the convective heat transfer coefficients of NaCl-KCl-ZnCl₂ (molar fraction: 13.8%-41.9%-44.3%) inside tubes has been accomplished to find the most suitable heat transfer correlations. This provides valuable information for the design of heat transfer devices in CSP plants that use molten chloride salts as heat transfer fluid and thermal energy storage material.

The second part of this dissertation mainly focuses on the analysis to the transient heat transfer phenomenon between the hot fluid and the cold pipe. Currently, most of the modern concentrated solar thermal power plants employ molten salts as the heat transfer fluid to carry the thermal energy from solar concentrators and deliver to thermal storage systems or thermal power plants for the

need of power generation. For the startup operation of solar concentrators, molten salts need to be pumped to flow into the pipes which may have lower temperature than the molten salt due to cold ambient overnight or over the suspend period of operation. As the freezing point of various molten salts ranges from 220 °C to 430 °C, preventing the freezing of molten salt flowing in cold pipe is a very important requirement for the safe operation of a concentrated solar thermal power plant. A basic heat transfer analysis of transient heat exchange between molten salts and the flow pipe is conducted to find a criterion or the critical condition of preventing molten salt from freezing. The effects of molten salt flow velocity, heat capacities of molten salt and pipe, dimensions of pipes, and the initial temperatures of salts and cold pipes are all correlated theoretically in the analysis through modeling of transient heat transfer between a pipe and the fluid. The results are very helpful to the understanding and management of a safe startup of hot molten salt flowing in cold pipes on cyclic operations.

The third part of this dissertation introduces details about the modeling that provides a fundamental approach for the comparison of various heat transport systems which may have different designs and using different heat transfer fluids/media (gas, liquid, or solid particles) in CSP systems. For various high temperature heat transfer fluids, such as, synthetic oils, various molten salts, and liquid metals, a general criterion is proposed in this work to evaluate the merit of fluids regarding their transport properties. For the goal of transferring a desired amount of heat, a fluid that causes less entropy production is believed to have better figure of merit (FOM). This is due to the fact that entropy production is associated with the destruction of exergy or useful energy. The entropy production in a heat transfer system in a solar thermal power plant includes the part due to the processes of heat addition and removal and the other part due to pressure losses in the flow in heat exchangers and pipes. Theoretical analysis and relevant equations for total entropy

production are derived. As an example, the FOM for several heat transfer fluids used in CSP industry are compared for the goal of heat transport in the range of 50 MW_{th} to 600 MW_{th}. This work offers one very important approach leading to the development and optimization of a heat transport system for CSP plant with all factors considered.

The investigations included in this dissertation for the heat transfer and system analysis in concentrating solar power technology are of particular interest to the renewable energy engineering community. It is expected that the proposed methods can provide useful information for engineers and researchers.

CHAPTER 1 INTRODUCTION

1.1 Background

Global energy and electricity consumption is increasing rapidly due to the growth in population, industrialization, and urbanization. As major conventional energy sources are depleting in nature and emit harmful emissions, the world is experiencing severe challenges in providing a clean and sustainable energy supply to mass populations [1,2,3]. Compared to global population growth, energy consumption is growing much faster and, within the next 15–20 years' time, electricity consumption will double [4,5]. The energy-consumption pattern of various energy sources, both conventional and renewable, will play the most important role in sustainable development, as this pattern is one of the critical indicators of resource use and environmental impact [6,7]. At present, 80% of the global primary energy supply comes from fossil fuels (e.g. coal, liquid petroleum and natural gas), which are now being considered a depleting energy source, and are responsible for emitting major greenhouse-gas (GHG) emissions such as CO₂ [2,8,9]. Moreover, fossil-fuel energy sources are responsible for an increasing pace of climate change, and developing countries especially should seek alternative energy sources for their respective power sectors to mitigate carbon emissions in the near future [10,11].

To eradicate such catastrophic scenario, global renewable-energy initiatives show that, with the existing development of the renewable energy infrastructure, renewables will contribute to an overall CO₂ reduction of 30% by 2050, compared to the year 2012 [12]. From such perspectives, the development, adoption, and dissemination of low carbon technologies, particularly of renewable-energy-harvesting technologies, has become the highest priority, to satisfy the energy requirement of society and contribute to a greater CO₂ reduction effort [13].

With high abundance and potential to be low-cost, solar energy is widely recognized as one of the most competitive alternatives among all the renewables [14]. There are two major technologies to utilize solar energy. Solar thermal technology and Solar electricity technology. The former transform solar energy into heat directly used in the field of low-to-high temperature applications such as active and passive water, space heating and cooling, industrial process heat, solar cooling and solar desalination [15-20].

Direct Solar-to-electricity technology is an early step utilization of solar energy by converting solar energy into electricity directly based on the photovoltaic (PV) effect [21]. It is cheap and easy to operate to obtain power from solar energy. However, the PV system has some disadvantages. First, the conversion efficiency from incident solar energy to electricity is low, only 15-20%, and will decrease without a tracking system [22]; Second, the problem of intermittency is serious in this technology. The power output of PV panels will decrease under cloudy weather and discontinue at night.

The second way to generate electricity from solar energy is to convert solar energy to thermal energy, then use thermal energy to generate electrical power. It is known as solar thermal electricity (STE) or concentrating solar power (CSP), which is distinctive compared to other renewable energy sources because it can be coupled with thermal energy storage (TES) as well as conventional fuels, making it highly dispatchable [23]. In a CSP system, the sunlight beams are reflected and concentrated onto an area of the solar receiver, creating a high temperature zone due to the radiation. Then the heat is absorbed by the heat transfer fluid (HTF) that pass through the receiver. The hot HTF flow through the heat exchangers, transferring the heat to the steam and causing its temperature and pressure to increase. Such high temperature and pressure steam is used in steam turbine to drive the electrical generator to generate electricity.

1.2 CSP Technology

Using the energy source, concentrating solar power (CSP) or solar thermal electricity (STE) is a technology that is capable of producing utility-scale electricity, offering firm capacity and dispatchable power on demand by integrating thermal energy storage or in hybrid operation [24]. Considering the high energy saving and high energy efficiency, CSP plants are predicted to produce a global electricity contribution of 7% by the year 2030 and 25% by the year 2050 [25]. It is envisioned that, with high levels of energy efficiency and advanced industry development, CSP could meet up 6% of the world's power demand by 2030 and 12% by 2050 [26]. Apart from the production of electricity, CSP also has tremendous potential in employment generation and reducing CO₂ emissions on a global scale [27].

Potential locations for CSP plants around the world are generally being identified by using the global distribution of Direct Normal Irradiance (DNI) [28]. North Africa, the Middle East, the Mediterranean, and vast areas in the United States including California, Arizona, Nevada, New Mexico are known as the “Sun Belt” where greater solar radiation is available from the sun. Geographically, the Belt is suitable for CSP plants, as there are massive land areas with extraordinary solar irradiation, well suited to install a large number of solar-energy harvesting systems. By 2020, CSP is expected to be an economically competitive source of bulk power generation for peak and intermediate loads, and by 2025–2030 for base-load power [29,30]. Commercially viable CSP plants should maintain a DNI of at least 2000–2800 kW h/m²/yr. Present commercial CSP plants are being developed based on this level of irradiance [28]. However, it is also argued that a DNI value > 1800 kW h/m²/yr is suitable for CSP plant development [31]. In the period 1984–1991, the first commercial CSP plant was constructed in the Mojave Desert, California, the USA by Luz International Ltd. However, due to a drop in the oil price at that time,

the regulatory initiatives that supported the progress of CSP collapsed. In 2006, CSP plant development initiatives were pursued in Spain and in the United States. The policy in regard to solar power generation was amended in those countries, and feed-in tariffs were introduced in Spain [20]. As of March 2014, the California Energy Commission approved licenses for five CSP plants with a total installed capacity of 2284MW [32]. In the United States, it has been assessed that CSP plants with a total capacity of 118GW could be installed by 2030, and by 2050 the capacity could be increased further to 1504GW [33]. As of 2015, the total installed capacity of CSP plants in Europe reached 5 GW, from 0.5GW in the year 2006 [34]. With the present development policy on CSP technology, six European Union (EU) countries, Cyprus, France, Greece, Italy, Portugal, and Spain, envision producing electricity of 20 TW h by the year 2020 [34]. By 2030, a total of 83GW could be installed in the sunniest regions and will reach 342GW by 2050; this expected power generation will be coming from the Middle East (55%) and Northern Africa (30%), and the remaining 15% will be from European countries, assuming a modest growth of CSP technology [25]. As of 2016, in Spain, the total installed capacity of the operational CSP plants is 2304MW [35], outperforming the estimate in the Spanish Renewable Energy Plan made for the time frame of 2005–2010 [25]. In the coming decades, it is expected that CSP will show prospects of exporting electricity generated from the desert regions of the Middle East and North Africa (MENA) to Europe. Moreover, it is found that the electricity demand of all Europe can be met by harvesting from only 0.4% of the Sahara Desert. Indeed, by using only 2% of the earth's total land surface, the global electricity demand can be entirely fulfilled [7]. By 2020, the annual electricity production from CSP plants is expected to reach 85 TW h, which will meet 2% of Europe's electricity production, and by 2030 the installed capacity will double, reaching 60 GW, and producing 70 TW h of electricity per annum [36].

Universities and major research institutions are producing high-quality research output that is contributing to CSP technology development and its dissemination all over the world. With a search term “concentrating solar power” in the SCOPUS database, a total of 15,998 patent documents was found. Fig. 1 shows the yearly number of patents in between 1981 and 2017 on CSP, which depicts the tremendous progress in the technology [1].

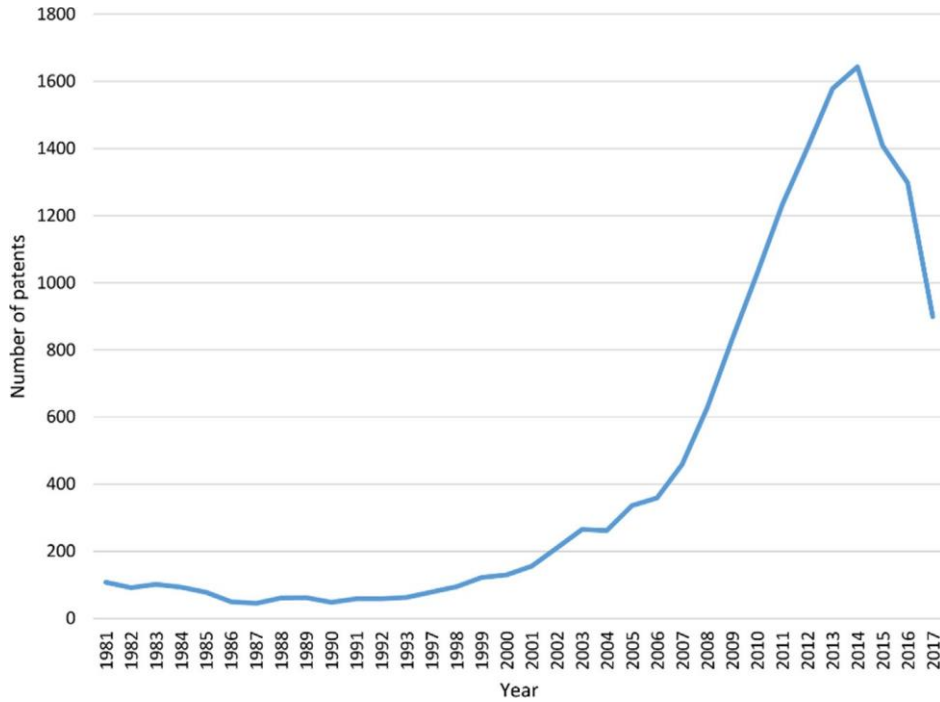


Fig. 1 Number of CSP technology-related patents

Depending on the way of concentrating the sunlight and the mobility of the receiver (fixed or mobile), four major CSP technologies have been identified in the past decades: parabolic trough collector (PTC) [37-41], linear Fresnel reflector (IFR), parabolic dish system (PDS), and solar power tower (SPT). Among these four types of CSP technologies, PTC and IFR are considered as a line-focus system, meanwhile, PDS and SPT are designed as a point-focus system. The conceptual drawings of those four technologies are shown in Fig. 2.

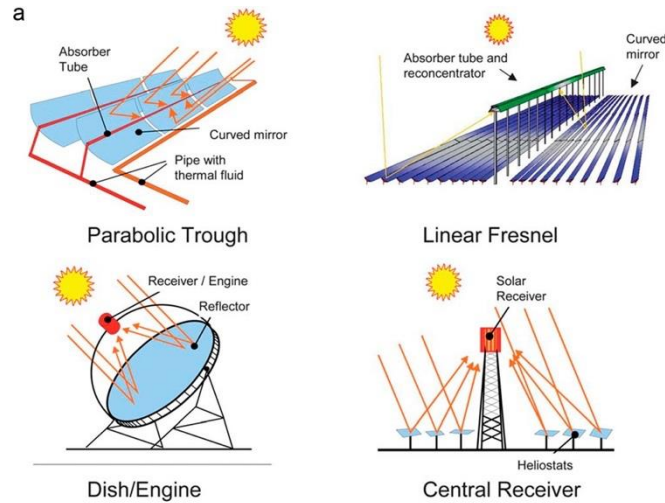


Fig. 2 Conceptual diagram for common CSP technology

Parabolic trough collector (PTC) is considered the most reliable, well-known, and commercially developed technology available for solar concentration technology [42]. By 2014, more than 90% of energy from CSP systems is provided by PTC technology [43, 44]. Generally, A PTC consists of parallel rows of reflectors curved like a parabolic shape in two dimensions and installed along a linear straight line in the third dimension, as shown in *Fig. 2a*. The sunlight is reflected and concentrated onto a receiver positioned along the reflector's focal line. Then a working fluid is pumped to pass through the tube and heated by the concentrated solar radiation. The receiver is a tube located directly above the symmetrical line of the parabolic mirror. The collector and the tube receiver in PTC are designed to be able to follow the movement of sun and keep toward it during the daylight hours by a single axis tracker.

Linear Fresnel reflectors (LFR) is another technology that uses line-focus method. It has a similar design with parabolic trough systems but the mirrors (reflectors) are flat or slightly curved that array along longer rows [45,46], as shown in *Fig. 2b*. The parallel beams of sunlight are reflected onto a linear straight fixed receiver with a downward-face. Benefiting from the simple design, the major advantage of this CSP application is the low area requirement of land field. The

Fresnel design uses less-expensive reflector materials and absorber components. Therefore, the investment, operation, and maintenance costs are much lower than other CSP applications [47]. However, the solar-to-electricity converting efficiency of LFR is less than parabolic troughs and it is hard to integrate thermal storage system into the design [40, 48,49].

Compared to the mobile receiver in PTCs, the design of fixed collectors in LFR allows for easy installation and maintenance and increasing the flexibility in the selection of working fluids. Since the mobile receivers in PTCs are considered technically challenging and required a lot of maintenance [48,50].

The Parabolic dish system is a point focusing system. PDSs are individual units with a receiver located at the focal point of the parabolic dish-shaped concentrator. The sunlight radiation is reflected and concentrated onto the absorber to be converted to thermal energy. Subsequently, the thermal energy is transferred to a Stirling engine or collected by a heat transfer fluid that carries the heat to a plant to generate power [51,52,53]. Similar to PTCs, the entire device of PDS tracks the movement of the sun, but with a two-axis tracking system [54,55]. Parabolic dishes system are usually considered to have the highest concentration ratios, the highest optical efficiency, and the highest overall conversion efficiency during all the CSP technologies [53,56]. The theoretical maximum concentration ratio of PDS is square of that of parabolic trough, which is 11513. It will produce high-temperature heat, which is above 1000 °C. Generally, The efficiency of PDS with the Stirling engine is found to be around 25% to 30% [57]. The main drawback of PDS technology is that it cannot be integrated with a thermal storage system and has less possibility of hybridization with other sources of energy.

There are many factors that can be affect the performance of a parabolic dish system, such as the material and the size of the aperture area of the concentrators; dimension, focal Length and

focal point diameter of the parabolic dish; the size of the aperture area and the receiver; geometric or area concentration ratio; and rim angle [58-68].

Solar power tower, which is also known as central receiver systems (CRS), is another type of point-focus CSP technology. Hundreds of thousands of small mirrors – which are also known as heliostats - are arrayed and located around the tower to reflect and concentrated the direct normal irradiation (DNI) onto a central receiver which is located on the top of the tower. By concentrating the sunbeam hundreds of times, the concentrating power of the tower is able to achieve a very high temperature [48]. Then the solar energy is absorbed and carried by working fluids that pass through the receiver and then used to generate power or saved in thermal storage systems. The higher temperature will increase the efficiency at which heat is converted into electricity and reduce the cost of thermal storage [40].

Generally, the mirrors in heliostats field use two-axis tracking systems to track the sun [69,70]. There are some patterns to array the heliostats, including vertical plane receiver with a north-facing heat transfer surface, cylindrical receiver with exterior heat transfer surface, and enclosed receiver with enclosed heat transfer surface [48, 71,72].

The first central receiver plant, named EURELIOS, with a capacity of 1 MWe was built in the 1980s in Europe [73]. The sun's beams were reflected onto the central receiver on the tower with the height of 55m by 182 mirrors arrayed on a 6200 m² heliostats field. The radiative power onto the receiver was 4800 kW and the temperature of fluid from the outlet of the receiver reached 512 °C [74]. It successfully generated power up to 5 kWh/m², 7 kWh/m², and 4 kWh/m² during spring, summer, and winter, respectively [75]. Following this successful operation, a growing number of commercial SPT plants have been established around the world. Solar one, the first commercial central receiver solar power plant built in the U.S., was built in California in 1982. it

comprised of 1818 mirrors each with an area of 40 m² mounted on a 72650 m² solar field [34]. The plant has an electric capacity of 10 MWe and the working fluid was heated to 304 °C [76]. In 1996, the Solar Two power plant was constructed by adding 108 mirrors each with 95 m² area and an aperture area of 10200 m² on Solar one project. The temperature of the working fluid increased from 285 °C to 565 °C after passing through the receiver [77]. The Solar two power plant provided 1633 MWh power, which exceeded the expected goal of 1500 MWh power production in one 30-day period [78]. Ivanpah Solar power facility, construction completed in 2014, is the world's largest CSP plant that uses solar power tower technology [79,80]. Ivanpah solar electricity generating system consists of a total of three separate units, one of them has a total capacity of 126 WM and the other two have a total capacity of 133 MW each. There are 173, 500 heliostats arrayed on a heliostat solar field with an aperture area of 2, 600, 000 m². The inlet and outlet temperature of the receiver is 249 °C and 1050 °C, separately [81,82].

The concept of a power tower has been confirmed to be highly technically flexible, a wide variety of heliostats, receivers, working fluids, and power blocks can be chosen to design an SPT plant [83,84]. Although solar power tower technology occupied less in the current market than the parabolic trough collector, SPT is considered to be the most feasible technology for the future CSP market [85,86].

1.3 Thermal Energy Storage for CSP systems

TES technology solves the time mismatch between solar energy supply and electricity demand, which provides a distinct advantage to CSP plants compared to other renewable energies, such as wind and photovoltaic. Also, electrical energy storage using battery has not proved to be economically viable [1,87]. Depending on the daily and yearly variation of solar radiation and the electricity demand profile, CSP plants integrated with thermal storage systems can have various

operational strategies and the storage system may offer the following functions [1,4,12]: (1) mitigating short fluctuations during transient weather conditions, e.g. cloudy periods; (2) shifting the generation period from peak hours of solar insolation to peak hours of power demand; (3) extending the generation period when solar is not available, which improves the annual capacity factor and requires a larger solar field than a system without storage.

Thermal energy for CSP systems can be stored in sensible heat storage by using either solid or liquid storage media, latent heat storage by using phase change materials (PCMs) and thermo-chemical storage through reversible chemical reactions. When designing a TES system for a CSP plant, the following factors need to be considered: (1) nominal temperature and specific enthalpy drop in load; (2) maximum load; (3) operational strategy and (4) integration into the powerplant [1,4].

1.4 Development of Liquid Heat Transfer Fluid

As motioned above, working fluid is one of the most important keys to the successful operation of a concentrated solar power (CSP) system, such fluids are also called heat transfer fluid (HTF). It is needed for a CSP system to collect and deliver heat from solar receiver to power block. Generally, there are three different destinations for varied application purposes. Firstly, some fluids can be directly transferred to the turbine to generate electricity power; Secondly, some heat HTFs are delivered to the heat exchanger to interchange heat to other working fluid those then will be transported to the turbine; The latest type of destination is thermal storage tank, where the heat can be stored and extracted once needed. Therefore, HTFs play a significant role in the modern solar thermal power system.

Many media can be served as heat transfer fluid. Depending on the states, HTF can be classified into three categories. (1) water and steam (2); Gas heat transfer fluid, including air,

supercritical CO₂, helium, and nitrogen [88]; (3) Liquid heat transfer fluid, such as thermal oils, molten salts, and liquid metals [89]. In this thesis, we are focusing on the liquid heat transfer fluids available in the commercial market and under development.

It is well known that a high temperature for solar thermal energy is desired for a concentrated solar thermal power (CSP) plant to have high energy conversion efficiency [90,91]. To obtain thermal energy at high temperatures, solar concentrators with high concentration ratio and a heat transfer fluid (HTF) being able to work at high temperatures are the two basic technical requirements [92,93]. Solar thermal concentrators with high concentration ratio provide high heat flux; while the heat transfer fluid is used to receive heat from the solar concentrator and then transfer the heat to another fluid (such as water, air, or super critical CO₂) which is the working substance in a thermal power cycle. Whereas the technology of concentrators with high solar concentration ratio has been developed in the current CSP industries, cost-effective and excellent heat transfer fluids for the working temperatures above 600 °C are still remaining to be found out [94].

So far, three generations of HTFs (other than air and water) have been developed particularly for the use in concentrated solar thermal power systems (CSP). The first generation HTF may be represented by the non-toxic petroleum-based oil (such as Xceltherm® 600—C₂₀ paraffin oil), which has an upper temperature limit of 315 °C [95,96]. The second-generation of HTFs are known as synthetic organic oils (such as Therminol®VP-1, a mixture of Diphenyl oxide and Biphenyl in weight percentage of 73.5% versus 26.5%), which has an upper temperature limit of 400 °C [97, 98] and a corresponding vapor pressure of 10 atm. To further improve the working temperature in a CSP system, the third generation HTF is based on nitrate molten salts [99] (having upper temperature limit of 580 °C), such as a mixture of sodium nitrate, sodium nitrite, and potassium

nitrate (in mole fraction of 7%NaNO₃ - 49%NaNO₂ - 44%KNO₃)known as Hitec® salt [100, 101]. Recently, one of the great efforts sponsored by the U.S. Department of Energy for CSP technologies is the development of the fourth generation HTF to approach a temperature limit of 850 °C by using either eutectic high temperature molten salts [102, 103] or eutectic metal mixtures [104-106].

The requirement to the properties of a HTF used in a concentrated solar thermal is multifold. First and foremost, the fluid should be able to remain as a liquid fluid in a wide range of temperatures while having low vapor pressures. Second, the fluid must have low corrosion to the pipes and containers of the heat transfer system. Third, the fluid must have favorable properties, including density, thermal conductivity, heat capacity, and viscosity, so that in overall the exergy (or the useful heat) destruction of the received solar thermal energy is minimal during the flow and heat transfer processes in the heat transfer system. Last, but not least, the cost of the materials for the HTF should be sufficiently low to be acceptable by industrial customers.

1.4.1 Thermal oil

Thermal oils are the initial generation of HTFs that have been used in the CSP plant. The major types of thermal oils include synthetic oils, mineral oil, and silicone oil. They have been developed and proved by commercial CSP applications in past decades [107]. Therminol VP-1 is a commercial synthetic oil that is served as HTF currently in large-scale commercial CSP applications, it contains biphenyl and diphenyl as a eutectic mixture. The upper operating temperature of this type of oil is 400 °C. With the aim of improving the performance and reducing the operation cost, D. Cabaleiro experimentally investigated thermophysical properties of the mixture of biphenyl and diphenyl with different molar ratios [108].

A good key feature of thermal oils is they can serve as both heat transfer fluid and thermal

storage system materials. The major limitation of the thermal oil is the upper operating temperature, which is less than 400 °C [109]. After being heated to a temperature higher than the limitation, hydrogen will be produced from the decomposition of the hydrocarbon mixture [110].

1.4.2 Molten salt

Molten salts, which are from the fusion of inorganic salts, are engineering fluids that can be used in a very large range of applications [111]. They were first utilized as the coolant in nuclear reactors [112]. Most recently, molten salts are considered as feasible substitute materials for thermal oil with the operating temperature higher than 400 °C in CSP plants. Generally, molten salts heat transfer fluid are eutectic molten salts composed of two or more components from nitrites, fluorides, carbonates, and chlorides.

1.4.2.1 Nitrate/nitrite molten salts

Benefiting from its low melting point, nitrate eutectic molten salts are the first type of molten salts to be widely used in large scale CSP plant. The primary advantages of molten nitrate salt serving as the heat transfer fluid in a solar tower power plant include a lower operating pressure, better heat transfer and higher allowable incident flux than a water/steam receiver. Depending on the composition, there are three major types of nitrate/nitrite molten salts being used in the commercial application: Solar salt, Hitec salt, and Hitec XL salt [113].

Solar salt is a binary mixture of NaNO_3 and KNO_3 in a molar ratio of $\text{NaNO}_3\text{-KNO}_3$: 60%-40%. It has a melting point of 220 °C and it is stable under 585 °C. At 300 °C, the specific heat, density, and viscosity of solar salt are 1.495 kJ/(kg•°C), 1899 kg/m³, and 3.26 cp, respectively [114]. Solar salt has the maximum operating temperature at 585 °C, which is much higher than thermal oil. Solar salt has been widely studied and commercially proven in past decades. Bauer et

al. [114] summarized and compared the thermophysical properties of solar salt from different pieces of literature. This work provides accurate information for the modeling and dimensioning of the design of the CSP plant. In commercial application, Solar Two project in the USA successfully produced 1633 megawatt-hours over one 30-day period by using solar salt as heat transfer fluid and thermal storage system media [100].

Hitec salt is the second type of commercial molten nitrate/nitrite salt, which is a ternary mixture consisting of 7% NaNO_3 , 53% KNO_3 , and 40% NaNO_2 in molar percentage. The adding of NaNO_2 effectively reduces the melting point to 142 °C but also lead to a reduction in the maximum operating temperature to 538 °C. From the SNL's (Sandia National Laboratory) report, the Hitec molten salt can be operating at 538 °C for a short period [115]. The heat capacity of Hitec salt is in the range of 1.39 -1.56 kJ/(kg•°C) from different researches, which is close to the heat capacity of solar salt [116]. The density and dynamic viscosity of Hitec salt are also reported in the work.

Another ternary salt mixture, which is named Hitec XL, includes 48% of $\text{Ca}(\text{NO}_3)_2$, 7% of NaNO_3 , and 45% of KNO_3 . Compared to solar salt and Hitec salt , it has the lowest melting point of 120 °C and the lowest upper limit operating temperature of 500 °C [35,117]. The specific capacity, density and viscosity are 1.447 kJ/(kg•°C), 1992 kg/m³ and 0.2 cp, correspondingly [118].

For a long-term period, chemical stability is a key concern to utilize nitrate molten salt mixture. Since molten nitrate salts may undertake several reactions due to the temperature and the property of the cover gas. The primary reaction is the decomposition of nitrate to nitrite and oxygen [119].

Corrosion of molten salt to the material of pipe and storage tank is another important factor for molten salts to serve as HTFs. The corrosion behavior of the above three nitrate/nitrite molten salt was studied by Fernandez's team [120-122]. From the corrosion test of Solar salt on stainless

steel, no corrosion products were observed at 390 °C. For Hitec salt, three steels (A516, T11, T22) showed excellent behavior against corrosion with 0.35 mg/cm² mass gains. From the experiments, the author found that stainless steel had very good corrosion resistance to Hitec XL salt. The corrosion rate was 0.00075 μm/h without any corrosion production during the 2000 h test period.

1.4.2.4 Chlorides molten salts

Chloride molten salts attracted much attention due to their good stability at ultra-high temperature. They have been used as the material of the thermal storage system for a while [123,124]. The phase diagrams of multiple binary and ternary molten salts from NaCl, KCl, MgCl₂, CaCl₂, MnCl₂, FeCl₂, CoCl₂, NiCl₂, ZnCl₂, LiCl, RbCl, and CsCl are evaluated and optimized by Robelin and Chartrand by employing Modified Quasichemical Mode [125-127]. The results indicate that many eutectic molten salts have the potential to serve as HTFs in the future. Myers [124] investigated the melting temperature, the heat of fusion, and cost for 17 pure chloride salts and 162 binary eutectic mixture systems taken from the single chloride salts. But the thermophysical properties of those eutectic molten salts were not discussed.

Chloride molten salts also have the potential to serve as heat transfer fluid in the solar thermal application. Armijo et al. [128] from SNL discussed operational modes of a 2.0 MW pilot-scale solar thermal system using chloride molten salts as heat transfer fluid in their paper. Vignarooban et al. [129] studied the corrosivity of NaCl-KCl-ZnCl₂ (13.4 mol% - 33.7 mol% -52.9 mol%) salt to three different alloy metals. The experimental results showed that all three materials had good resistance against corrosion. The corrosion rates can be noticeably reduced when the materials and salts are keeping away from oxygen. The entropy generation of chloride molten salts consisting of NaCl, KCl, and ZnCl₂ were calculated and compared to solar salt and carbonate salts by Xu et al. [130]. The entropy generation of these chloride salts was found to be much lower than carbonate

salts and a little higher than solar salt at the same condition. It indicates that the Carnot cycle efficiency of using chloride salt is close to employing solar salt and much higher than carbonate salts.

Wei's team designed a novel ternary chloride salts with the compound of NaCl, KCl, and CaCl₂ by calculating the phase diagram and studied its thermophysical properties [131-134]. The melting point and heat of fusion of this ternary salt were found to be 420.83 °C and 201.5 J/g [131], separately. The results of TG (Thermal Gravimetry) show that the mass loss of this eutectic salt increases rapidly when the temperature is higher than 700 °C. Long-term isothermal stability tests indicate the salt is stable by holding 70 hours at the temperature of 500 - 650 °C, but the mass loss is obvious when the salt is kept at 700 °C. The heat capacity of this ternary chloride molten salt was measured to be 1.19 – 1.40 kJ/(kg•°C) during the temperature range of 486 °C to 616 °C [135]. The experimental results show the density and viscosity of this NaCl-KCl-CaCl₂ eutectic salt are 2630 - 1940 kg/m³ and 3.78 - 3.10 cp in the temperature range of 500 - 750 °C and 500 - 650 °C, respectively [135].

1.4.3 Liquid metals

In order to promote the conversion efficiency, and subsequently reduce the cost, future CSP plant need larger scale, higher concentration ratio, and higher working temperature [136-138]. Recently, Liquid metals and their mixture, which have been successfully used as coolants for nuclear power [140], attracted much attention to serving as HTFs in CSP because of their wide operating temperature range [137,139]. Lorenzin and Abanades reviewed and investigated the properties and feasibility of liquid metals to serve as HTF in CSP technologies. They selected five candidates among Alkali, heavy and fusible metal groups including: molten tin (Sn), gallium (Ga), lithium (Li), sodium (Na), and lead-bismuth (PbBi). Yuan et al. [141,142] introduced a new design

of a solar fuel reactor depending on liquid metal heat transfer fluid and the simulation results indicated that it can promote more than 80% heat recuperation of sensible heat. Bachelier and Jager [143] evaluated and compared the thermal and hydraulic performance of molten and liquid metal operating in an LFR solar collector and the results showed that compared to molten salt, employing liquid sodium as HTF had the benefits of wider operation temperature range, faster start-up procedures, quicker response of the control system and ultimately potentially higher energy yield. Prabu and Sekar [144] studied and compared the performance of hybrid solar system using GaInSn liquid metal, air and water as heat transfer fluid. The simulation results designate that use of liquid metal provides the highest exergy efficiency.

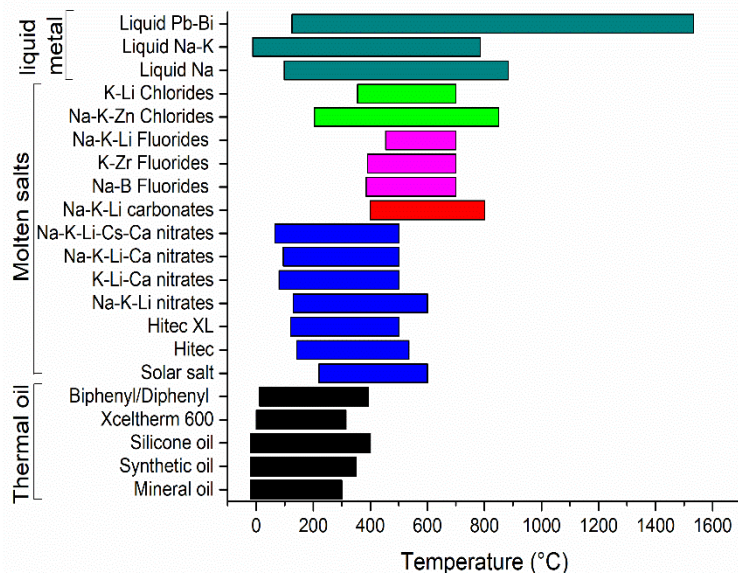


Fig. 3 Operating temperature range for different liquid HTFs

Depending on the above review about HTFs, pressured gases are hard to serve as the media of the thermal energy storage system because of their high pressure at superheat or supercritical state. For liquid heat transfer fluid, the comparison of the operating temperature range is shown in Fig. . Thermal oils are good HTFs for low operating temperature range but will decompose when

the temperature is higher than the upper limit (less than 400 °C). Liquid metals and their eutectic alloys have the advantages of a large operation temperature range and low viscosity. However, the disadvantages are still significant, much higher cost restricts the application in large scale CSP plant. Therefore, employing molten salts to serve as both HTFs and TES media is a more feasible way. Because the upper limit operating temperature of nitrate molten salts is less than 600 °C, the higher corrosivity of fluoride molten salts, and the lower reserves of carbonate molten salts, chloride molten salts are desirable candidates to serve as heat transfer fluid and thermal storage system media in large scale concentrated solar plant. [145]

1.5 Gaps in Literature

From reviewing the previous work done for the liquid heat transfer fluids in CSP systems, there are three gaps in literature found.

First, in recent years, heat transfer of liquid salts has become a highlighted research area again, due to the fast developments of CSP and nuclear technologies, where reliable heat transfer data and correlations with high accuracies are desired for the designs of heat transfer devices. From 2009 to now, the heat transfer performance of two liquid salts has been investigated by testing some shell-and-tube heat exchangers (STHX) when the salt flows in the tubes, where Hitec [146] and LiNO_3 [147] were employed. From the experimental studies, Wu et al. [148] concluded that the errors between most experimental results and existing correlations including Gnielinski's equation [149], and Hansen's equation [150] are within $\pm 25\%$ for the tested nitrate molten salt. Two systems of eutectic molten chloride salts, NaCl-KCl-ZnCl_2 , NaCl-KCl-MgCl_2 were highlighted by the authors' team at the University of Arizona, targeting at obtaining a new high-temperature HTF with a working temperature of up to 800°C and acceptable thermal and transport properties [151-153]. However, there have no heat transfer data and correlations reported for these

molten chloride salts, which are needed for the designs of heat transfer devices in the next generation CSP systems or nuclear power plants that may use these molten salts.

Second, molten salts freezing points are typically much higher above atmosphere temperature, for example, eutectic nitrate molten salt, $\text{KNO}_3\text{-NaNO}_3$, freezes at 220 °C [154], and $\text{MgCl}_2\text{-KCl}$ and $\text{MgCl}_2\text{-KCl-NaCl}$ freeze at 430 °C and 400 °C, respectively [151,153,155]. If the temperature of flow pipes is below the molten salt, it may cause freeze while flowing in pipes. There are two scenarios when the freeze happens in flowing molten salt. One is that the continuous flow of molten salt carries sufficient heat so that the front of the flow will never freeze completely, and the flow can move forward to build up a normal flow; the other is that the pipe is too cold in respect to the flowing molten salt and the freeze makes the flow difficult to set up and eventually is fully frozen/blocked which will cause the failure of the circulation of molten salt. There is no reported work on this to help the industry to understand the flowing freezing phenomenon better and prevent such disastrous situation from happening.

Third, although there are many proposed liquid heat transfer fluids as shown in Section 1.4, there is not criterion to understand the benefits of using one heat transfer fluid against another in CSP plant. It is difficult to make a fair comparison between two heat transfer fluids by comparing individual transport properties. For example, one fluid may have higher thermal conductivity and higher viscosity than another fluid. While the high thermal conductivity contributes to better heat transfer, the high viscosity will contribute to larger pressure loss during the flow [156-158]. It is therefore necessary to find one criterion that can entail all the transport properties of a heat transfer fluid so that comparison of benefit or advantage between HTFs can be made possible.

From above review and investigation, the major objectives and tasks are listed in section 1.6.

1.6 Objectives of this work

The main objectives of the work presented in this dissertation includes three parts. First is to systematically study the convective heat transfer performance of the selected molten chloride salt NaCl-KCl-ZnCl₂ (Molar fraction: 13.8%-41.9%-44.3%) inside tubes. A high temperature molten chloride salt circulation loop was designed and constructed for address this challenge.

Second is to carry out analysis for the transient heat transfer phenomenon between the hot fluid and the cold pipe. In this way, a fundamental discovery of the critical length's connection with various parameters is gained. Such parameters include the heat capacity, density, and thermal conductivity of both the fluid and pipe, viscosity and flow velocity of the fluid, the diameter and wall thickness of the pipe, as well as the temperature of the fluid entering the pipe and the temperature of the initially cold pipe.

Third is to propose a general criterion to evaluate the merit of various high temperature HTFs regarding their transport properties, in order to address the challenge of lacking such in the industry. Through this analysis, it can provide insights for a further development for the selection criterion of different heat transfer fluids associated to the cost of electrical energy of a CSP plant.

CHAPTER 2 EXPERIMENTAL STUDY ON HEAT TRANSFER

PERFORMANCE OF HIGH TEMPERATURE MOLTEN

CHLORIDE SALTS IN CSP SYSTEMS

2.1 Introduction

The global warming and worsening environment on the earth are alarming signals to human society that reducing the use of fossil fuels and cutting emission of CO₂ become contingent. The major solution to the problem is to use clean and renewable energies for electricity generation. Many countries around the world have drawn their roadmaps and plans to dramatically improve the proportion of renewable energy in their energy supply for electricity generation [158-161] by the time of 2050. The most viable approach for accomplishing the goal is to significantly increase the harvest and utilization of solar energy and wind power.

Because of the intermittency of availability of wind power and solar energy, energy storage and dispatch are very important should a stable electrical power supply is basically required. Therefore, technologies of storage of various types of energy, electrical, chemical, thermal, mechanical, potential, etc., have attracted a great amount of research and studies in the recent 10 years.

For energy storage in a concentrating solar power (CSP) system, thermal energy storage (TES) is mostly viable and cost-effective [162]. It is also typical that high temperature heat source is demanded in a thermal power plant to obtain high energy conversion efficient. Therefore, a fluid being able to take the heat from solar concentrator and being able to be stored with compact volumes will be ideal.

In the state-of-the-art CSP plant, solar energy is concentrated to a power tower, where the radiation energy is converted to thermal energy and a fluid carries the thermal energy away. A part of the thermal energy is utilized to produce high temperature steam for driving the power cycle for electricity generation, while the remaining part of thermal energy can be stored in a TES unit for use at night or under unfavorable weather. As a result, a CSP with TES can minimize the fluctuation of power generation, maintaining a reliable power output with solar energy. There is a significant development and construction of solar thermal power plants around the world. The global cumulative CSP capacity has been growing quickly in recent years and has reached 6,430 MWe by the end of 2019 [163-166].

The fluid medium, or heat transfer fluid (HTF) in a CSP system is very important. It is required to be able to work as a fluid at high temperatures (such as up to 750°C) and vapor pressure below 1.0 atm in the next generation CSP, making minimum corrosion to solar receiver, pipes, heat exchanger, and storage tanks, as well as having reasonable thermal transport properties for convective heat transfer and thermal storage. In the recent CSP technology, molten salts are the most promising HTF and heat storage media [167,168]. Besides the application for solar thermal energy, molten salts are also applied in nuclear technologies. For example, molten fluoride salts are considered as promising heat transfer fluids in the state-of-the-art fourth-generation nuclear power plants [169, 170]. These are because the molten salts have numerous advantages such as low vapor pressure, good thermostability, and low price [171, 172]. For improving the performance and ensuring the safe operation of these devices in CSP plants and nuclear power plants, it is critical to understand the flow and heat transfer features of the liquid salts in pipes. As the consequence, experimental investigation to the heat transfer is needed.

It was found from literature survey that several experimental studies from the 1940s to 1970s

investigated the heat transfer performance of some liquid salts in pipes heated with uniform wall heat flux. Typical liquid fluorides including $\text{ThF}_4\text{-BeF}_2\text{-UF}_4\text{-LiF}$ [15, 16], FLiNaK [173-177] and NaF-NaBF_4 [173], and liquid nitrate salts (Hitec salts [178,179]) had been experimentally studied. During the following thirty years from 1970s, there was almost no progress on this topic, and no experimental result had been openly reported.

In recent years, heat transfer of liquid salts has become a highlighted research area again, due to the fast developments of CSP and nuclear technologies, where reliable heat transfer data and correlations with high accuracies are desired for the designs of heat transfer devices. From 2009 to now, the heat transfer performance of two liquid salts has been investigated by testing some shell-and-tube heat exchangers (STHX) when the salt flows in the tubes, where Hitec [146] and LiNO_3 [146] were employed. From the experimental studies, Wu et al. [148] concluded that the errors between most experimental results and existing correlations including Gnielinski's equation [149], and Hansen's equation [150] are within $\pm 25\%$ for the tested nitrate molten salt. Two systems of eutectic molten chloride salts, NaCl-KCl-ZnCl_2 , NaCl-KCl-MgCl_2 were highlighted by the authors' team at the University of Arizona, targeting at obtaining a new high-temperature HTF with a working temperature of up to 800°C and acceptable thermal and transport properties [151-153]. There have no heat transfer data and correlations reported for these molten chloride salts, which are needed for the designs of heat transfer devices in the next generation CSP systems or nuclear power plants that may use these molten salts.

In the current work, the molten chloride salt NaCl-KCl-ZnCl_2 at one of its ternary eutectic molar fractions (13.8%-41.9%-44.3%) was selected for study. For the first time, challenging high temperature experiments was carried out to investigate the convective heat transfer inside a tube. The experiments covered the typical range of Re from 3000 up to over 1.0×10^4 at sufficiently high

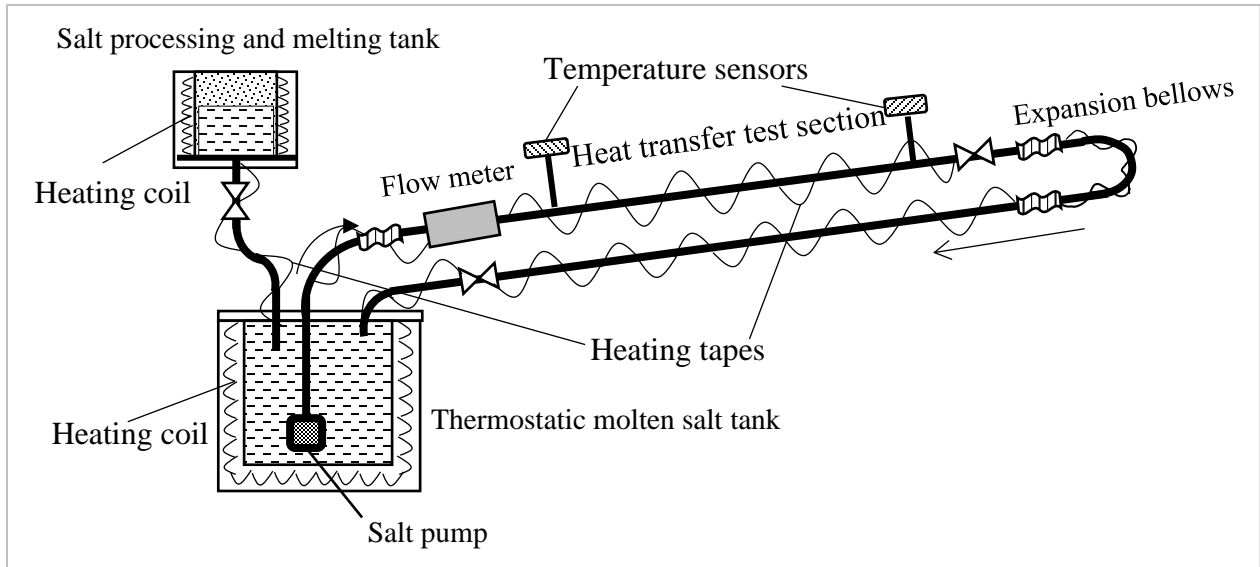
temperatures. The experimental data of heat transfer coefficient were compared with predictions from classical heat transfer correlations to examine whether they are applicable to the newly developed chloride salts, or otherwise a new correlation needs to be developed. Since NaCl-KCl-ZnCl₂ and NaCl-KCl-MgCl₂ are similar ionic chloride salts and Newtonian fluids at above melting points, it is a cautious inference that the selected heat transfer correlations can also be applicable to NaCl-KCl-MgCl₂.

2.2 Molten Salt Convective Heat Transfer Experimental Setup and Data Reduction

2.2.1 Molten salt flow loop

As shown in Fig. 4, the molten salt test loop is comprised of a molten salt tank or reservoir, a pump, an ultrasonic flow meter, the heat transfer test section, control valves, sensors and instrumentation for measurement of temperatures in the test section, and heat tapes adding heat flux to the test section. The materials for the flow pipes of the test loop are high temperature alloys of Hastelloy C-276. The molten salt tank and the pump are made of stainless steel.

The molten salt tank seats in a furnace with temperature controlled, and therefore, serves as a thermostatic reservoir of the high temperature fluid for the test loop. The molten salt temperature in the reservoir can be controlled from room temperature to 650oC. After being pumped out, the molten salt flows into test section for convective heat transfer coefficient measurement. For the molten salt to automatically flow back and drain down to the thermostatic reservoir after the test and operation, the pipes of the test section and the returning pipe of the flow were arranged to have a slope of 5 degrees as schematically shown in Fig.4a and a photograph shown in Fig.4b.



(a) Schematic



(b) Photograph

Fig. 4 The chloride molten salt flow loop for the experiments

The cylindrical thermostatic molten salt tank or reservoir has 304.8 mm in inner diameter and 381 mm in height. The volume for molten salt is about 21.96 Liters. The pipes of the flow loop could hold a volume of molten salt of 3.24 Liters, which is due to the flow pipes of 6.4m in

total length, 25.4mm in outer diameter, and a wall thickness of 1.65 mm.

The pump in the molten salt tank can discharge molten salt at the flow rate of up to 0.63 Liter/s. The molten salt flow velocity was measured using an ultrasonic flow meter.

Heating tapes with controlled power were used in the heat transfer test section and extra heating tapes were also used to keep all the pipes at a temperature above 300oC for the startup of operation of the test loop. Proportional, Integral, and Derivative (PID) heating controllers were used to control temperature of the pipes beyond the test section. Power controller was used to monitor the power supplied to the heat transfer test section. A multifunction I/O device has a module for temperature measurement using thermocouples, which allows LabVIEW engineering software to obtain temperatures sensed by thermocouples. The specifics and information of the employed instruments including measurable parameters, accuracy, model and maker, and measurable range are listed in Table 1.

Table 1 Specifics of instruments used in the high temperature molten salt loop

Name	Measurable parameter	Accuracy	Model and maker	Range
Molten salt tank	Volume	N/A	Wenesco, LLC.	27.80 liters T <650°C
Pipe	Outer diameter & wall thickness	OD ± 0.127 mm, Wall tolerance ± 0.051 mm	Hastelloy C276 American Special Metal.	25.4 mm OD & 1.65 mm thick. T <800°C
Molten salt pump	Volume flow rate	N/A	Wenesco, LLC.	0-0.63 (liter/s) T <650°C
Ultrasonic flow meter	Flow velocity	$\pm 1.6\%$ of reading in addition to ± 0.01 m/s	FLUXUS ADM 7407 by Flexim Americas Co.	0.01-25 m/s, T < 650°C
Heating tape for none test section	Power	N/A	STH051-080 by Omega Engineering, Inc.	0-627W, T <760°C
Heating tape at test section	Power	N/A	A401-UNAZ0515-88 by HTS/Amptek Co.	0-1567W, T < 760°C

Micro Fusion SCR Power Controller	Power	±0.5% of reading	uF1HXTA0-16-P1R00, by Control Concepts Inc.	0-10 kW
PID Heating controllers	Temperature	±3°C of reading	SDC240KC-A, by Semi-conductor Smart Solutions, LLC.	T < 700°C
Thermocouples	Temperature	±1.1°C or 0.4% of reading (whichever is greater)	KQXL-116G-24, KQXL-116G-18 by Omega Engineering, Inc.	0-1038°C
Multifunction I/O Device	Voltage	±0.03% of reading	NI cDAQ-9178, NI9229, National Instruments.	-60 V to +60 V
Ceramic fiber blanket	Thermal conductivity		3R2300, by Industries 3R Inc.	0.06-0.16 W/(m.K)
Expansion bellows	N/A	N/A	Customized by Duraflex Inc.	T < 800°C
Stainless steel valves	N/A	N/A	F313L by Dixon Eagle	T < 650°C

2.2.2 Detail of test section

The heat transfer test section is a pipe made of Hastelloy C276. The length of the test section is 1860 mm, with outer and inner diameters of 25.4 mm and 22.1 mm, respectively. Thermocouples were inserted into the pipe at the inlet, mid-point, and outlet of the test section to measure the fluid temperatures. The test pipe was wrapped with heating tape to provide heat flux to the flow of molten salt inside the pipe. Reliability of the heating tape was particularly required. At the outer surface of the pipe and beneath the heating tape there were thermocouples to measure surface temperature of the pipe. On top of the heating tape, the first layer of thermal insulation was wrapped. The ceramic fiber insulation blanket has thermal conductivity of 0.06-0.16 W/m·K under temperature of 300 °C to 600 °C, correspondingly. The diameter at the outside of the first layer of thermal insulation is 69.57 mm. At this location of diameter, thermocouples were set to measure the temperature in the thermal insulation material. On top of that, a second layer of thermal

insulation material was wrapped with an outer diameter of 111.06 mm. At this location of the diameter, thermocouples were set and one more layer of thermal protection was wrapped. The temperature reading from thermocouples at the two radial locations, D1 and D2, as shown in Fig. 5 allowed us to calculate the temperature gradient in thermal insulation and thus the outward heat loss. With the heating tape power subtracting the heat loss outward, the remaining heat is assumed going into the flowing molten salt inside the tube.

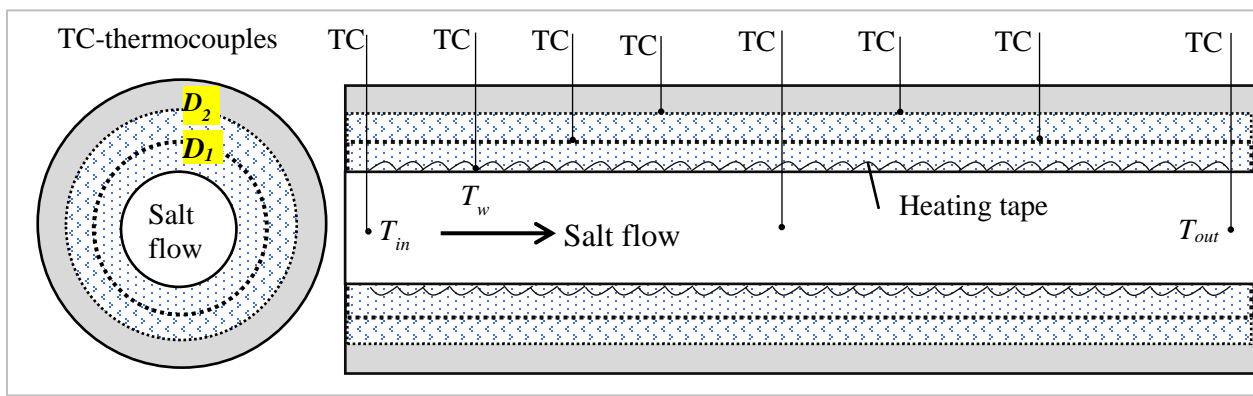


Fig. 5 The allocation of thermocouples for temperature and heat flux measurement at test section

2.2.3 Procedures of a test and operation

The purchased anhydrous salt powder of NaCl, KCl and ZnCl₂ were prepared at the required eutectic molar composition (mole: 13.8% NaCl, 41.9% KCl, 44.3% ZnCl₂) or mass composition (8.1% NaCl, 31.3% KCl, 60.6% ZnCl₂). The three salts were then ground and mixed in a tumbler mixer for more than 200 hours so that the salts were made into very fine particles and eutectic mixture at solid state was formed. The powder of eutectic mixture was loaded into a salt melting tank, which sits in a furnace (Model KM714 from SKUTT AUTOMATIC KILN) as shown in Fig. 6. After the salt was loaded to the melting tank, the tank was vacuumed to get rid of air and moisture and then charged with dry nitrogen gas. When the salt was heated to a temperature of 150

°C, it was maintained for over 1 hour to let water vapor (if there was any) get out. After the salt was melted, dry nitrogen gas sparging was applied to get rid of bonded water and the air trapped inside the salt. The vent was connected to tubes leading to humidity sensor and oxygen sensor. When all the moisture and air was removed from the molten salt in the melting tank, the liquid salt was drained to the molten salt reservoir of the test loop. The test loop was pre-vacuumed and filled with nitrogen.

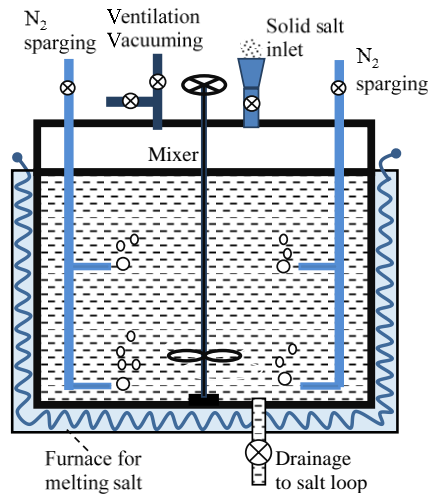


Fig. 6 Salt melting and purification in salt processing tank

The experimental test was at high temperatures; therefore, the first step of the experiment was to always keep the molten salt at a temperature sufficiently above the melting point. It took about 2 hours for the tank's heater to heat and fully melt the salt. All pipes and valves of the flow loop were also warmed up to keep at 360 °C, a temperature sufficiently above the melting point of the molten salt.

The flow rate of the liquid salt could be controlled through adjustment of the frequency of the molten salt pump. The flow rate was read from the molten salt flow meter. All the thermocouples were connected to the data acquisition system including the NI-DAQ units and the LabVIEW software to read and record the temperature history during a test. The heating power or heat flux

from the heating tape on the test section was measured through the power control system. Depending on the change of test temperatures, it took about 60-90 minutes for one test condition to reach a steady state for measurement. To prevent heaters having a too fast temperature rise, all the heating process were managed to go slowly in 1 hour interval to make sure that heaters did not heat up excessively and fail.

The measured parameters included the mass flow rate (or flow velocity), the fluid temperatures at the inlet and outlet of the test section, the heat flux of the heating tape, the temperatures at the outer wall of the pipe, and temperatures at different diameters in the thermal protection layer. These parameters allowed the calculation of the heat transfer coefficient of the internal flow of the molten salt.

After recording all readings at steady state for 2 hours, heating power or flow rate could be changed to do the next measurement under a new condition. If the experiment was finished, the remaining first step was to turn down and stop the pump, thereafter, the heaters should be kept on for another 2 hours before turning off, so that molten salt could be hot enough and automatically flow back and drained down to the thermostatic reservoir.

2.2.4 Data reduction and uncertainty analysis

The directly measured data include wall temperatures at desired locations of test section, flow rate of the molten salt, the heat flux from the heating tape at the surface of the test section, the dimensions of the tubes of the test section, and the coordinate of the locations of thermocouples.

The energy generated from the heating tape is partly lost outward to the ambient, and the remaining part is consumed to heat up the fluid inside the tube, which gives

$$\dot{Q}_{heater} = \dot{Q}_{in} + \dot{Q}_{loss} \quad (4)$$

The heat loss can be calculated using the measured temperatures in the thermal insulation layer at locations of diameters of D_1 and D_2 as shown in Fig. 5.

$$\dot{Q}_{loss} = 2\pi L k_{th} \frac{T_1 - T_2}{\ln(D_2/D_1)} \quad (5)$$

\dot{Q}_m is the energy absorbed by the molten salt inside the tube. Therefore, this energy satisfies the following three equations:

$$\dot{Q}_{in} = \dot{m} C_p (T_{f-out} - T_{f-in}) \quad (6)$$

$$\dot{Q}_{in} = 2\pi L k_w \frac{T_{wo} - T_{wi}}{\ln(D_{wo}/D_{wi})} \quad (7)$$

$$\dot{Q}_{in} = \pi D_{wi} L h (T_{wi} - T_f) \quad (8)$$

where h is heat transfer coefficient, which can be determined as:

$$h = \dot{Q}_{in} / \left\{ \pi D_{wi} L \left[T_{wo} - \frac{\dot{Q}_{in} \ln(D_{wo}/D_{wi})}{2\pi L k_w} - \frac{(T_{f-out} + T_{f-in})}{2} \right] \right\} \quad (9)$$

$$Nu = \dot{Q}_{in} / \left\{ \pi L k_f \left[T_{wo} - \frac{\dot{Q}_{in} \ln(D_{wo}/D_{wi})}{2\pi L k_w} - \frac{(T_{f-out} + T_{f-in})}{2} \right] \right\} \quad (10)$$

Consequently, the following two steps show how to find the convective heat transfer coefficient inside the tube.

1) The analysis starts with calculating \dot{Q}_{loss} using the measured temperatures at the interfaces of the thermal insulation layers at locations of diameters of D_1 and D_2 . The reading of \dot{Q}_{heater} subtracting \dot{Q}_{loss} will be the energy \dot{Q}_{in} , which can also be checked by the value calculated from Eq. (6).

2) The heat transfer coefficient h and Nusselt number can be obtained step by step from calculation using Eq. (7) and Eq. (8), which result in the equations for h and Nu as given in Eq. (9)

and Eq. (10). The fluid temperature in Eq. (8) is the average temperatures at the inlet and outlet of the test section, which gives $T_f = (T_{f-out} + T_{f-in})/2$.

The energy \dot{Q}_{in} could be calculated in two ways, one through the Eq. (4) and (5), and the other through the measured fluid temperature at inlet and outlet and the flow rate of molten salt in Eq. (6). The difference of the energy calculated by these two ways helps one to check the heat balance.

The uncertainties of Re, \dot{Q}_{in} , h, and Nu were evaluated using the method presented in Refs. [13,30-32]. The uncertainties of the measurement instruments can be found in Section 3.1. The uncertainties of thermal physical properties of the heat transfer fluid can be found from previous work [26]. The relative uncertainties for density, thermal conductivity, heat capacity, and viscosity are 0.89%, 7.9%, 3.48% and 3.76%, respectively. The uncertainties of the dimensions and properties of pipes and thermal insulation materials are neglected. Consequently, using the method presented in reference [13,30], the relative uncertainties of Re can be calculated by the square root of the sum of the squares (RSS).

The calculated results showed relative uncertainties of Re as 4.26%. Similarly, the relative uncertainties of \dot{Q}_{in} , h, Nu, and the percentage of deviation, $(Nu - Nu_{predicted})/Nu_{predicted}$, were found to be 4.06%, 4.08%, 9.14%, and 9.88%, respectively. The uncertainties for Nusselt number are reflected by the error bars in the plots in Section 2.3.

2.3 Results and discussions

The molten salt loop was operated continuously for 11 days at high temperatures to have the convective heat transfer coefficients measured.

Figure 7 shows the energy balance checked at different tested Re. The deviations of heat

calculated in two ways are around $\pm 6\%$ in most experimental conditions. The one point with the highest deviation in the tests was 9.4%, the standard deviation of heat balance is 5.9%, which can confirm the reliability of the tests.

The obtained results of Nusselt number at different Reynolds numbers under six different temperatures are shown in Fig. 8. The experiments covered a Reynolds number range from 3000 to 14000 and a temperature range from 400°C to 600°C. It is noted that a higher Reynolds number should be tested to cover much stronger turbulent flow, however, technical difficulties (severe vibration) of the high temperature pump at high rotating speed hindered the effort, which incentivizes the development of more reliable molten salt pump in the future. Nonetheless, the Reynolds number tested still covered sufficient turbulent flow regime, which provides a very valuable reference and the checking for the validity of heat transfer correlations for CSP industry to design heat transfer devices.

For comparison between the experimental data and predictions from empirical correlations, two famous heat transfer correlations for internal turbulent flow, Gnielinski equation and Dittus-Boelter equation, were applied to calculate the Nusselt number with given Reynolds number and Prandtl number of the molten salt.

As seen in Fig. 8, the tested Nu and the prediction by Gnielinski equation agree very well, within a deviation of less than 5% at low Reynolds number range and a deviation less than 15% at high Reynolds numbers. In general, this empirical correlation gives slight over-prediction of the Nusselt number compared to the experimentally obtained data at the tested Reynolds numbers.

The Dittus-Boelter correlation was also applied to predict the heat transfer coefficient and compared to the tested data. It over predicts the heat transfer coefficient for about 20% for all the tested cases. This deviation of the prediction against experimental data is still acceptable in the

heat transfer community. As the conclusion of heat transfer test, we recommend Gnielinski equation for the prediction of internal turbulent flow heat transfer coefficient of the current molten chloride salts.

Fig. 9 shows the comparison of all the experimental data with the prediction from Gnielinski equation. There are 22 data out of 24 showing a percentage deviation of less than $\pm 15\%$ between the experimental data and the prediction by the empirical correlations. The other two points have percentage deviations above $\pm 15\%$ but less than $\pm 16\%$ between the prediction and the experimental results. Figure 10 shows that the mean value of the percentage deviation between measured and predicted value of Nu from Gnielinski's correlation is 7.2%, standard deviation of the $(N_{\text{tested}} - N_{\text{predicted}}) / N_{\text{predicted}}$ is 7.4%. In general, both two empirical correlations tend to overpredict the heat transfer coefficient, however, prediction from Gnielinski correlation is more acceptable. We also found that at high temperatures, the deviation between prediction and tested results becomes higher. Higher random error in the test at high temperatures could also be the reason. At high temperature test, the waiting time for reaching steady state was shorter due to the increased vibration of pump, which may cause less accuracy of getting reliable data. Nonetheless, in overall the deviation of tested data and the prediction still agreed reasonably well.

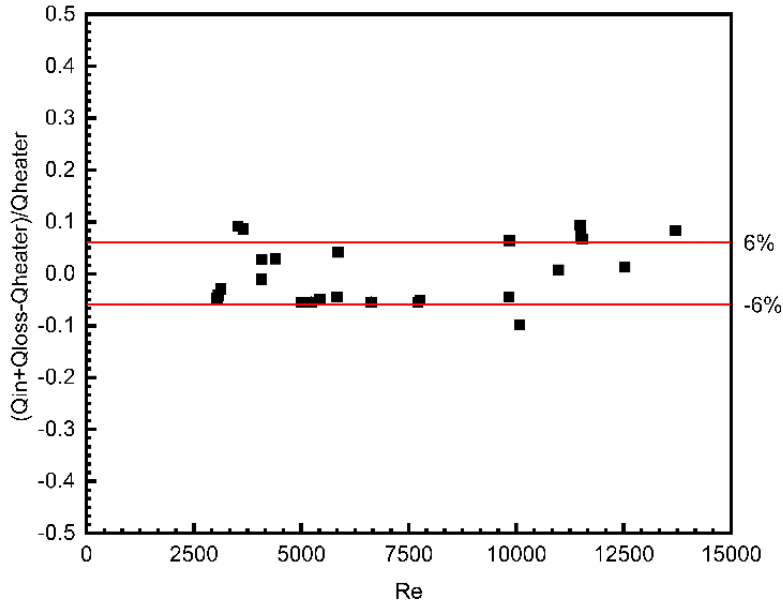
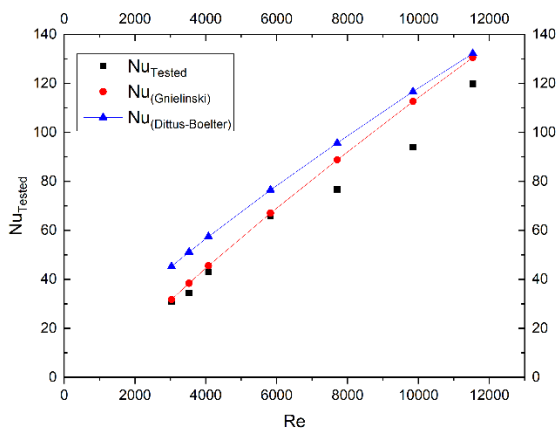
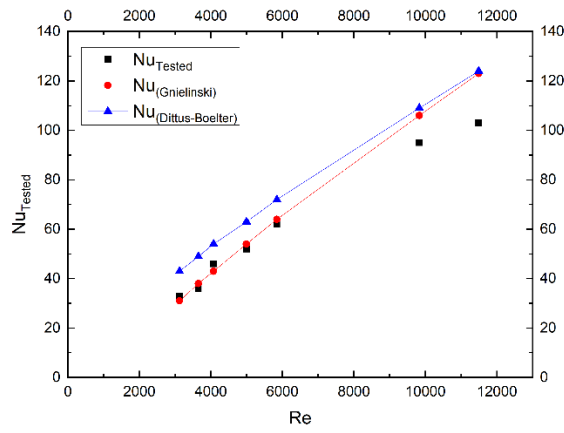


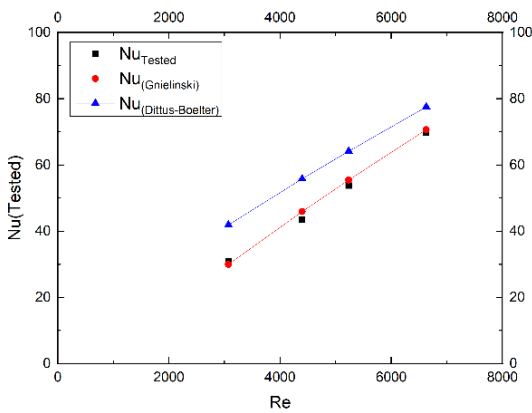
Fig. 7 Heat balance in the tests. Heat flux $q_{in}=7743\text{W/m}^2$, and temperatures ranged from 400°C to 600°C .



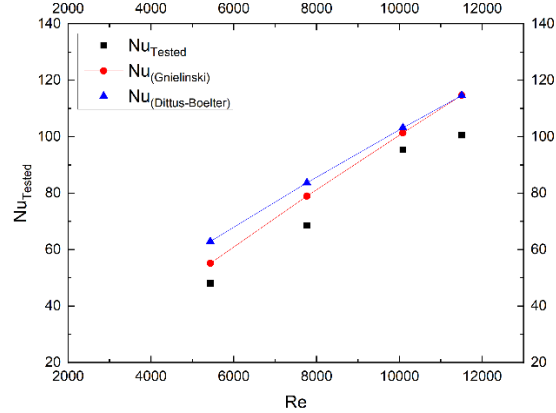
(a) $T_{f-in}=400^\circ\text{C}$



(b) $T_{f-in}=450^\circ\text{C}$



(c) $T_{f-in}=480^\circ\text{C}$



(d) $T_{f-in}=550^\circ\text{C}$

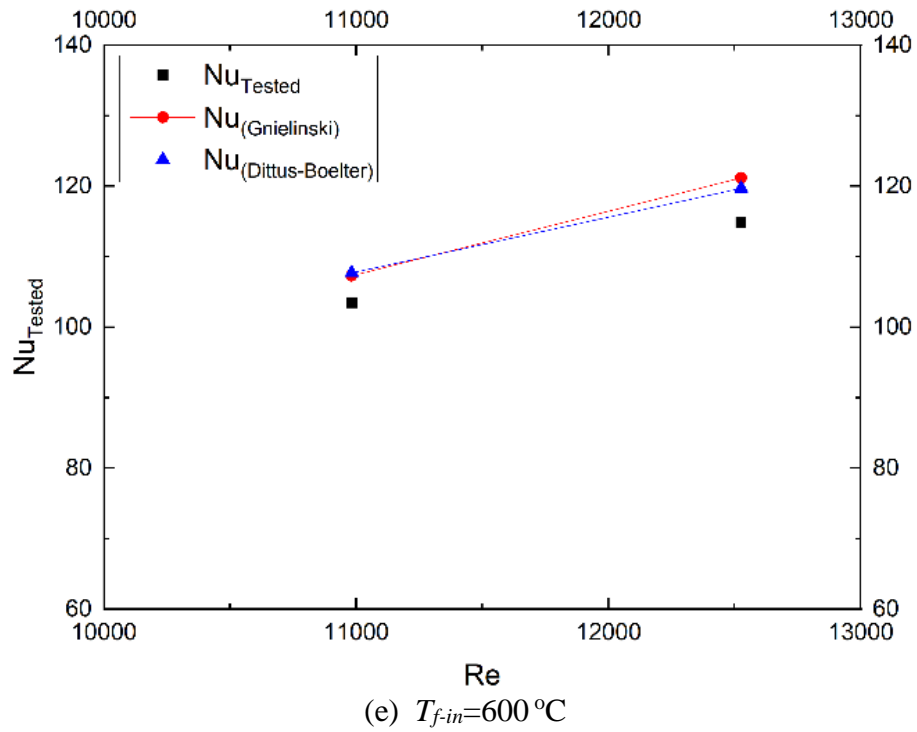


Fig. 8 Experimental data of heat transfer coefficient and predictions using empirical correlations. Heat flux $q_{in}=7743\text{W/m}^2$ for the tests.

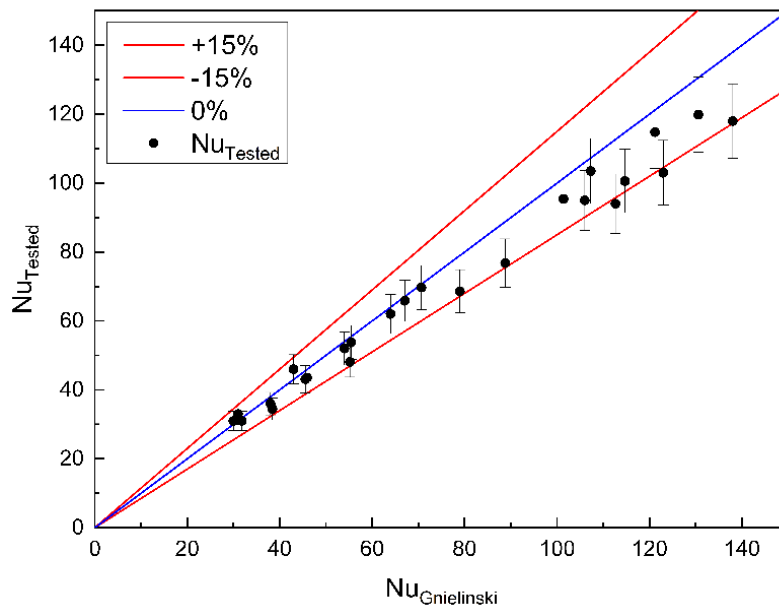


Fig. 9 The agreement of all the tested Nu number between experimental data and predictions by Gnielinski correlation. Temperatures of tests ranged from $400\text{ }^{\circ}\text{C}$ to $600\text{ }^{\circ}\text{C}$.

2.4 Conclusions

Eutectic chloride salts NaCl-KCl-ZnCl₂ (molar fraction: 13.8%-41.9%-44.3%) is designated as a new heat transfer fluid for high temperature application in concentrated solar power system. The process and preparation to obtain eutectic salt mixture was successfully practiced in this work. Behavior of hygroscopicity of the salts was observed to help prevent salts from absorbing water from air.

Experimental measurement of the convective heat transfer coefficients of the eutectic salt inside tubes has been conducted to check the validity of heat transfer correlations for application to the new heat transfer fluid. Experimental data of Nusselt number, Reynolds number, were provided for comparison with the prediction by the Dittus-Boelter correlation and Gnielinski's correlation. Gnielinski equation predicts the heat transfer coefficients within a deviation of less than 5% at low Reynolds number range (less than 6000) and a deviation less than 15% at high Reynolds numbers. The Dittus-Boelter correlation can over-predict the heat transfer coefficient for about 20% for all the tested cases. Based on the comparison, Gnielinski's correlation is recommended for better prediction of heat transfer coefficients of the current molten salt. It is the cautious inference that the Gnielinski's correlation may be applicable to similar eutectic ionic molten chloride salts system NaCl-KCl-MgCl₂ with corresponding thermal and transport properties.

CHAPTER 3 ANALYSIS OF THE HEAT TRANSFER AND CRITERION OF FREEZING OF MOLTEN SALT STARTUP FLOW IN RELATIVELY COLD PIPES

3.1 Introduction

Because of the capability of large amount of solar thermal energy storage for power generation in nighttime and in the time of bad weather, concentrated solar thermal power (CSP) technology has been widely recognized as a viable approach for power generation and dispatch using solar energy. Based on the latest data, concentrated solar thermal power generation capacity in the world has reached to 5.5GW with the power plants typically having extended operation of 4 to 6 hours every day after sunset [179].

In the current CSP technologies, synthetic oil Therminol VP-1 is used as the heat transfer fluid for trough solar concentrators to reach to a maximum temperature of 400 °C [180]; while eutectic nitrate molten salt, $\text{KNO}_3\text{-NaNO}_3$, is used for heliostat power tower solar collectors to a maximum temperature of 560 °C [181]. In the next generation of solar power tower technology eutectic molten chloride salts, $\text{MgCl}_2\text{-KCl}$, or $\text{MgCl}_2\text{-KCl-NaCl}$ might still be considered, which can have a high temperature up to 800 °C [182, 154].

There are multiple important criteria for a molten salt being accepted as a proper heat transfer fluid, which include favorable thermal and transport properties, low corrosion rate to pipes and tanks, low freezing point, high boiling point, and low cost to meet the need of large quantity of mass for thermal storage.

Molten salts freezing points are typically much higher above atmosphere temperature, for

example, eutectic nitrate molten salt, $\text{KNO}_3\text{-NaNO}_3$, freezes at $220\text{ }^\circ\text{C}$ [154], and $\text{MgCl}_2\text{-KCl}$ and $\text{MgCl}_2\text{-KCl-NaCl}$ freeze at $430\text{ }^\circ\text{C}$ and $400\text{ }^\circ\text{C}$, respectively [151,155]. If the temperature of flow pipes is below the molten salt, it may cause freeze while flowing in pipes. There are two scenarios when the freeze happens in flowing molten salt. One is that the continuous flow of molten salt carries sufficient heat so that the front of the flow will never freeze completely, and the flow can move forward to build up a normal flow; the other is that the pipe is too cold in respect to the flowing molten salt and the freeze makes the flow difficult to set up and eventually is fully frozen/blocked which will cause the failure of the circulation of molten salt. Therefore, having a better understanding of the flowing freezing is important towards a safe and reliable operation of molten salt flow loop for solar thermal and molten salt nuclear power plants [183]. The focus of this work is the analysis of the heat transfer and freezing of flowing molten salt in a pipe, which will help the industry to understand the phenomenon and prevent the disastrous situation from happening in a concentrated solar power plant or salt nuclear power plant.

3.2 Physical Model and Mathematical Description

3.2.1 Transient heat transfer between hot fluid and cold pipe being viewed as energy storage process

When hot fluid flows passing inside a cold pipe, the pipe wall absorbs heat from the fluid, which can make the fluid temperature drops. If the fluid temperature drops below its freezing point, solidification of the fluid will block the continuous flow of the fluid inside the pipe. The objective of the current analysis is to find out how far the hot fluid can flow into the cold pipe before its temperature drops below the freezing point.

Typically, the fluid adjacent to the cold wall may freeze first, however, if the flow mixing is

sufficiently strong, one may make assumption that the temperature of fluid at a cross section is the same. This is a strong approximation; however, it will greatly reduce the complexity of the problem and makes it possible to have a basic understanding to the phenomenon through analytical study. The effect of various parameters to the freezing starting point along the pipe can be fundamentally understood.

As has been studied in the previous work by Li et al. [184], when hot molten salt flowing through a cold pipe, the heat transfer between the fluid and the pipe can be essentially viewed as a thermal energy storage process, namely, the thermal energy from the fluid is stored in the cold pipe. Fundamentally, the thermal energy storage from a fluid given to packed solid materials, as shown in Fig. 10 (a) and (b), can be treated the same from the perspective of mathematical description, which has been discussed in detail in Ref. [184, 185]. The similarity of these two cases in Fig. 10 (a) and (b) lies on the fact that a fluid flowing through the packed solid materials which is a porous media, except the porous structure is different. For the case in Fig. 10(b), one can see the structure as a stack of multiple pipes of solid materials that have fluid flowing inside. There is heat transfer between the fluid and the solid material, which makes the fluid temperature decreases, while the temperature of the solid material rises. In case that freeze of the fluid is a concern, temperature of the fluid should be managed above the freeze point through the analysis of the transient heat transfer between the solid and fluid.

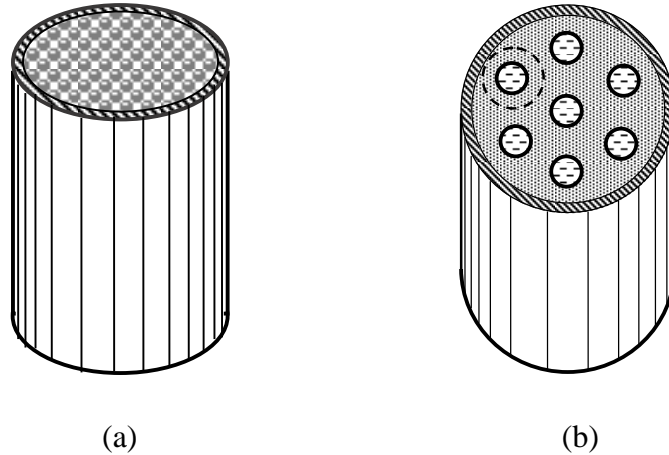

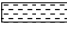


Fig. 10 Similarity of structure of hot fluid flowing through packed solid material which can be viewed as a porous material ( solid thermal storage material;  heat transfer fluid)

To study the temperature variation against time in the solid material and the fluid, transient equations governing the energy conservation in the solid material and the fluid, which are coupled through the heat transfer between the solid and fluid, will have to be constructed. For the case in Fig. 10(a), a 1D model of fluid flowing through a uniformly packed porous material can be used as seen in Fig. 11(a). For the case in Fig. 10(b), one can study the temperature variation of the solid material pipe, as shown in Fig. 11(b), with fluid flowing inside.

In a previous work conducted by Van Lew et al. [186], one- dimensional governing equations for the energy conservation in the solid material and the fluid in a differential unit of Δz , as shown in Fig. 11(a), have been established with the following assumptions:

- 1) Radial distribution of the fluid flow and solid material through the storage system is assumed uniform to make the problem to a one-dimensional problem along the axis, z , of the storage tank.
- 2) The contacts between solid spheres are point contacts and therefore heat conduction between rocks are negligible.
- 3) The Peclet number ($Pe=LU/\alpha$) of fluid flow in the tank packed with porous solid material

is large ($Pe \gg 100$), and therefore, the heat conduction in the axial direction in the fluid is negligible [10], where L is a characteristic length, U is the fluid velocity, and α is the thermal diffusivity of the fluid.

4) The Biot number ($Bi=hL/k$) [11] of the transient heat conduction in a single solid sphere is small enough that lumped heat capacitance method is applicable to the heat conduction in the sphere. However, if the Biot number is large, a correction to the heat transfer coefficient between fluid and solid is introduced [11].

5) There is no heat loss from the storage tank to the surroundings. However, if there is heat loss to be considered, it may be considered by an equivalent larger cooling heat capacity of the pipe.

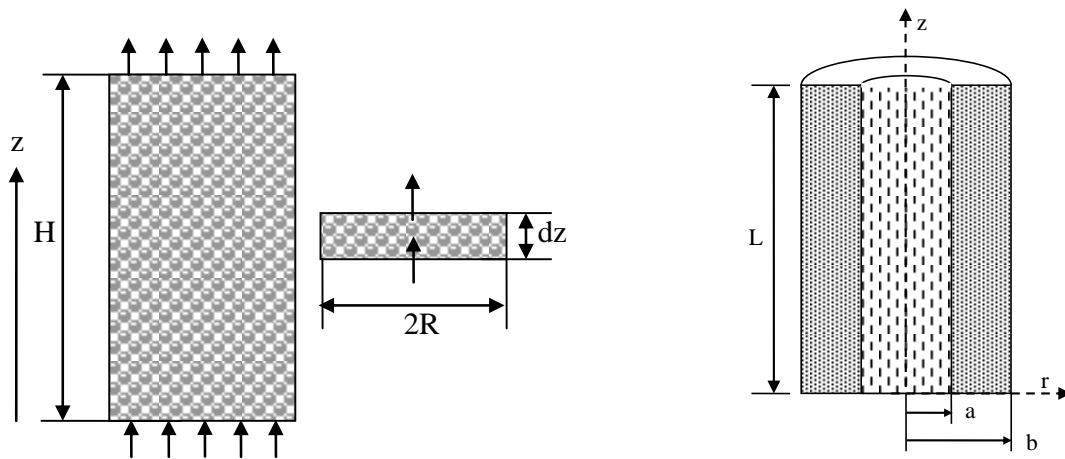


Fig. 11 Model used to analyze the heat transfer between hot fluid flowing through packed solid material.

Because of the analogous feature of the heat transfer for the cases in Fig. 11(a) and (b), the same type of governing equations of the energy conservation in the solid pipe wall and the fluid can be established. However, the heat transfer coefficient between the solid pipe and the fluid will be correspondingly applied to. In case the Biot number is large than 0.1, an extra correction on top

of the heat transfer coefficient between the solid pipe and fluid will be introduced. This work has been conducted by Li [184] and Xu [185] in previous work. They provided the so-called effective heat transfer coefficient between the solid pipe and fluid for large Biot numbers. The effective heat transfer coefficient in the lumped capacitance method of this structure is found and proven being able to accurately predict the energy storage in solid pipe, or the thermal energy storage material [184]. With the effective heat transfer coefficient, the lumped capacitance method can be applied to modelling the thermal storage in the case of Fig. 10(b) or Fig. 11(b). In the solid-material pipe the heat conduction in the fluid flow direction is ignored, only leaving the heat conduction in the thickness of the pipe for analysis.

Although the heat transfer analysis for the fluid flowing in a solid material pipe was originated from the perspective of energy storage, it is now can be used to understand the transient temperature variation in the hot fluid when it flows through a cold pipe. The objective of the analysis in this work is to find the onset length of pipe where fluid starts to freeze at various heat transfer conditions. From the entrance to the onset of fluid freezing is named as the critical length in this study.

3.2.2 Fluid energy balance equation

The governing equation for the energy conservation in the one-dimensional fluid flow in the case in Fig. 11(b) is [186]:

$$\frac{h_{eff}S_s}{\rho_f C_f \varepsilon \pi R^2} (T_s - T_f) = \frac{\partial T_f}{\partial t} + U \frac{\partial T_f}{\partial z} \quad (11)$$

where h_{eff} is effective heat transfer coefficient between the fluid and the solid wall, U is the flow

velocity of the fluid, ε is the porosity of the system, S_s is the heat transfer surface area between the fluid and the solid surface per unit of length of the flow pipe. According to the above definitions, the equations for the parameters are as follows:

$$U = \frac{\dot{m}}{\rho_f a_f} \quad (12)$$

$$a_f = \varepsilon \pi b^2 \quad (13)$$

$$\varepsilon = a^2 / b^2 \quad (14)$$

$$S_s = 2\pi a \quad (15)$$

Introducing the following dimensionless variables,

$$\theta_f = (T_f - T_l) / (T_h - T_l) \quad (16.a)$$

$$\theta_s = (T_s - T_l) / (T_h - T_l) \quad (16.b)$$

$$z^* = z / H \quad (16.c)$$

$$t^* = t / (H / U) \quad (16.d)$$

A dimensionless governing equation for fluid in the pipe is obtained as:

$$\frac{\partial \theta_f}{\partial t^*} + \frac{\partial \theta_f}{\partial z^*} = \frac{1}{\tau_r} (\theta_s - \theta_f) \quad (17)$$

where a dimensionless parameter by a cluster of properties and dimensions is

$$\tau_r = \frac{U \rho_f C_f \varepsilon \pi b^2}{H h_{eff} S_s} \quad (18)$$

The effective heat transfer coefficient h_{eff} (W/m² K) in the above equations is defined as the original heat transfer coefficient between the fluid and the pipe with consideration of the modification due to the correction for the case that the Biot number of the heat conduction in the solid pipe is larger than 0.1.

For the fully developed flow in a pipe, Dittus-Boelter equation [187, 188] or Gnielinski equation [189] can be used to decide the basic heat transfer coefficient h . In the current study, we use Dittus-Boelter equation. With the correction considered as described in detail in Ref. [184], the effective heat transfer coefficient is:

$$h_{eff} = \frac{1}{\frac{1}{h} + \frac{1}{k_s} \frac{a^3 (4b^2 - a^2) + ab^4 (4Ln[b/a] - 3)}{4(b^2 - a^2)^2}} \quad (19)$$

3.2.3 Energy balance equation for the cold pipe wall

For the energy balance of the solid material of the pipe wall, the same approach of energy conservation analysis can be applied for a control volume dz of the pipe. The solid pipe extracts heat from the passing fluid at the cost of a change in the internal energy of the filler. The energy balance equation is:

$$\rho_s C_s (1 - \varepsilon) \pi b^2 dz \frac{\partial T_s}{\partial t} = -h_{eff} S_s (T_s - T_f) dz \quad (20)$$

With substitution of the dimensionless variables given in Eq. (6), to the above governing equation, there is

$$\frac{\partial \theta_s}{\partial t^*} = -\frac{H_{CR}}{\tau_r} (\theta_s - \theta_f) \quad (21)$$

$$H_{CR} = \frac{\rho_f C_f \varepsilon}{\rho_s C_s (1 - \varepsilon)} \quad (22)$$

The dimensionless form of governing equations allows a generalized solution to the problem, where the dimensionless parameter τ_r and H_{CR} determines the results of solutions [190].

3.2.4 Numerical solution using method of characteristics

The non-dimensional energy balance equations for heat transfer fluid and pipe wall can be solved numerically along the characteristics, as has been discussed in Ref. [12]. Equation (17) can be reduced along the characteristic line of $t^* = z^*$, so that,

$$\frac{D\theta_f}{Dt^*} = \frac{1}{\tau_r} (\theta_s - \theta_f) \quad (23)$$

Separating and integrating along the characteristic, we can get integral equation

$$\int d\theta_f = \int \frac{1}{\tau_r} (\theta_s - \theta_f) dt^* \quad (24)$$

Similarly, Eq.(11) for the energy balance of pipe wall is reposed along characteristic, $z^* = \text{constant}$, so that

$$\frac{d\theta_s}{dt^*} = -\frac{H_{CR}}{\tau_r}(\theta_s - \theta_f) \quad (25)$$

The solution for Eq.(15) is very similar to that for Eq.(13) but with an additional factor of H_{CR} . The term H_{CR} is simply a fractional ratio of fluid heat capacitance to rock heat capacitance. Therefore, the equation for solution of θ_s will have interrelation with θ_f , as the pipe wall material must have the capacity to store the energy being delivered to it, or vice versa. Finally, separating and integrating along the characteristic for Eq. (15), there is

$$\int d\theta_s = \int -\frac{H_{CR}}{\tau_r}(\theta_s - \theta_f)dt^* \quad (26)$$

There are now two characteristic equations bound to intersections of time and space. A discretized grid of points, laid over the time and space dimensions, will have nodes at these intersecting points, as shown in the diagram of a matrix in Fig.12 [186].

In space, there are $i = 1, 2, \dots, M$ nodes broken up into step sizes of Δz^* to span all of z^* . Similarly, in time, there are $j = 1, 2, \dots, N$ nodes broken up into time-steps of Δt^* to span all of Δt^* . Looking at a grid of the ϑ nodes, a clear picture of the solution can arise. To demonstrate a calculation of the solution we can look at a specific point in time, along z^* where there are two points, $\vartheta_{1,1}$ and $\vartheta_{2,1}$. These two points are the starting points of their respective characteristic waves described by Eq. (13) and (15). After the time Δt^* there is a third point $\vartheta_{2,2}$ which has been reached by both wave equations. Therefore, Eq. (14) can be definitely integrated numerically as:

$$\int_{\vartheta_{1,1}}^{\vartheta_{2,2}} d\theta_f = \int_{\vartheta_{1,1}}^{\vartheta_{2,2}} \frac{1}{\tau_r} (\theta_s - \theta_f) dt^* \quad (27)$$

The numerical integration of the right-hand side is performed via the trapezoidal rule and the solution is:

$$\theta_{f_{2,2}} - \theta_{f_{1,1}} = \frac{1}{\tau_r} \left(\frac{\theta_{s_{2,2}} + \theta_{s_{1,1}}}{2} - \frac{\theta_{f_{2,2}} + \theta_{f_{1,1}}}{2} \right) \Delta t^* \quad (28)$$

where $\theta_{f_{1,1}}$ is the value of θ_f at $\vartheta_{1,1}$, and $\theta_{f_{2,2}}$ is the value of θ_f at $\vartheta_{2,2}$, and similarly so for θ_s . The integration for Eq. (16) along $z^* = \text{constant}$ is

$$\int_{\vartheta_{2,1}}^{\vartheta_{2,2}} d\theta_s = \int_{\vartheta_{2,1}}^{\vartheta_{2,2}} -\frac{H_{CR}}{\tau_r} (\theta_s - \theta_f) dt^* \quad (29)$$

The numerical integration of the right-hand side is also performed via the trapezoidal rule and the solution is:

$$\theta_{s_{2,2}} - \theta_{s_{2,1}} = -\frac{H_{CR}}{\tau_r} \left(\frac{\theta_{s_{2,2}} + \theta_{s_{2,1}}}{2} - \frac{\theta_{f_{2,2}} + \theta_{f_{2,1}}}{2} \right) \Delta t^* \quad (30)$$

Equations (18) and (20) can be reposed as a group of algebraic equations for two unknowns of $\theta_{f_{2,2}}$ and $\theta_{s_{2,2}}$, while θ_f and θ_s at grid points $\vartheta_{1,1}$ and $\vartheta_{2,1}$ are known.

$$\begin{bmatrix} 1 + \frac{\Delta t^*}{2\tau_r} & -\frac{\Delta t^*}{2\tau_r} \\ -\frac{H_{CR}\Delta t^*}{2\tau_r} & 1 + \frac{H_{CR}\Delta t^*}{2\tau_r} \end{bmatrix} \begin{bmatrix} \theta_{f_{2,2}} \\ \theta_{s_{2,2}} \end{bmatrix} = \begin{bmatrix} \theta_{f_{1,1}} \left(1 - \frac{\Delta t^*}{2\tau_r}\right) + \theta_{s_{1,1}} \frac{\Delta t^*}{2\tau_r} \\ \theta_{f_{2,1}} \left(\frac{H_{CR}\Delta t^*}{2\tau_r}\right) + \theta_{s_{2,1}} \left(1 - \frac{H_{CR}\Delta t^*}{2\tau_r}\right) \end{bmatrix} \quad (31)$$

Since Eq. (21) is only for two linear equations, it can be easily solved. It is also important to note that all coefficients/terms in Eq. (21) are one-time determined from Δz^* , Δt^* , τ_r , H_{CR} . Therefore, the solution does not need heavy computations.

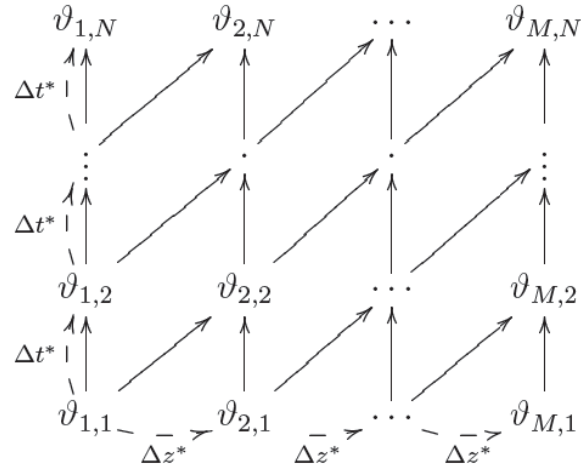


Fig. 12 Interception points of characteristics of Eq. (7) and (11)

From the grids (or interception point matrix) in Fig.3 it is seen that the temperatures of pipe wall and fluid at grids $\vartheta_{i,1}$ are the initial conditions. The temperatures of fluid and pipe wall at grids $\vartheta_{1,j}$ are the inlet conditions which vary with time. The inlet temperature for fluid versus time is given. The pipe wall temperature (as a function of time) at inlet can be easily obtained using Eq.(15), for which inlet fluid temperature is known. Now, as the conditions at $\vartheta_{1,1}$, $\vartheta_{1,2}$, and $\vartheta_{2,1}$ are known, the temperatures of pipe wall and fluid at $\vartheta_{2,2}$ will be easily calculated from Eq.(21).

Extending the above sample calculation to all points in the ϑ grid of time and space will give the entire matrix of solutions in time and space for both pipe wall and fluid. While the march of Δz^* steps is limited to $z^* = 1$ the march of time Δt^* has no limitation.

3.3 Results and discussion

The established analytical model is applied to the startup flow of hot molten chloride salt $MgCl_2-KCl-NaCl$ (wt% of 45.98–38.91–15.11) in a cold metal pipe. The freeze point of the molten salt is $401.4\text{ }^\circ\text{C}$. The study will consider the scenarios that the metal pipe is initially cold at different levels of low temperatures below the freeze point of the fluid, while the molten salt entering to the cold pipe has temperatures above the freeze point. In the computation, the length from the entrance where the fluid temperature is getting close to the molten salt freeze point will be identified as the critical length of the pipe that only beyond that the freeze of fluid may occur. The significance of this critical length is obvious that in the engineering application the flow pipe should be shorter than the critical length.

The physical properties of fluid and pipe are listed in Table 2 for reference. With these properties used, the results of computations are presented to understand the effects of various parameters on the critical length of the pipe, including fluid velocity u , pipe outer diameter D_o (at 0.0254 m) pipe wall thickness δ (at 2 mm), and initial pipe temperature T_1 .

The Pe number in this study ranges from 44121 to 829643, which satisfies the requirement of $Pe > 100$ to support the assumption that the heat conduction in the axial direction in the fluid is negligible. The character length for Pe number is the inner diameter of the pipe. The Bi number (based on tube wall thickness as the characteristic length) in this study ranges from 4.57×10^{-3} to 5.2×10^{-2} which is much smaller than 0.1. In fact, since the effective heat transfer coefficient h_{eff} is introduced in Eq. (8), the current model works irrespective of the value of Biot number.

Table 2 Key properties of molten salt fluid and metal pipe

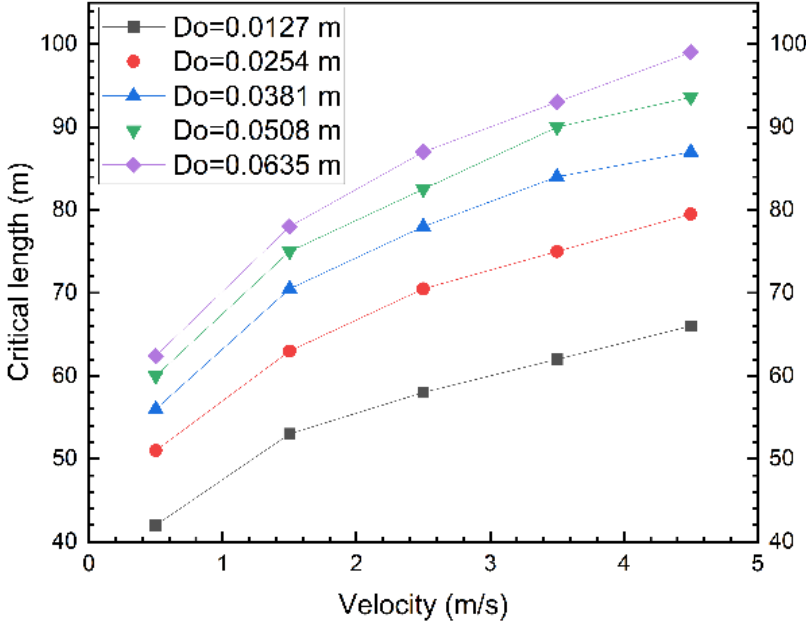
Parameters	Cp	ρ	T_{freeze}	k	μ
	J/(kg °C)	kg/m ³	°C	W/(m °C)	(Pa s)

Fluid (salt)	1090.4	1706.7	401.4	0.4724	3.79E-3
Pipe (metal)	460	8690	-	15.5	-

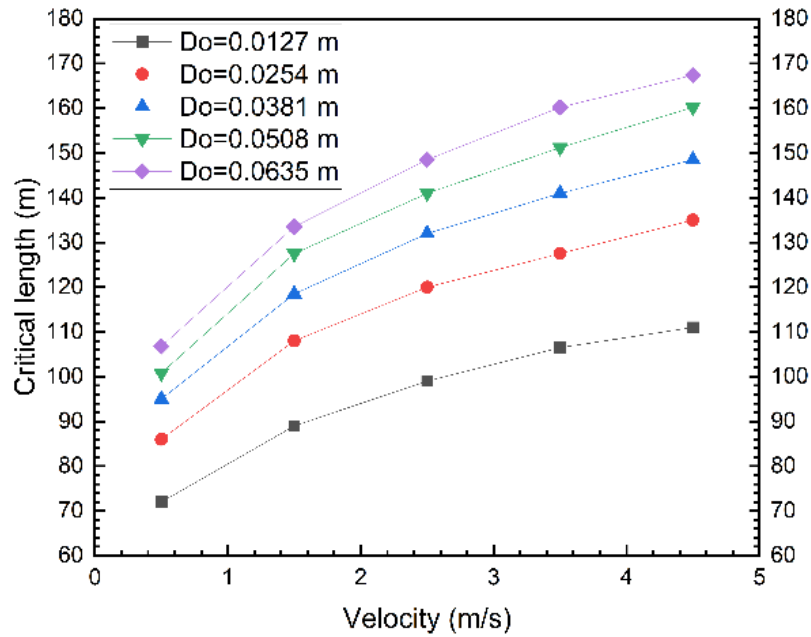
3.3.1 Effect of fluid velocity to the critical length

The higher velocity the fluid enters the pipe, there is more thermal energy carried into the pipe per unit time. This means that there is less possibility the fluid getting frozen due to the cold pipe. Correspondingly, the critical length of the pipe is longer for high flow velocity, as seen in Fig. 13 (a) and (b).

The Reynolds number corresponding to the velocities in Fig. 4 covers a range from 3500 to 1.21×10^5 . It is observed that the increase of fluid velocity at low range of velocities has more significant impact to the prolong of the critical length of the pipe. This also means that when the flow velocity of the hot fluid is too low, there is a high possibility of freeze of liquid in the entrance of pipe. Therefore, the flow velocity entering to the cold pipe should be sufficiently high to avoid freeze of the fluid. The obtained data for critical length of pipe is very important for the design of the molten salt flow system to avoid freeze problem.



(a) $T_l=300\text{ }^\circ\text{C}$



(b) $T_l=350\text{ }^\circ\text{C}$

Fig. 13 Variation of the critical length of pipe due to different flow velocity. $T_h=450\text{ }^\circ\text{C}$, pipe wall thickness=2mm.

3.3.2 Effect of pipe diameter to the critical length

The increase of pipe diameter means the increase of the cross-section flow area of fluid and thus the flow can bring in more hot fluid to the pipe per unit time. This makes the freeze of the fluid less possible. Therefore, the increase of pipe diameter will cause a longer critical length of the pipe, as shown in Fig. 14 (a) and (b). It is also observed that the increase of the critical length due to the increase of the pipe diameter is more significant at the low range of pipe diameter. Above a certain level, further increase of pipe diameter causes less increase of the critical length.

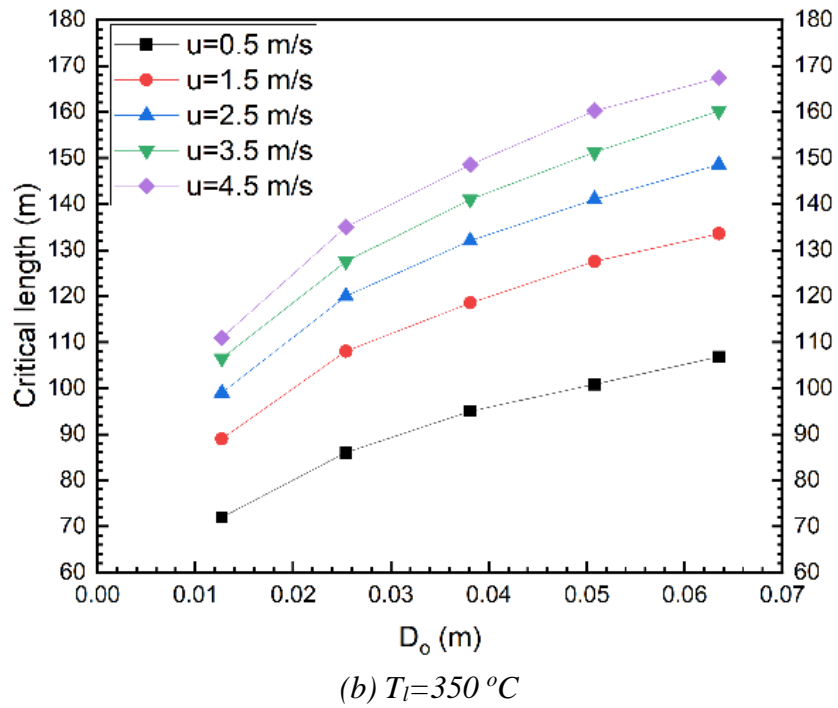
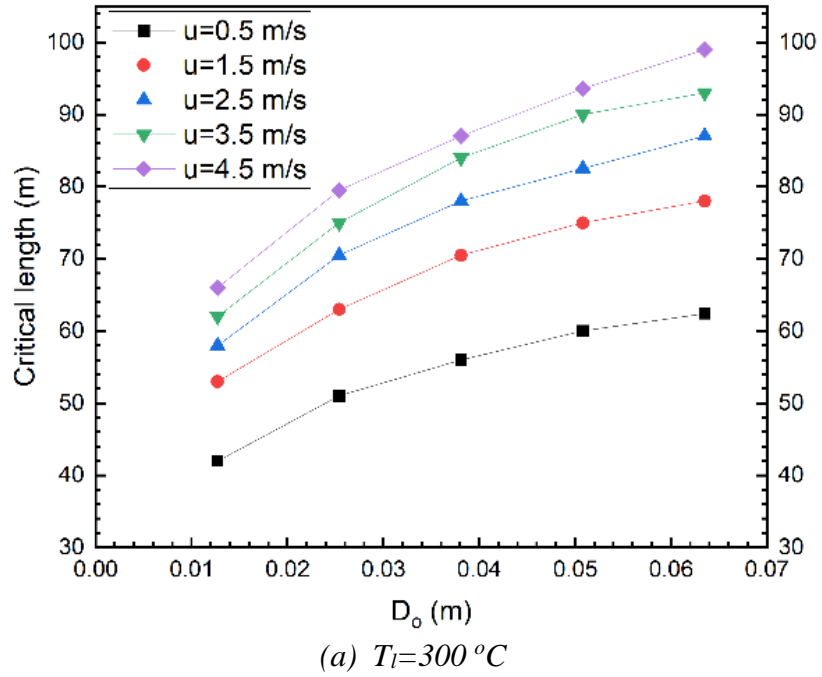


Fig. 14 Variation of the critical length of pipe due to different diameter of the pipe. $T_h=450\text{ }^\circ\text{C}$, pipe wall thickness=2mm.

3.3.3 Effect of pipe wall thickness to the critical length

A larger wall thickness of the cold pipe means more cold mass of metal material that can

absorb more heat and cause the hot fluid to freeze more. The critical length shows a linear decrease with the increase of the pipe wall thickness. In the current study, since the heat capacity of the pipe is rather lower than that of the molten salt, the increase of pipe wall thickness does not cause dramatic drop of the critical length. If the heat capacity of the solid material of the pipe is large, the increase of wall thickness will cause more significant shorter critical length.

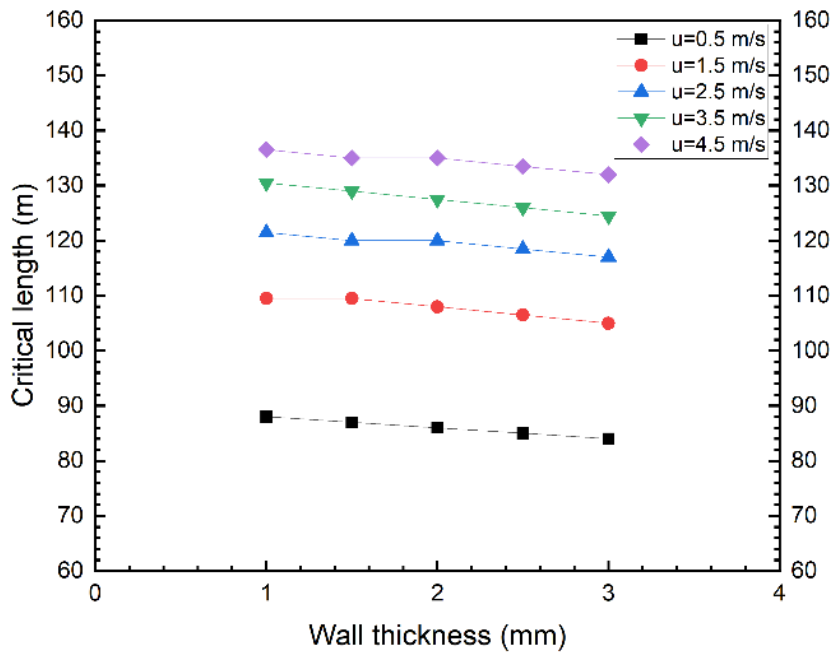


Fig. 15 Variation of the critical length of pipe due to different pipe wall thickness. $T_h=450$ °C, $T_l=350$ °C, $D_o=0.0254$ m.

3.3.4 Effect of pipe wall temperature to the critical length

The very important effect to the critical length before occurrence of freezing is the temperature of the cold pipe. When the temperature of cold pipe is higher, the critical length increases

significantly more than a linearity increase. This is an important scenario for reference in engineering application that warming up the cold pipe can have a significant effect to prevent the freeze of the fluid when it starts to flow into a cold pipe.

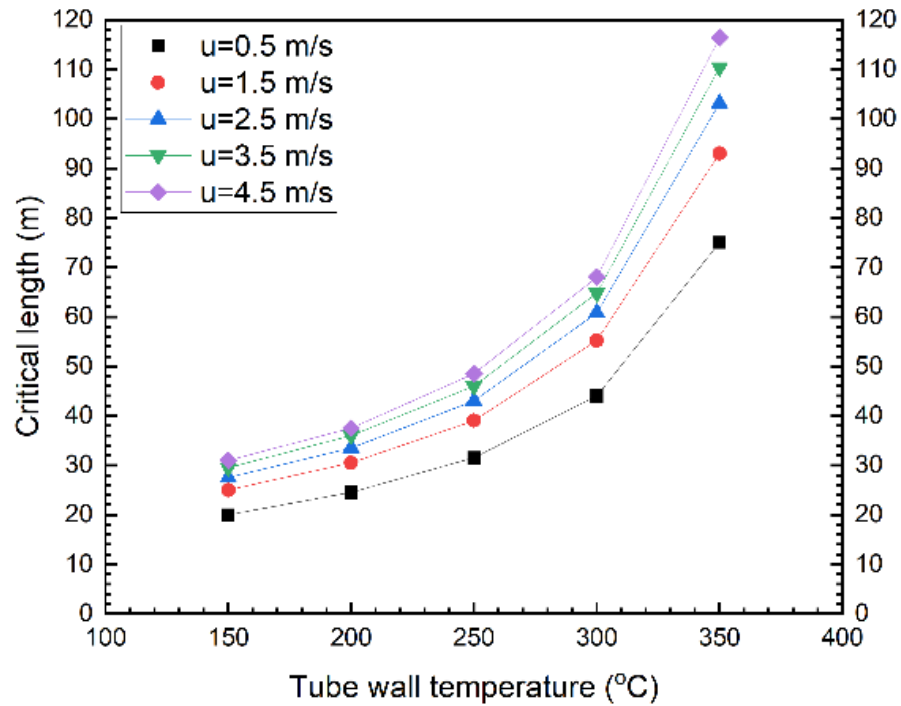


Fig. 16 The variation of critical length of pipe due to different pipe wall temperature. $T_h=450$ °C, $D_o=0.0127$ m, pipe wall thickness=1.0mm.

3.4 Conclusions

When hot molten salt flows into cold pipes, freeze of the salt will occur after a critical length, which is a scenario that must be avoided in the startup operation of a CSP or nuclear power plant that uses molten salt as heat transfer fluid. The current study carried out an analysis to the transient heat transfer phenomenon between the hot fluid and the cold pipe. The analysis fundamentally discovered that the critical length is affected by various parameters including: the heat capacity, density, and thermal conductivity of both the fluid and pipe, viscosity and flow

velocity of the fluid, the diameter and wall thickness of the pipe, as well as the temperature of the fluid entering the pipe and the temperature of the initially cold pipe. The analysis and computation allow one to find the critical length based on the above-mentioned parameters and thus adjustment may be made to avoid freeze of fluid at the cold startup operation.

The analytical solution was applied to a case of hot chloride molten salt NaCl-KCl-MgCl₂ flowing to a low temperature pipe made of Hastelloy C-22. The study has obtained a set of resultant data with the given parameters, from which several discoveries have been obtained:

1) The flow velocity of the fluid can significantly affect the critical length. At low velocity range, the increase of flow velocity makes more significant increase of the critical length. This also implies that a sufficiently high flow velocity of the hot fluid is very critical to avoid freeze of the fluid in the cold pipe.

2) The increase of pipe diameter is also very helpful to have a longer critical length of the pipe. It is easier to have freeze of molten salt in a small cold pipe and should be avoided.

3) The wall thickness of the pipe has linear effect on the critical length. With the increase of the wall thickness of the pipe, the critical length of the pipe will decrease. However, the decrease of the critical length due to the increase of wall thickness is not very large.

4) The temperature of the cold pipe has a significant effect on the critical length. When the initial pipe temperature is sufficiently high, the critical length can be significantly longer.

In overall, a high flow speed, larger pipe diameter, and higher initial pipe temperature will greatly help to reduce the potential of salt freeze in the startup operation.

CHAPTER 4 MODELING AND ANALYSIS OF ENTROPY PRODUCTION FOR SELECTION OF HTFS IN CSP SYSTEMS

4.1 Introduction

It is well known that a high temperature for solar thermal energy is desired for a concentrated solar thermal power (CSP) plant to have high energy conversion efficiency [90,91]. To obtain thermal energy at high temperatures, solar concentrators with high concentration ratio and a heat transfer fluid (HTF) being able to work at high temperatures are the two basic technical requirements [92,93]. Solar thermal concentrators with high concentration ratio provide high heat flux; while the heat transfer fluid is used to receive heat from the solar concentrator and then transfer the heat to another fluid (such as water, air, or super critical CO₂) which is the working substance in a thermal power cycle. Whereas the technology of concentrators with high solar concentration ratio has been developed in the current CSP industries, cost-effective and excellent heat transfer fluids for the working temperatures above 600 °C are still remaining to be found out [94].

So far, three generations of HTFs (other than air and water) have been developed particularly for the use in concentrated solar thermal power systems (CSP). The first generation HTF may be represented by the non-toxic petroleum-based oil (such as Xceltherm® 600—C₂₀ paraffin oil), which has an upper temperature limit of 315 °C [95,96]. The second-generation of HTFs are known as synthetic organic oils (such as Therminol®VP-1, a mixture of Diphenyl oxide and Biphenyl in weight percentage of 73.5% versus 26.5%), which has an upper temperature limit of 400 °C [97, 98] and a corresponding vapor pressure of 10 atm. To further improve the working temperature in a CSP system, the third generation HTF is based on nitrate molten salts [99] (having upper

temperature limit of of 580 °C), such as a mixture of sodium nitrate, sodium nitrite, and potassium nitrate (in mole fraction of 7%NaNO₃ - 49%NaNO₂ - 44%KNO₃)known as Hitec® salt [100, 101]. Recently, one of the great efforts sponsored by the U.S. Department of Energy for CSP technologies is the development of the fourth generation HTF to approach a temperature limit of 850 °C by using either eutectic high temperature molten salts [102, 103] or eutectic metal mixtures [104-106].

The requirement to the properties of a HTF used in a concentrated solar thermal is multifold. First and foremost, the fluid should be able to remain as a liquid fluid in a wide range of temperatures while having low vapor pressures. Second, the fluid must have low corrosion to the pipes and containers of the heat transfer system. Third, the fluid must have favorable properties, including density, thermal conductivity, heat capacity, and viscosity, so that in overall the exergy (or the useful heat) destruction of the received solar thermal energy is minimal during the flow and heat transfer processes in the heat transfer system. Last, but not least, the cost of the materials for the HTF should be sufficiently low to be acceptable by industrial customers. The analysis in this work will discuss the evaluation of transport properties of HTFs.

It is difficult to make a fair comparison between two heat transfer fluids by comparing individual transport properties. For example, one fluid may have higher thermal conductivity and higher viscosity than another fluid. While the high thermal conductivity contributes to better heat transfer, the high viscosity will contribute to larger pressure loss during the flow [156-158]. It is therefore necessary to find one criterion that can entail all the transport properties of a heat transfer fluid so that comparison of benefit or advantage between HTFs can be made possible.

It is easy to understand that the benefit or advantage of using one heat transfer fluid against another in a CSP plant should be found consequently from the generated electrical energy per

capital cost over the lifetime of a CSP power plant due to the use of the fluid and the associated materials of pipes and containers. This requires the evaluation of the thermal efficiency and exergy destruction in the heat transfer processes from solar concentrator to the working fluid of thermal power cycle so that the produced electrical energy from a given amount of concentrated solar thermal energy can be determined.

The entropy production in the heat transfer processes contributes to the exergy (useful energy) destruction, as well as the thermal energy efficiency of the power cycle [191]. The entropy production should include two parts, one from heat transfer processes and the other from the pressure loss due to friction of fluid in the flow circulation [192]. Therefore, the entropy production in the heat transfer system from using a HTF can be defined as a primary figure of merit (FOM) for a HTF. After heat transfer, the temperature of the heat for the thermal power plant is important, which can indicate the ideal value of the thermal efficiency for the power cycle. In the following work, theoretical analysis is conducted to the heat transfer system to find the entropy production.

4.2 Analysis of Entropy Production in Heat transfer System in a CSP Plant

The objective of the following analysis is to find the relationship of the system entropy production to all the relevant fluid properties at given conditions. The properties, including thermal conductivity, viscosity, density, and heat capacity, jointly determine the heat transfer, pressure loss and thus the entropy production.

As show in Fig. 1, the application of a HTF in a concentrated solar thermal power plant is associated to two heat transfer processes and the circulation of the HTF in the system. The system has heat addition to the HTF from the solar field (or solar concentrator), and after that the heat is removed (through a heat exchanger) and delivered to the working fluid in the thermal power cycle of the power plant.

Due to the demand of high temperature for the heat source in a power plant, one may define the desired fluid temperatures at inlet and outlet of the solar collection section as T_i and T_o , respectively. This gives the average temperature of the HTF as $(T_i + T_o)/2$ in the heat receiving solar collector. Correspondingly, after getting to the temperature of T_o from the solar collector, the HTF flows into the heat exchanger to deliver heat to the working fluid of the power cycle, which makes the HTF temperature going back to T_i . For the given amount of heat transfer rate, \dot{Q} , and the temperatures of T_i and T_o , a good HTF should render the heat transfer to be so accomplished that the wall temperature, T_{h-w} , in the solar collector should not be too high, and also the wall temperature, T_{l-w} , in the heat delivery heat exchanger should not be too low. In fact, T_{l-w} represents the temperature of the high-temperature heat reservoir of the thermal power cycle, which is critical to the overall energy efficiency of the CSP system. Furthermore, one also does not want to use too much of pumping power to achieve the goal of transferring the heat \dot{Q} from the solar collector to the working fluid of the power cycle.

It is assumed that the dimensions of pipes and heat exchangers in the system illustrated in Fig. 17 have been decided based on the properties of a known HTF and the demanded heat transfer rate \dot{Q} , which is the total thermal energy supply per unit of time for a CSP plant. The entropy production rates in such a system will be obtained for a HTF of interest.

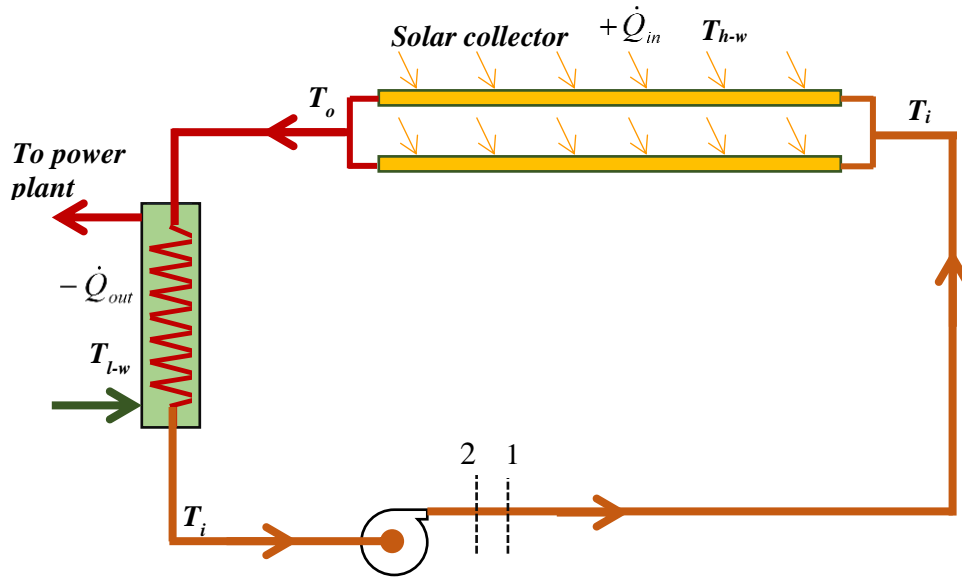


Figure 17. Flow loop that a HTF is used to transfer heat from solar collectors to the power plant

From the knowledge of second law analysis in thermodynamics, the steady state entropy production rate in the system (a control volume from location 1 to location 2 including the pipes and heat exchangers) should be expressed as:

$$s_2 \dot{m} = s_1 \dot{m} + \int_{\text{collector}} \frac{\delta \dot{Q}_{in}}{T_{h-w}} - \int_{\text{exchanger}} \frac{\delta \dot{Q}_{out}}{T_{l-w}} - \dot{m} \frac{v}{T_m} \Delta P + \dot{m} s_{gen} \quad (32)$$

where the system inlet is at location 1 and outlet is at location 2; T_{h-w} is the wall temperature of the heat source (concentrated solar energy) that is added to the system, and T_{l-w} is the wall temperature of heat exchanger that HTF gives out heat.

In order to conveniently observe how fluid properties affect the entropy production in the system, the heat transfer in the solar collector and the heat exchanger (in Fig. 17) is assumed to have uniform heat flux across the boundary walls. In fact, for solar heat collector and a countercurrent heat exchanger, this assumption is quite reasonable. Therefore, the integral terms

$\int_{collector} (1/T_{h-w}) \delta \dot{Q}_{in}$ and $\int_{exchanger} (1/T_{l-w}) \delta \dot{Q}_{out}$ in Eq. (1) can be simplified to ratios of the total heat rate

and the average temperatures of the walls, which give \dot{Q}_{in}/T_h and \dot{Q}_{out}/T_l . Here T_h and T_l are the average values respectively for T_{h-w} and T_{l-w} . The authors did a numerical test for the

accuracy of approximating the term $\int_{collector} (1/T_{h-w}) \delta \dot{Q}_{in}$ by \dot{Q}_{in}/T_h . For a linear variation of 300 K

for the wall temperature from inlet to outlet and an inlet wall temperature above 400 °C (673K)

the deviation of \dot{Q}_{in}/T_h from $\int_{collector} (1/T_{h-w}) \delta \dot{Q}_{in}$ is below 1.5% or even smaller for higher wall

temperatures and smaller temperature difference between inlet and outlet. With such a sufficient

accuracy, the analysis hereafter will use \dot{Q}_{in}/T_h to replace $\int_{collector} (1/T_{h-w}) \delta \dot{Q}_{in}$ and \dot{Q}_{out}/T_l to

replace $\int_{exchanger} (1/T_{l-w}) \delta \dot{Q}_{out}$.

Since the HTF circulates in the system, we can choose point 1 and 2 to be the same point, meaning the fluid circulated from a starting point and back to the starting point. Therefore, there

must have $s_2\dot{m} = s_1\dot{m}$, which results in the following expression for the system entropy production rate:

$$\dot{m}s_{gen} = \dot{S}_{gen} = \frac{\dot{Q}_{out}}{T_l} - \frac{\dot{Q}_{in}}{T_h} + \dot{m} \frac{v}{T_m} \Delta P = \frac{\dot{Q}_{out}}{T_l} - \frac{\dot{Q}_{in}}{T_h} + \frac{\dot{V}}{T_m} \Delta P \quad (33)$$

where \dot{S}_{gen} is the system entropy production in a steady state operation, \dot{V} is the volume flow rate of the HTF; \dot{Q}_{in} and \dot{Q}_{out} are the absolute values of the heat rates added to and delivered out of the system, respectively. It is clear to see from Eq. (33) that the entropy production is due to the two heat transfer processes and the pressure loss in the system, which needs the pump to overcome. Ideally, the heat added into the system and removed from the system have the same absolute value. For convenience, we give $\dot{Q}_{out} = \dot{Q}_{in} = \dot{Q}$ in the analyses hereafter.

The fluid temperature at the inlet and outlet of the solar collection field is defined as T_i and T_o , respectively. When considering the heat removal in the heat exchanger to deliver the heat to the fluid in the thermal power cycle, the temperature of the HTF at the inlet and exit becomes T_o and T_i , respectively. The average temperatures of the HTF in the solar collection field and the heat exchanger are the same as $T_m = 0.5(T_o + T_i)$. The average temperature of the HTF in the circulation pipes should also be $T_m = 0.5(T_o + T_i)$. The temperature differences that drive the heat exchange in the solar collection field and in the heat exchanger are $T_h - 0.5(T_o + T_i)$ and $0.5(T_o + T_i) - T_l$, respectively.

Considering the heat transfer processes in the solar collection field and in the heat exchanger, there are:

$$\dot{Q} = A_h h_h [T_h - 0.5(T_o + T_i)] \quad (34)$$

$$\dot{Q} = A_l h_l [0.5(T_o + T_i) - T_l] \quad (35)$$

where A_h and A_l are heat transfer surface areas; h_h and h_l are heat transfer coefficients. From these two equations, we can find that,

$$T_h = \frac{\dot{Q}}{A_h h_h} + 0.5(T_o + T_i) \quad (36)$$

$$T_l = 0.5(T_o + T_i) - \frac{\dot{Q}}{A_l h_l} \quad (37)$$

Substitute Eqs. (36) and (37) into Eq. (33), the system entropy production rate is obtained as,

$$\dot{S}_{gen} = \frac{\dot{Q}}{0.5(T_o + T_i) - \dot{Q}/(A_l h_l)} - \frac{\dot{Q}}{0.5(T_o + T_i) + \dot{Q}/(A_h h_h)} + \frac{\dot{V}}{0.5(T_o + T_i)} \Delta P \quad (38)$$

For the purpose of evaluating the transport properties of a HTF, this analysis needs to give the demanded heat rate \dot{Q} , the desired temperatures of T_i and T_o . The flow rates of HTF can be decided as,

$$\dot{Q} = \dot{m} C_p (T_o - T_i) \quad (39)$$

$$\dot{m} = \dot{V} \rho \quad (40)$$

$$\dot{V} = \frac{\dot{Q}}{\rho C_p (T_o - T_i)} \quad (41)$$

Substitute Eq. (41) into Eq. (38), the entropy production rate is further expressed as

$$\dot{S}_{gen} = \frac{\dot{Q}}{0.5(T_o + T_i) - \dot{Q}/(A_l h_l)} - \frac{\dot{Q}}{0.5(T_o + T_i) + \dot{Q}/(A_h h_h)} + \frac{\dot{Q}}{0.5\rho C_p(T_o + T_i)(T_o - T_i)} \Delta P \quad (42)$$

where the first two terms are due to heat transfer processes, which is defined as \dot{S}_{gen-ht} , and the last term is due to pressure loss when the HTF circulates in the system (including in heat exchangers and in circulation pipes), which may be defined as \dot{S}_{gen-fl} .

From Eq. (42), it is understandable that a large value of h_l and h_h will result in less entropy production, while the pressure loss ΔP will contribute to higher entropy production. Furthermore, it is also easy to understand that if the heat transfer is improved (either due to surface enhancement or better properties of HTF), the entire heat transfer task can be achieved with the temperature T_l closer to T_h , which therefore is beneficial to the thermal energy efficiency in the thermal power plant. The pressure loss in the entire system includes the losses from two heat exchangers and from fluid circulation pipes, which may be defined as ΔP_{HE-h} , ΔP_{HE-l} , and ΔP_c , respectively. With the volume flow rate of the HTF available from Eq. (41), the pressure losses in the system can be conveniently obtained.

In the next section, the heat transfer coefficients, h_h and h_l , will be expressed in terms of the fluid properties, the prescribed temperatures, as well as the heat rate which determines the flow rate and velocities of the fluid in given devices.

4.2.1 Entropy production in heat transfer processes

4.2.1.1 Heat transfer due to turbulent flow

For the heat transfer of turbulent flow in pipes with Reynolds number (Re) close to 1.0×10^4 or above, $0.7 \leq \text{Pr} \leq 160$, and length-to-diameter ratio $L/d \geq 10$, we take the famous Dittus-Boelter equation [193] to obtain heat transfer coefficients as follows:

$$Nu_h = \frac{h_h d_h}{k} = 0.023 \text{Re}_h^{0.8} \text{Pr}^{0.4} \quad (\text{fluid is heated}) \quad (43)$$

$$Nu_l = \frac{h_l d_l}{k} = 0.023 \text{Re}_l^{0.8} \text{Pr}^{0.3} \quad (\text{fluid is cooled}) \quad (44)$$

Assume the heat transfer design analysis already found the number (n) of tubes (in diameter of d) for the heat exchanger. The flow velocity in the tubes of a heat exchanger can be obtained as:

$$u = \frac{\dot{V}}{n(0.25\pi d^2)} = \frac{\dot{Q}}{\rho C_p (T_o - T_i) n(0.25\pi d^2)} = \frac{\dot{Q}}{\rho C_p (T_o - T_i) N d^2} \quad (45)$$

where we define $N = 0.25n\pi$. Using Eq. (45), the Reynolds number for the flow in the heat transfer tubes is obtained as

$$\text{Re} = \frac{\dot{Q}}{\rho C_p (T_o - T_i) N d^2} \frac{\rho d}{\mu} = \frac{\dot{Q}}{C_p (T_o - T_i) N \cdot d \cdot \mu} \quad (46)$$

Bring the expression for Reynolds numbers into Eqs. (43) and (44), the heat transfer coefficients are obtained as follows:

$$h_h = \frac{k}{d_h} 0.023 \left[\frac{\dot{Q}}{\rho C_p (T_o - T_i) N_h d_h^2} \frac{\rho d_h}{\mu} \right]^{0.8} \left(\frac{\mu C_p}{k} \right)^{0.4} = 0.023 \left[\frac{\dot{Q}}{N_h (T_o - T_i)} \right]^{0.8} \frac{1}{d_h^{1.8}} \frac{k^{0.6}}{C_p^{0.4} \mu^{0.4}} \quad (47)$$

$$h_l = \frac{k}{d_l} 0.023 \left[\frac{\dot{Q}}{\rho C_p (T_o - T_i) N_l d_l^2} \frac{\rho d_l}{\mu} \right]^{0.8} \left(\frac{\mu C_p}{k} \right)^{0.3} = 0.023 \left[\frac{\dot{Q}}{N_l (T_o - T_i)} \right]^{0.8} \frac{1}{d_l^{1.8}} \frac{k^{0.7}}{C_p^{0.5} \mu^{0.5}} \quad (48)$$

Substituting Eqs. (47) and (48) into Eq. (42), the entropy generation due to heat transfer in the system is

$$\begin{aligned} \dot{S}_{gen-ht}^{Turbulent} &= \frac{\dot{Q}}{0.5(T_o + T_i) - \frac{\dot{Q}}{4N_l^{0.2} L_l} \frac{1}{0.023} \left[\frac{(T_o - T_i)}{\dot{Q}} \right]^{0.8} \frac{d_l^{0.8} C_p^{0.5} \mu^{0.5}}{k^{0.7}}} \\ &\quad - \frac{\dot{Q}}{0.5(T_o + T_i) + \frac{\dot{Q}}{4N_h^{0.2} L_h} \frac{1}{0.023} \left[\frac{(T_o - T_i)}{\dot{Q}} \right]^{0.8} \frac{d_h^{0.8} C_p^{0.4} \mu^{0.4}}{k^{0.6}}} \end{aligned} \quad (49)$$

It is worth noting that we can choose equations of dimensionless parameters of Nu against Re and Pr from several correlations [193, 194], which are widely accepted in heat transfer society with comparable accuracy. The authors chose Dittus-Boelter correlation [193] for the convenience that the effect or impact of the transport properties to the entropy generation in the heat transfer process can be more explicitly seen in Eq. (49). For slightly better accuracy for heat transfer coefficient when Reynolds number is high up to 5.0×10^6 a correlation such as Gnielinski equation [193, 194] may be used for the above analysis. Nevertheless, selection of the heat transfer correlations will not change the basic conclusion of the relative comparison of FOM of different heat transfer fluids

in respect to the system entropy production determined from the transport properties of the fluids, as long as the selected correlation is used consistently for every fluid.

4.2.1.2 Heat transfer due to laminar flow

For laminar flow in heat exchangers, the Nusselt number for a constant wall heat flux case is a constant (which gives $Nu_h=Nu_l=4.36$) [193, 195]. Therefore, the heat transfer coefficient is obtained to be $h = 4.36 \cdot k/d$. This allows us to calculate the entropy production due to laminar flow heat transfer in the form of:

$$\dot{S}_{gen-ht}^{Laminar} = \frac{\dot{Q}}{0.5(T_o + T_i) - \frac{\dot{Q}}{4.36k4N_hL_h}} - \frac{\dot{Q}}{0.5(T_o + T_i) + \frac{\dot{Q}}{4.36k4N_lL_l}} \quad (50)$$

4.2.2 Entropy production rate due to pressure losses

4.2.2.1 Flow with $2300 \leq Re \leq 2 \times 10^4$

The following equation [193] is chosen to calculate the pressure loss due to turbulent flow in the heat transfer tubes in heat exchangers.

$$\Delta P_{HE} = \frac{f \cdot \rho u^2 L}{2d} \quad (51)$$

where f is Darcy friction factor. Taking Blasius equation ($f = 4 * 0.079 Re^{-0.25}$) for Darcy friction factor, the pressure drop is obtained as:

$$\Delta P_{HE} = 0.079 \frac{2 \cdot \rho u^2 L}{d} \left(\frac{ud\rho}{\mu} \right)^{-0.25} = 0.158 \frac{\rho^{0.75} u^{1.75} L \mu^{0.25}}{d^{1.25}} \quad (52)$$

where L is the length of the tubes subject to study. Substituting velocity u (by Eq. (45)) into Eq. (52), there is

$$\Delta P_{HE} = 0.158 \frac{\rho^{0.75} L \mu^{0.25}}{d^{1.25}} \left[\frac{\dot{Q}}{\rho C_p (T_o - T_i) N d^2} \right]^{1.75} = 0.158 \frac{L \mu^{0.25}}{\rho C_p^{1.75} d^{4.75}} \left[\frac{\dot{Q}}{(T_o - T_i) N} \right]^{1.75} \quad (53)$$

For the pressure loss in the fluid circulation pipes (in a total length of L_c and pipe diameter of d_c), the same expression of pressure loss is

$$\Delta P_c = 0.158 \frac{\rho^{0.75} L_c \mu^{0.25}}{d_c^{1.25}} \left[\frac{\dot{Q}}{\rho C_p (T_o - T_i) N_c d_c^2} \right]^{1.75} = 0.158 \frac{L_c \mu^{0.25}}{\rho C_p^{1.75} d_c^{4.75}} \left[\frac{\dot{Q}}{(T_o - T_i) N_c} \right]^{1.75} \quad (54)$$

where N_c is definition as $N_c = 0.25 n_c \pi$, and n_c is the number of pipes that are used to circulate the fluid.

The total system pressure drop includes three parts, from fluid circulation pipes, as well as from the heat exchangers (one has heat added to the HTF, and the other has heat removed from the HTF). Therefore, the total pressure drops in heat exchangers and in the circulation pipe is

$$\Delta P = \Delta P_{HE-h} + \Delta P_{HE-l} + \Delta P_c \quad (55)$$

Substituting pressure losses into the third term in Eq. (42), the entropy production rate due to pressure loss is

$$\dot{S}_{gen-fl}^{T-1} = \frac{\dot{Q}}{0.5(T_o + T_i)(T_o - T_i)} \frac{0.158 \mu^{0.25}}{\rho^2 Cp^{2.75}} \left[\frac{\dot{Q}}{(T_o - T_i)} \right]^{1.75} \left(\frac{L_h}{d_h^{4.75} N_h^{1.75}} + \frac{L_l}{d_l^{4.75} N_l^{1.75}} + \frac{L_c}{d_c^{4.75} N_c^{1.75}} \right) \quad (56)$$

where \dot{S}_{gen-fl}^{T-1} designates the first case of turbulent flow, which has $2300 \leq Re \leq 2 \times 10^4$.

4.2.2.2 Flow with $Re \geq 2 \times 10^4$

Under the condition of $Re \geq 2 \times 10^4$, the equation for pressure loss of turbulent flow in the heat transfer tubes of heat exchangers is

$$\Delta P_{HE} = 0.184 \frac{\rho u^2 L}{2d} \left(\frac{ud\rho}{\mu} \right)^{-0.2} = 0.092 \frac{\rho^{0.8} u^{1.8} L \mu^{0.2}}{d^{1.2}} \quad (57)$$

Bring the expression of velocity given in Eq. (45) into the above expression, there is

$$\Delta P_{HE} = 0.092 \frac{\rho^{0.8} L \mu^{0.2}}{d^{1.2}} \left[\frac{\dot{Q}}{\rho Cp (T_o - T_i) N d^2} \right]^{1.8} = 0.092 \frac{L \mu^{0.2}}{\rho Cp^{1.8} d^{4.8}} \left[\frac{\dot{Q}}{(T_o - T_i) N} \right]^{1.8} \quad (58)$$

Similarly, the pressure drop in a circulation pipe with $Re \geq 2 \times 10^4$ is

$$\Delta P_c = 0.092 \frac{\rho^{0.8} L_c \mu^{0.2}}{d_c^{1.2}} \left[\frac{\dot{Q}}{\rho Cp (T_o - T_i) N_c d_c^2} \right]^{1.8} = 0.092 \frac{L_c \mu^{0.2}}{\rho Cp^{1.8} d_c^{4.8}} \left[\frac{\dot{Q}}{(T_o - T_i) N_c} \right]^{1.8} \quad (59)$$

In case that the Reynolds numbers of the flow in heat exchangers and in HTF circulation pipes are all larger than 2×10^4 , the entropy production rate due to all pressure losses is

$$\dot{S}_{gen-fl}^{T-2} = \frac{\dot{Q}}{0.5(T_o + T_i)(T_o - T_i)} \frac{0.092 \mu^{0.2}}{\rho^2 C_p^{2.8}} \left[\frac{\dot{Q}}{(T_o - T_i)} \right]^{1.8} \left(\frac{L_h}{d_h^{4.8} N_h^{1.8}} + \frac{L_l}{d_l^{4.8} N_l^{1.8}} + \frac{L_c}{d_c^{4.8} N_c^{1.8}} \right) \quad (60)$$

where \dot{S}_{gen-fl}^{T-2} designates the second case of turbulent flow when $Re \geq 2 \times 10^4$.

It is worth noting that equations for Darcy friction factor of turbulent flow with slightly better accuracy, such as developed by Petukhov [193, 196], may be used to calculate the pressure loss. However, the above Blasius equation results in rather explicit expression of the entropy production as a function of transport properties, which is helpful for us to directly observe the effects of fluid properties to the entropy production due to frictional loss. It is true and important that both Blasius equation [193] and Petukhov equation [193, 196] are widely accepted in the society of fluid mechanics for sufficient accuracy. The selection of these correlations will not change the basic conclusion of the comparison of the entropy production in different fluids, as long as the selected correlation is used consistently for every fluid.

4.2.2.3 With laminar flow in heat exchangers and circulation pipes

Although the flow of HTF in a solar thermal power plant can rarely be laminar, to include all possibilities, an analysis is still provided here. The Darcy friction factor for laminar flow [193] is $f = 64/Re$. Bring the expression of velocity into the Reynolds number, the pressure losses in the tubes of heat exchanger and in a circulation tube are given as follows, respectively.

$$\Delta P_{HE} = \frac{\rho u^2 L}{2d} \cdot 64 \cdot \left(\frac{ud\rho}{\mu} \right)^{-1} = 32 \frac{L\mu}{d^2} \frac{\dot{Q}}{\rho C_p (T_o - T_i) N d^2} \quad (61)$$

$$\Delta P_c = \frac{\rho u_c^2 L_c}{2d_c} \cdot 64 \cdot \left(\frac{u_c d_c \rho}{\mu} \right)^{-1} = 32 \frac{L_c \mu}{d_c^2} \frac{\dot{Q}}{\rho C_p (T_o - T_i) N_c d_c^2} \quad (62)$$

If all flows are laminar, the entropy production rate due to all pressure losses in heat exchangers and circulation tubes can be expressed as:

$$\dot{S}_{gen-fl}^L = \frac{\dot{Q}}{0.5(T_o + T_i)(T_o - T_i)} \frac{32\mu}{\rho^2 C_p^2} \left[\frac{\dot{Q}}{(T_o - T_i)} \right] \left(\frac{L_h}{d_h^4 N_h} + \frac{L_l}{d_l^4 N_l} + \frac{L_c}{d_c^4 N_c} \right) \quad (63)$$

4.2.2.4 Different Reynolds numbers in different devices

It needs to be noted that the Reynolds number of the flow in heat exchangers and in HTF circulation tube can be different depending on the flow rate and designs of the devices. One has to check the Reynolds numbers in each device and choose the proper terms from Eq. (56), Eq. (60), and Eq.(63) accordingly to calculate the total entropy generation rate due to pressure losses. Similarly, one also needs to check the Reynolds number of the flow in the heat transfer pipes in solar collector and heat exchanger in order to select the proper equations for heat transfer from Eqs. (49) and (50).

4.3 Discussion and Evaluation of Several Heat Transfer Fluids

4.3.1 Applications of the analysis for various heat transport systems

Evaluation of the heat transfer fluid properties is one of the applications of the present analysis. The model can also be generally used to evaluate the performance of heat transport systems. It is important to note that all the analyses need to set a target/goal of heat transfer rate \dot{Q} and

prescribed conditions of temperatures of T_i , T_o . Under these conditions, different heat transport systems can be designed, and system entropy production can be compared for evaluation of the merit.

For the merit evaluation about the transport properties of HTF, the prescribed parameters are the required heat transfer rate \dot{Q} for the system, the desired working temperatures of fluid, T_i , T_o , and dimensions of the devices including d_h , d_l , d_c , L_h , L_l , L_c , n_h , n_l , and n_c . These dimensions must be obtained through a preliminary design of the heat exchangers and the entire system, which is based on constrains of given diameters of the heat transfer tubes, tube materials, and the desired temperatures of fluid T_i and T_o . With the conditions of \dot{Q} , T_i , T_o , and dimensions keeping the same, different transport properties of HTFs will result in different system entropy production and thus the merit of the fluid properties is evaluated.

4.3.2 Cluster of properties contributing to entropy production

For heat transfer of turbulent flow, it is interesting to examine Eq. (49) that the clusters of properties $d_i^{0.8} C_p^{0.5} \mu^{0.5} / k^{0.7}$ and $d_h^{0.8} C_p^{0.4} \mu^{0.4} / k^{0.6}$ actually influence the entropy production in the heat transfer processes. For heat transfer of laminar flow, the cluster of properties contributing to entropy production in the heat transfer processes is $1/k$. Large values of these clusters of properties will result in lager entropy production in the system.

For the entropy production due to pressure loss in the heat exchangers and in the circulation pipe, the property clusters are $\mu^{0.25} / (\rho^2 C_p^{2.75} d^{4.75})$ and $\mu^{0.2} / (\rho^2 C_p^{2.8} d^{4.8})$ for turbulent flow with Reynolds number less than 2×10^4 , and larger than 2×10^4 , respectively. For laminar flow the cluster of properties to entropy production due to pressure loss is $\mu / (\rho^2 C_p^2 d^4)$. Large values of these cluster

of properties will result in large entropy production in the system. The clusters of HTF properties contributing to larger entropy generation due to heat transfer and pressure drop are summarized in Table 3.

In case one wants to use other heat transfer correlations such like Gnielinski equation [194] for the entropy generation analysis, Equation (42) should be directly used, where the heat transfer coefficient is obtained from the heat transfer correlations.

It is important to note that a large viscosity always contribute to a large entropy production either from heat transfer or from pressure loss. A high thermal conductivity contributes to a less entropy production in heat transfer process. However, the effect of fluid heat capacity to the entropy production in heat transfer processes is interesting to examine. From Eq. (49), it seems that C_p has a positive effect to the entropy production. On the other hand, because of large heat capacity, the heat transfer task can be achieved with less mass flow, which means that smaller flow tubes may be used. This is seen in the cluster of properties, $d_i^{0.8} C_p^{0.5} \mu^{0.5} / k^{0.7}$, where for large C_p the tube diameter d_i may be reduced.

Generally, the pressure loss causes a relatively less proportion of the total entropy production. However, it is still important to calculate the total entropy production from both heat transfer and pressure loss to evaluate the merit of a HTF.

Table 3 Clusters of properties contributing entropy production in the system

Heat transfer		Pressure drop	
Fluid is heated	Fluid is cooled		
$Re \geq 1 \times 10^4 :$ $d_h^{0.8} C_p^{0.4} \mu^{0.4} / k^{0.6}$	$Re \geq 1 \times 10^4 :$ $d_i^{0.8} C_p^{0.5} \mu^{0.5} / k^{0.7}$	$Re \leq 2 \times 10^4 :$ $\mu^{0.25} / (\rho^2 C_p^{2.75} d^{4.75})$	$Re \geq 2 \times 10^4 :$ $\mu^{0.2} / (\rho^2 C_p^{2.8} d^{4.8})$
$Re \leq 2300 :$ $1/k$	$Re \leq 2300 :$ $1/k$	$Re \leq 2300 :$ $\mu / (\rho^2 C_p^2 d^4)$	

4.3.3 Examples of entropy production rate due to different HTFs for heat transport tasks

As has been mentioned before, the system entropy production rate is viewed as the FOM for a HTF. To show a comparison of the FOM of different HTFs, analysis was conducted to a system that transport thermal energy of several selected values from 50 MW_{th} to 600 MW_{th} from a solar concentrator to the working substance in the power plant. The following cases of given conditions of temperatures and HTFs are selected for the study.

(1) The average working temperature T_m is 200 °C with T_i and T_o being 150 °C and 250 °C, respectively. Three HTFs, Xceltherm-600 , Therminol VP-1 , and Lead-Bismuth Eutectic (LBE) liquid metal alloy [198] are compared.

(2) The average working temperature T_m is 340 °C with T_i and T_o being 290 °C and 390 °C, respectively. Comparison is made between HTFs of Therminol VP-1 , nitrate molten salt (KNO₃-NaNO₂-NaNO₃) , and Lead-Bismuth Eutectic (LBE) liquid metal alloy [198].

(3) The average working temperature T_m is 450 °C with T_i and T_o being 400 °C and 500 °C, respectively. Comparison is made between HTFs of nitrate molten salt (KNO₃-NaNO₂-NaNO₃) , halide molten salt (NaCl-KCl-ZnCl₂) [197], and Lead-Bismuth Eutectic (LBE) liquid metal alloy [198].

(4) The average working temperature T_m is 700°C, and T_i and T_o are 650 °C and 750 °C, respectively. Entropy production rate using halide molten salt (NaCl-KCl-ZnCl₂) [197] and Lead-Bismuth Eutectic (LBE) liquid metal alloy [198] is studied. Targeted properties for a HTF at such a high level of temperature set by U.S. DOE are also used to calculate the entropy production for comparison [197].

For the task of transporting 50 MW_{th} using the system, the calculated results of entropy production and the Carnot efficiency ($\eta = 1 - 300(K)/T_i(K)$) based on the temperatures (T_i) of the heat delivered to the power cycle for all the above cases are listed in Tables 4 to 7. The corresponding conditions of temperature, the property of the fluids, and the dimensions of the heat exchangers are also given in the tables. The properties for the Lead-Bismuth Eutectic (LBE) liquid metal alloy are separately given in Table 8. For this analysis, the authors tested the use of Dittus-Boelter correlation [193] and Gnielinski equation [194] for heat transfer coefficient, and Blasius equation [193] and Petukhov equation [193, 196] for Darcy friction factors, respectively. The conclusion of the relative comparison of the system entropy production (as the FOM) of different fluids did not change by the use of the correlations, as long as the selected pair of equations are consistently used for every fluid.

The results of entropy production using Dittus-Boelter correlation and Blasius equation are provided in Tables 4-7. For slightly better accuracy, entropy production calculated using Gnielinski equation [194] for Nu and Petukhov equation [196] for Darcy friction factor are provided in the parenthesis in the tables. These results of entropy production rates are plotted in Fig. 18 for comparison.

As seen in Fig. 18, the heat transfer system at low temperature level has high entropy generation rate. Importantly, comparison of the entropy generation rate between every three different HTFs at the same operating temperature of $(T_i + T_o)/2$ shows us which HTF has better performance. Obviously, Therminol VP-1 is better than the earliest HTF, Xceltherm-600, at working temperature of $T_m = 200$ °C (473K) level; while Lead-Bismuth Eutectic (LBE) liquid metal alloy could have the lowest entropy production. When working at temperature level of $T_m = 340$ °C (613K), Therminol VP-1 and nitrate molten salts show very close entropy production, and Lead-

Bismuth Eutectic (LBE) liquid metal alloy could have the lowest entropy production. Going to a higher temperature of $T_m=450\text{ }^\circ\text{C}$ (723K), nitrate molten salt and halide molten salt are compared. Because of the lower thermal conductivity, the halide molten salt has higher entropy production, whereas the Lead-Bismuth Eutectic (LBE) liquid metal alloy has the lowest entropy production. When the operating temperature is at $T_m=700\text{ }^\circ\text{C}$ (973K) level, the entropy production with the use of the molten halide salt reaches a low level. Again Lead-Bismuth Eutectic (LBE) liquid metal alloy results in even lower entropy production than the molten salt. When those HTF except metal alloy are compared, the molten halide salt at working temperature of $T_m=700\text{ }^\circ\text{C}$ (973K) makes the lowest entropy generation. This clearly shows the benefit of operating the heat transfer system at higher temperatures using the halide molten salt. Nevertheless, if Lead-Bismuth Eutectic (LBE) liquid metal alloy is used, it gives the lowest entropy production at all working temperatures compared to other HTFs.

The analysis can also be employed to study and predict the gain for reduction of entropy generation if one can improve or change some properties of a HTF through adding additives or other measures. For example, in Table 9, targeted better properties of thermal conductivity and heat capacity for halide salt HTF were evaluated to indicate how much gain is possible regarding the reduction of entropy generation rate. This result is also given in Fig. 18 at $T_m=700\text{ }^\circ\text{C}$ (973K).

Table 4 Properties of HTFs at average temperature of 200 °C and the results of entropy production rate

	Xceltherm-600 at 200°C [7]	Therminol VP-1 200°C [9]	Lead-Bismuth Eutectic (LBE) [15, 16, 28]
ρ kg/m ³	743.2	913	Eq. in Table 6.
μ m Pa s	0.623	0.395	Eq. in Table 6.
k W/m-K	0.1216	0.114	Eq. in Table 6.
C_p kJ/kg-K	2.61	2.048	Eq. in Table 6.
T_h K	573 (564)	552 (541)	(485) Eq. in Table 6 for Nu
T_l K	373 (382)	399 (405)	(461) Eq. in Table 6 for Nu
\dot{S}_{gen} J/(K-s)	46793 (42212)	34872 (30869)	(5432) Eq. in Table 6 for Nu
$\eta = 1 - 300 / T_l (K)$	0.196 (0.215)	0.247 (0.260)	(0.349) Eq. in Table 6 for Nu
$T_i=423$ K; $T_o=523$ K; $d_i=d_h=0.02$ m; $n_i=n_h=820$; $L_h=7.7$ m; $L_l=7.7$ m; $d_c=0.5$ m; $n_c=4$; $L_c=200$ m			

Note: Results in parenthesis is based on Gnielinski equation for Nu [194], or otherwise specified, and Petukhov equation for Darcy friction factor[196]. This is the same for the results in the parenthesis in Table 3-5.

Table 5 Properties of HTFs at average temperature of 340 °C and the results of entropy production rate

	Therminol VP-1 340°C [9]	KNO ₃ -NaNO ₂ -NaNO ₃ (7-49-44 %mole) 340°C [10]	Lead-bismuth Eutectic (LBE) [15, 16, 28]
ρ kg/m ³	773	1833.921	Eq. in Table 6.
μ m Pa s	0.185	2.56394	Eq. in Table 6.
k W/m-K	0.089	0.51	Eq. in Table 6.
C_p kJ/kg-K	2.425	1.89	Eq. in Table 6.
T_h K	723 (705)	713 (715)	(639) Eq. in Table 6 for Nu
T_l K	523 (521)	526 (511)	(587) Eq. in Table 6 for Nu
\dot{S}_{gen} J/(K-s)	26448 (25027)	24956 (27792)	(7023) Eq. in Table 6 for Nu
$\eta = 1 - 300 / T_l (K)$	0.426 (0.424)	0.429 (0.413)	(0.489) Eq. in Table 6 for Nu
$T_i=563$ K; $T_o=663$ K; $d_i=d_h=0.02$ m; $n_i=n_h=820$; $L_h=5.1$ m; $L_l=5.1$ m; $d_c=0.5$ m; $n_c=4$; $L_c=200$ m			

Table 6 Properties of HTFs at average temperature of 450 °C and the results of entropy

production rate

	KNO ₃ -NaNO ₂ -NaNO ₃ (7-49-44 %mole) 450°C [10]	NaCl-KCl-ZnCl ₂ @450 °C [27]	Lead-bismuth Eutectic (LBE) [15, 16, 28]
ρ kg/m ³	1751	2150	Equation in Table 6.
μ m Pa s	1.375	7.0	Equation in Table 6.
k W/m-K	0.51	0.32	Equation in Table 6.
C_p kJ/kg-K	1.7596	0.81	Equation in Table 6.
T_h K	793 (788)	853 (868)	(740) Eq. in Table 6 for Nu
T_l K	623 (658)	511 (583)	(705) Eq. in Table 6 for Nu
\dot{S}_{gen} J/(K-s)	17206 (12522)	39287 (27806)	(3327) Eq. in Table 6 for Nu
$\eta = 1 - 300 / T_l (K)$	0.518 (0.544)	0.413 (0.486)	(0.575) Eq. in Table 6 for Nu
T _i =673 K; T _o =773 K; d _i =d _h =0.02 m; n _i =n _h =820; L _h =5.5 m; L _l =5.5 m; d _c =0.5 m; n _c =4; L _c =200 m			

Table 7 Properties of HTFs at average temperature of 700 °C and the results of entropy

production rate

	NaCl-KCl-ZnCl ₂ 700 °C [27]	NaCl-KCl-ZnCl ₂ 700 °C (Target)	Lead-bismuth Eutectic (LBE) [15, 16, 28]
ρ kg/m ³	1950	1950	Equation in Table 6.
μ m Pa s	4.0	4.0	Equation in Table 6.
k W/m-K	0.31	Targeted: 0.51	Equation in Table 6.
C_p kJ/kg-K	0.90	Targeted: 1.50	Equation in Table 6.
T_h K	1083 (1082)	1074 (1039)	(989) Eq. in Table 6 for Nu
T_l K	800 (864)	815.5 (907)	(957) Eq. in Table 6 for Nu
\dot{S}_{gen} J/(K-s)	16355 (11616)	14745 (6974)	(1752) Eq. in Table 6 for Nu
$\eta = 1 - 300 / T_l (k)$	0.625 (0.653)	0.632 (0.669)	(0.686) Eq. in Table 6 for Nu
T _i =923 K; T _o =1023 K; d _i =d _h =0.02 m; n _i =n _h =820; L _h =5.5 m; L _l =5.5 m; d _c =0.5 m; n _c =4; L _c =200 m			

Table 8 Summary of correlations for thermophysical properties of molten LBE ($P \sim 0.1$ MPa)

Properties	Unit	Correlations T(K)	Temperature range (K)	Uncertainty
Density	kg m^{-3}	$\rho = 11096 - 1.3236 T$	403-1300	0.8%
Specific heat	$\text{J kg}^{-1} \text{K}^{-1}$	$C_p = 159 - 2.72 \times 10^{-2} T + 7.12 \times 10^{-6} T^2$	430-605 (Extrapolation is applicable in 430-1900K)	7%
Dynamic viscosity	Pa s	$\mu = 4.94 \times 10^{-4} \times \exp(754.1/T)$	400-1100	5%
Thermal conductivity	$\text{W m}^{-1} \text{K}^{-1}$	$k = 3.61 + 1.517 \times 10^{-2} T - 1.741 \times 10^{-6} T^2$	403-1100	5%
Constant heat flux [28]: $Nu = 6.3 + 0.0167Re^{0.85}Pr^{0.93}$ at $0.004 \leq Pr \leq 0.1$ & $10^4 \leq Re \leq 10^6$				

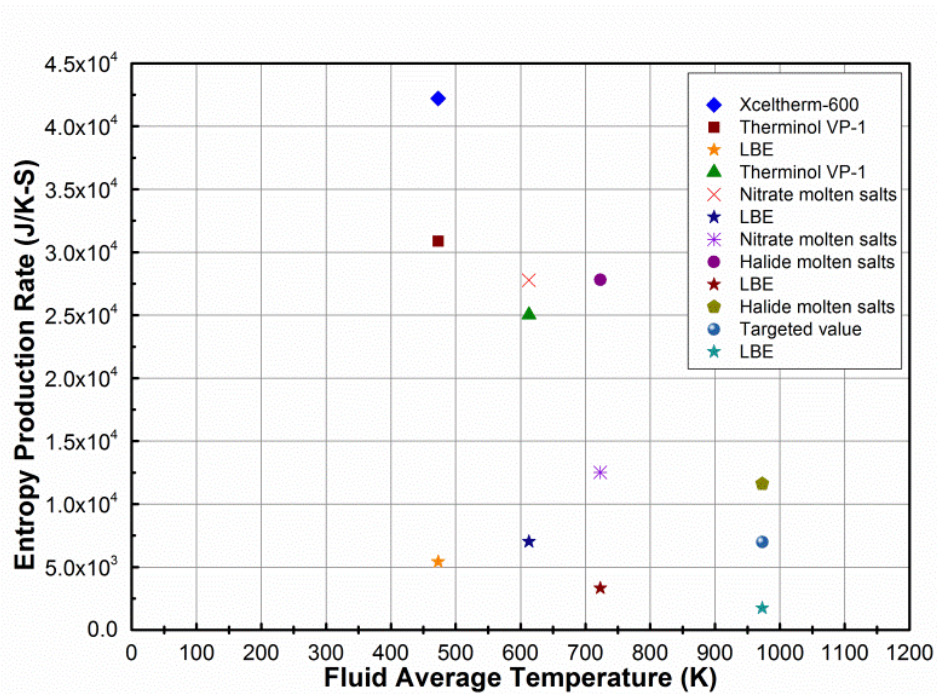


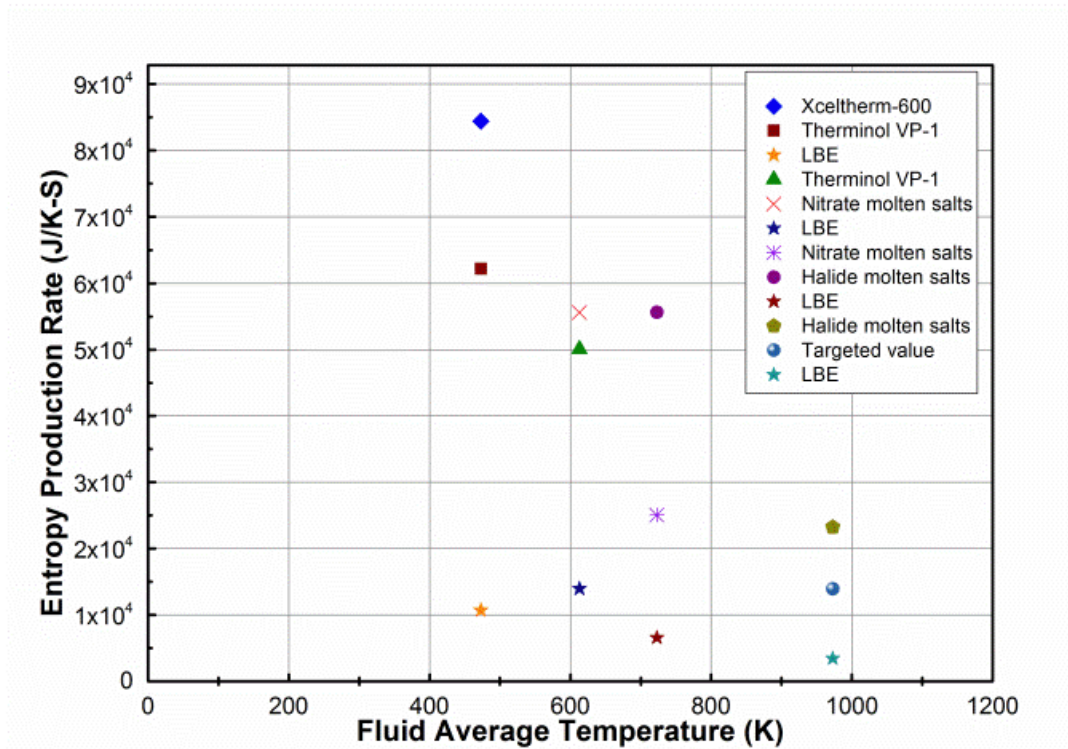
Fig. 18 The entropy production rate of a system using different HTFs at different operating temperatures for the task of transmitting 50 MW_{th} heat.

Similar analyses were conducted for the task of transporting heat in the range of 100MW_{th} to 600MW_{th} in the system. The used parameters for the analyses were given in Table 7. The results of entropy production for different level of heat transport using different HTFs are shown in Fig. 3(a) to (e). When more heat transport is needed, more entropy production is resulted in. However, it is also clear that the high-to-low sequence of entropy production rates from different HTF under one same T_m has no change in all the five figures different in \dot{Q} . This consistency shows that if a fluid is good and has low entropy production at a low heat transport rate, it will be good also for larger heat transport rate.

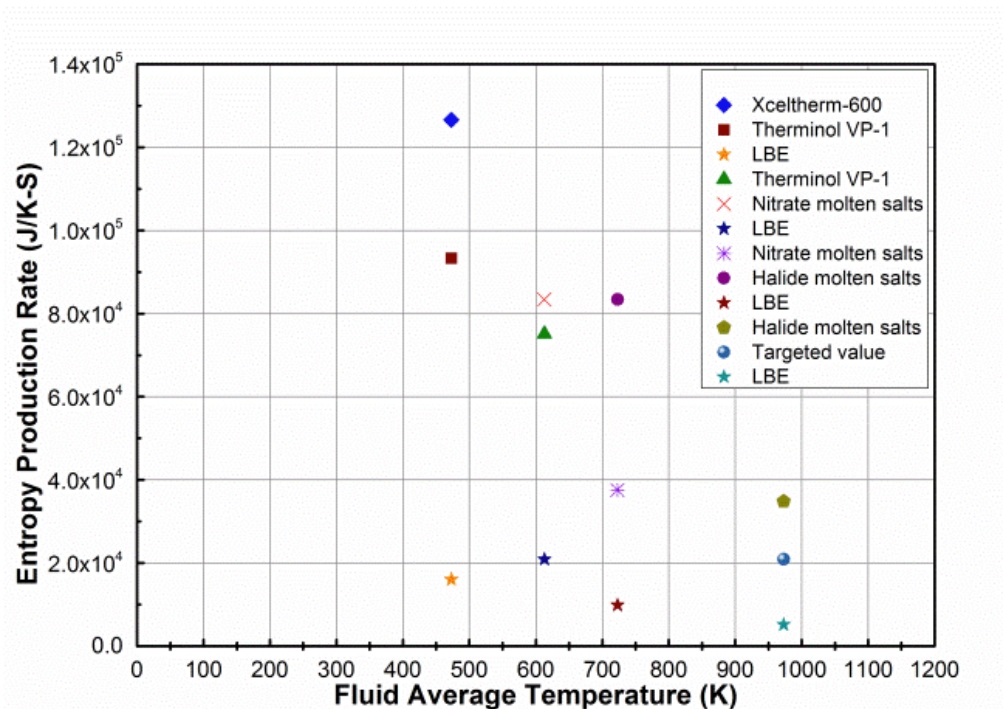
Table 9 Parameters in the analysis for different average fluid temperatures and several heat transfer tasks

Heat transmit Tasks(MW)	Fluid average temperature T_m (K)	T_i (K)	T_o (K)	d_l (m)	d_h (m)	n_l	n_h	L_h (m)	L_l (m)	d_c (m)	n_c	L_c (m)
50	473	423	523	0.02	0.02	820	820	7.7	7.7	0.5	4	200
	613	563	663	0.02	0.02	820	820	5.1	5.1	0.5	4	200
	723	673	773	0.02	0.02	820	820	5.5	5.5	0.5	4	200
	973	923	1023	0.02	0.02	820	820	5.5	5.5	0.5	4	200
100	473	423	523	0.02	0.02	1640	1640	7.7	7.7	0.5	4	200
	613	563	663	0.02	0.02	1640	1640	5.1	5.1	0.5	4	200
	723	673	773	0.02	0.02	1640	1640	5.5	5.5	0.5	4	200
	973	923	1023	0.02	0.02	1640	1640	5.5	5.5	0.5	4	200
150	473	423	523	0.02	0.02	2460	2460	7.7	7.7	0.5	4	200
	613	563	663	0.02	0.02	2460	2460	5.1	5.1	0.5	4	200
	723	673	773	0.02	0.02	2460	2460	5.5	5.5	0.5	4	200
	973	923	1023	0.02	0.02	2460	2460	5.5	5.5	0.5	4	200
200	473	423	523	0.02	0.02	3280	3280	7.7	7.7	0.5	4	200
	613	563	663	0.02	0.02	3280	3280	5.1	5.1	0.5	4	200
	723	673	773	0.02	0.02	3280	3280	5.5	5.5	0.5	4	200
	973	923	1023	0.02	0.02	3280	3280	5.5	5.5	0.5	4	200
400	473	423	523	0.02	0.02	6560	6560	7.7	7.7	0.5	4	200

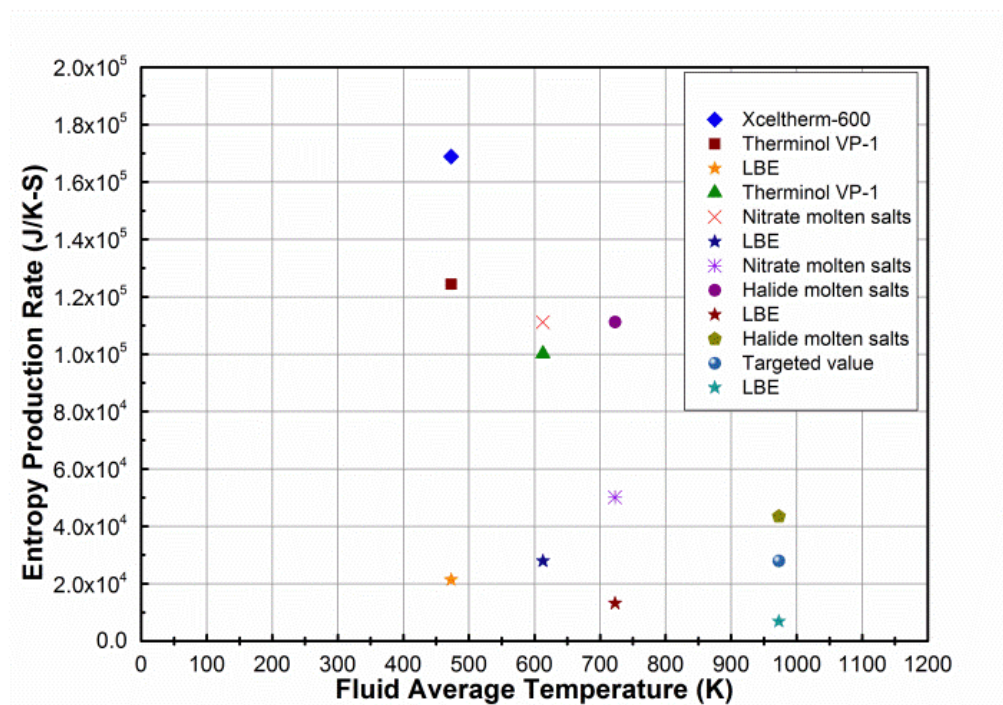
	613	563	663	0.02	0.02	6560	6560	5.1	5.1	0.5	4	200
	723	673	773	0.02	0.02	6560	6560	5.5	5.5	0.5	4	200
	973	923	1023	0.02	0.02	6560	6560	5.5	5.5	0.5	4	200
600	473	423	523	0.02	0.02	9840	9840	7.7	7.7	0.5	4	200
	613	563	663	0.02	0.02	9840	9840	5.1	5.1	0.5	4	200
	723	673	773	0.02	0.02	9840	9840	5.5	5.5	0.5	4	200
	973	923	1023	0.02	0.02	9840	9840	5.5	5.5	0.5	4	200



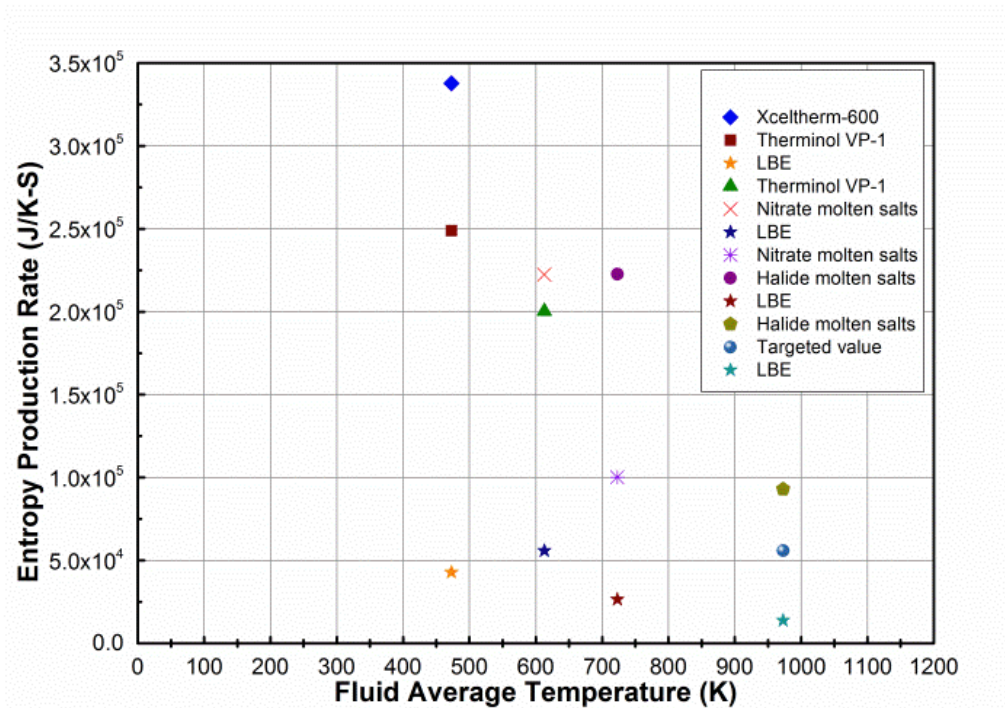
(a) 100 MW_{th}



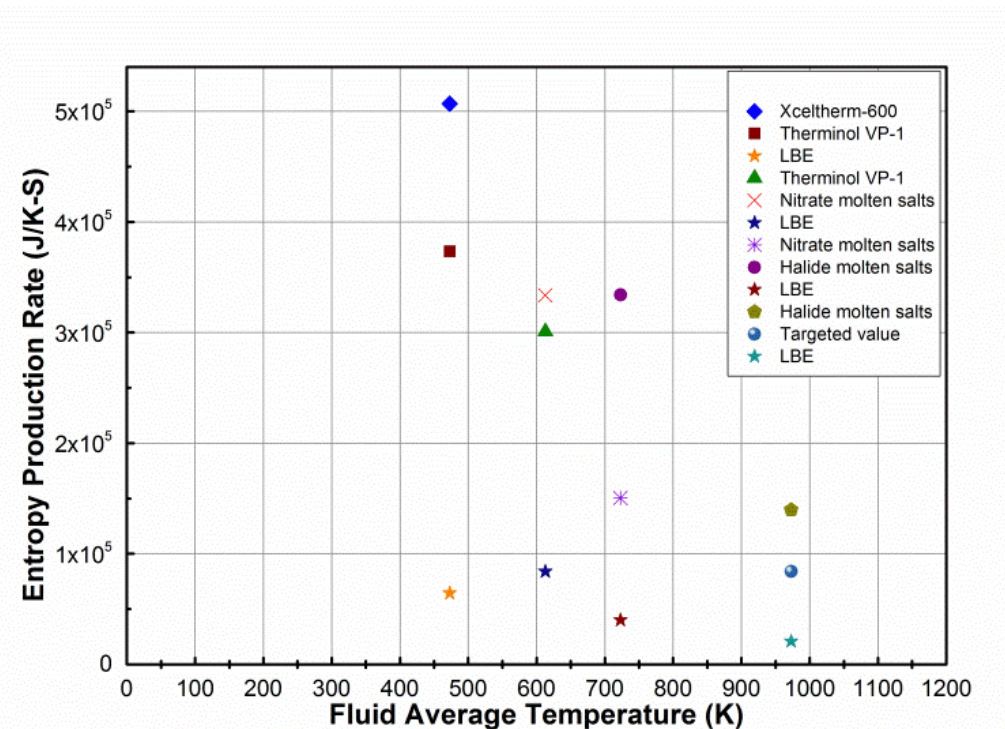
(b) 150 MW_{th}



(c) 200 MW_{th}



(d) 400 MW_{th}



(e) 600 MW_{th}

Fig. 19 The entropy production rates from different THFs at different operating temperatures for the task of transferring heat from 100 MW_{th} to 600 MW_{th} . Results are based on Gnielinski equation for Nu [194] of all fluids except for LEB that used equation in Table 6; and Petukhov equation [196] was used for Darcy friction factor.

4.3.4 The Carnot efficiency of the power system using the heat transported from solar collector

As has been discussed before, it is also important to examine the Carnot efficiency ($\eta = 1 - 300(K)/T_l(K)$), which is based on the temperatures (T_l) of the heat delivered to the power cycle. Because the number of heat transfer tubes in heat exchangers proportionally increase with the increase of heat transport tasks, the results for the Carnot efficiency does not vary with the increase of heat transport tasks, but only vary with the operating temperature T_m and the types of HTFs. Figure 20 shows the Carnot efficiency for all cases of temperatures and HTFs. It is needless to say that moving to higher temperature will obviously generate higher efficiency. For example, with the use of the halide molten salt working at temperature of $700 \text{ }^\circ\text{C}$ (973K), the efficiency (η) reaches 65.3%; whereas at a temperature of $450 \text{ }^\circ\text{C}$ (723K) using nitrate molten salt the efficiency is only 54.4%.

More importantly, the FOM of different heat transfer fluids can be compared at any desired operating temperature. For example, at the temperature of $450 \text{ }^\circ\text{C}$ (723K), the transport properties of LBE lead to higher η than that of the nitrate molten salt and halide molten salt, while halide molten salt results in the lowest η . At the temperature of $700 \text{ }^\circ\text{C}$ (973K), the η from the halide molten salt is also lower than that of LBE but approaches the targeted value based on target properties of a desired new fluid. Although from the transport property point of view LBE is a good HTF, however, it has severe corrosion issues which is not a favorable HTF [198].

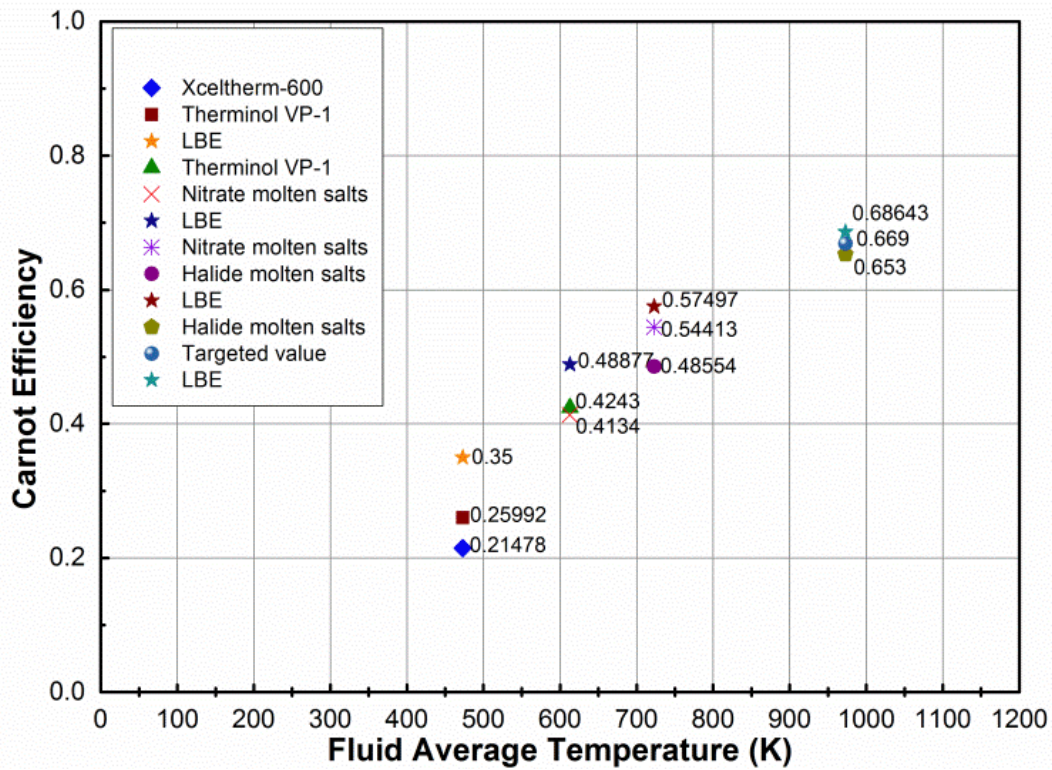


Fig. 20 The resulted Carnot efficiencies of the system using different HTFs at different operating temperatures for the tasks of transferring heat. Results are based on Gnielinski equation for Nu [24] of all fluids except for LEB that used equation in Table 6; and Petukhov equation [196] was used for Darcy friction factor.

4.4 Conclusions

This work tried to provide a standard of evaluating the FOM of heat transfer fluids that serves the objective of transporting heat from a concentrated solar collector and delivering to a thermal power plant. Entropy production of the heat transfer system is used to appreciate the FOM of different HTFs at different temperature levels. Through analysis, the role and contribution of each

of the transport properties to the minimized system entropy generation can be found, and a figure of merit (FOM) based on all the transport properties was able to be compared. In order to get lower entropy production, the conclusions for the studies HTFs are:

(1) for heat transport at temperature below 300 °C, Therminol VP-1 (applicable <400 °C) is better than Xceltherm-600 (applicable <315 °C).

(2) at temperatures between 300 °C and 400 °C, Therminol VP-1 is better than nitrate molten salt (applicable <580 °C).

(3) at temperatures between 400 °C to 500 °C, nitrate molten salt is better than halide molten salt (applicable <800 °C).

(4) at temperature above 600 °C and up to 800 °C, halide eutectic salts are applicable and the entropy production from the currently available halide salt properties are slightly higher than that from targeted properties for halide salts at high temperatures.

(5) LBE showed best overall transport properties to make least entropy production at all the temperatures compared to other HTFs. The issues restrict the application of LBE are not transport properties, but corruptions, too heavy to lift to high tower, and cost etc.

Since the entropy production is related to the exergy destruction (defined as $T_0 \dot{S}_{gen}$) or the reduction of useful work, this analysis can be eventually associated to cost analysis to the system, which will be further pursued by the authors in the future. Through such analysis, the selection of different heat transfer fluids will be associated to the cost of electrical energy of a CSP plant.

The basic equations and approaches of entropy production analysis may also be applied to the evaluation of the effectiveness of heat transfer enhancement measures which is at the expenses of increased pressure loss. The work also provides a fundamental criterion for the comparison of various heat transport systems which may have different designs and using different heat transfer

fluids/media (gas, liquid, or even solid particles) in CSP systems if the heat transport rate \dot{Q} and conditions of temperatures of T_i , T_o are prescribed.

Finally, it is noted that the analyses in this work only evaluate the transport properties and thermal performance of HTFs. Other issues such as material cost, corrosion of the HTF to pipes and containers can also significantly affect the selection of a HTF. Therefore, the current FOM still cannot serve as one uttermost criterion to make judgement of a HTF. Nevertheless, this work still offers one very important approach leading to the development and optimization of a heat transport system for CSP plant with all factors considered.

CHAPTER 5 CONCLUDING REMARKS AND FUTURE WORK

5.1 Concluding Remarks

In this dissertation, the heat transfer and entropy production of high temperature molten chloride salts circulation in CSP systems have been investigated using experimental methods and modeling analysis.

In the first part of this dissertation, the experimental study of the convective heat transfer of the molten chloride salt at high temperatures was conducted systematically for the first time. A circulation system and instrumentation of flow and heat transfer was designed and constructed so to accomplish measurement of the convective heat transfer coefficients of NaCl-KCl-ZnCl₂ (molar fraction: 13.8%-41.9%-44.3%) inside tubes and check the validity of heat transfer correlations for application to the new heat transfer fluid. Experimental data of Nusselt number, Reynolds number, were provided for comparison with the prediction by the Dittus-Boelter correlation and Gnielinski's correlation. Based on the comparison, Gnielinski's correlation is recommended for better prediction of heat transfer coefficients of the current molten salt. It is the cautious inference that the Gnielinski's correlation may be applicable to similar eutectic ionic molten chloride salts system NaCl-KCl-MgCl₂ with corresponding thermal and transport properties. This provides valuable information for the design of heat transfer devices in CSP plants that use molten chloride salts as heat transfer fluid and thermal energy storage material.

For the analysis to the transient heat transfer phenomenon between the hot fluid and the cold pipe, the second part of this dissertation proposed a method based on the perspective of energy storage. In this analysis, the transient temperature variation in the hot fluid when it flows through a cold pipe is better understood and the onset length of the pipe when fluid starts to freeze at

various heat transfer conditions are found. The effects of molten salt flow velocity, heat capacities of molten salt and pipe, dimensions of pipes, and the initial temperatures of salts and cold pipes are all correlated theoretically in the analysis through modeling of transient heat transfer between a pipe and the fluid. The results are very helpful to the understanding and management of a safe startup of hot molten salt flowing in cold pipes on cyclic operations.

The third part of this dissertation introduces details about the modeling that provides a fundamental approach for the comparison of various heat transport systems which may have different designs and using different heat transfer fluids/media (gas, liquid, or solid particles) in CSP systems. For various high temperature heat transfer fluids, such as, synthetic oils, various molten salts, and liquid metals, a general criterion was proposed in this work to evaluate the merit of fluids regarding their transport properties. For the goal of transferring a desired amount of heat, a fluid that causes less entropy production is believed to have better figure of merit (FOM). Theoretical analysis and relevant equations for total entropy production are derived. As an example, the FOM for several heat transfer fluids used in CSP industry were compared for the goal of heat transport in the range of 50 MW_{th} to 600 MW_{th}. Through analysis, the role and contribution of each of the transport properties to the minimized system entropy generation can be found, and a figure of merit (FOM) based on all the transport properties was able to be compared. Since the entropy production is related to the exergy destruction (defined as $T_0 \dot{S}_{gen}$) or the reduction of useful work, this analysis can be eventually associated to cost analysis to the system, which will be further pursued by the authors in the future. This work offered one very important approach leading to the development and optimization of a heat transport system for CSP plant with all factors considered.

The investigations included in this dissertation for the heat transfer and system analysis in concentrating solar power technology are of particular interest to the renewable energy engineering

community. It is expected that the proposed methods can provide useful information for engineers and researchers.

5.2 Future Work

1) Conduct the enthalpy study based on the mass and heat capacity of the pipe for consideration of the heat loss to surroundings including pipe insulation. This detailed modeling and simulation will be greatly helpful to the CSP industry for a thorough understanding of the phenomenon so to avoid freezing issue and clog in CSP system for a cold start up.

2) Further the modeling analysis from the minimized system entropy production to cost analysis for the concentrated solar power system. Since the entropy production is related to the exergy destruction or the reduction of useful work, this analysis can be eventually associated to cost analysis to the system. Through such analysis, the selection of different heat transfer fluids or designs of heat transfer devices will be associated to the cost of electrical energy of a CSP plant.

3) Summarize the experience of high temperature molten salt system design, construction, operation and maintenance, write a review journal to provide the precious knowledge for the researchers and industry engineers

4) Finishing the submission for the journal paper “*In-situ* Thermophysical Measurement of Flowing Molten Chloride Salt Using Modulated Photothermal Radiometry” together with the team in Univesity of California San Diego. For the first time, the feasibility of applying MPR method, as an in-situ measurement method for high temperature fluids was demonstrated in November 2021 as a key accomplishment in the project of “Non-contact Thermophysical Characterization of Solids and Fluids for Gen3 Concentrating Solar Power”.

APPENDIX PAPERS REFERRED TO IN THIS DISSERTATION

The work presented in this dissertation is based on the following published and prepared for publication papers.

Manuscript

1. Zhang, Y., Wang, X.X., Haddad, F., Gervasio, D., Li, P.W., Critical issues and solutions—a review for MgCl₂, NaCl, KCl eutectic mixture being used as high temperature heat transfer fluid and thermal storage in CSP, In Preparation.

Publications in peer-reviewed journals

1. Zhang, Y., Li, P.W., 2017. Minimum system entropy production as the FOM of high temperature heat transfer fluids for CSP systems. *Solar Energy*, 152, pp.80-90.

2. Zhang, Y., Wang, X., Liu, Q., Xu, B. and Li, P., 2022. Convective heat transfer of NaCl-KCl-ZnCl₂ eutectic molten salt at high temperatures inside a tube for application in CSP. *Journal of Solar Energy Engineering*, Accepted.

3. Chung, K.M. #, **Zhang, Y.#**, Zeng, J.#, Haddad, F., Chen, R.K., Li, P.W., In-situ Thermophysical Measurement of Flowing Molten Chloride Salt Using Modulated Photothermal Radiometry, Ready for submission

4. Chung Ka Man, Zeng Jian, Sarath Reddy Adapa, Feng Tianshi, Zhao Andrew, Garay Javier, Zhang Ye, Li Peiwen, Zhao Youyang, Chen Renkun, Thermal Conductivity Measurement of Molten Salt Using Modulated Photothermal Radiometry, Under Review

Publications in peer-reviewed conference proceedings

1. Li, P.W., Zhang, Y., 2015. Minimum system entropy production for the figure of merit of high temperature heat transfer fluid properties. In Energy Technology 2015 (pp. 359-372). Springer, Cham.
2. Zhang, Y., Li, Y. and Li, P., Evaluation of Several Types of High Temperature Heat Transfer Fluids for Concentrated Solar Power System. In ASTFE Digital Library. Begel House Inc.. Proceedings of the 3rd Thermal and Fluid Engineering Summer Conference, March 4- March 7, 2018, Fort Lauderdale, FL, USA.
3. Zhang, Y., Li, Y.Y., Li, P.W., Total Entropy Production in Flow and Heat Transfer for Evaluation of Performance of Heat Transfer Devices. In ASTFE Digital Library. Begel House Inc.. Second Thermal and Fluids Engineering Conference 2017, April 2- April 5, Las Vegas, NV, USA.
4. Zhang, Y., Li, P., Analysis of the Heat Transfer and Criterion of Freezing of Molten Salt Startup Flow in Relatively Cold Pipes, ASME 2022 Heat Transfer Summer Conference, July 11- July 13, 2022, TBD, Accepted.

REFERENCES

- [1] Islam, M.T., Huda, N., Abdullah, A.B., Saidur, R.. *A comprehensive review of state-of-the-art concentrating solar power (CSP) technologies: Current status and research trends*. *Renew Sustain Energy Rev* 2018;91:987–1018.
- [2] Islam, M.T., Shahir S., Uddin, T.I., Saifullah, A.. *Current energy scenario and future prospect of renewable energy in Bangladesh*. *Renew Sustain Energy Rev* 2014; 39:1074–88.
- [3] Mekhilef, S., Saidur, R., Safari, A.. *A review on solar energy use in industries*. *Renew Sustain Energy Rev* 2011; 15:1777 – 90.
- [4] Pavlović, T.M., Radonjić, I.S., Milosavljević, D.D., Pantić, L.S.. *A review of concentrating solar power plants in the world and their potential use in Serbia*. *Renew Sustain Energy Rev* 2012; 16:3891-902.
- [5] Hasan, M., Mahlia, T., Nur, H.. *A review on energy scenario and sustainable energy in Indonesia*. *Renew Sustain Energy Rev* 2012; 16:2316-28.
- [6] WPB. *World population balance population and energy consumption*. Available from (http://www.worldpopulationbalance.org/population_energy); 2015 [Last accessed on 10 October 2016].
- [7] Zhang, Z., Yuan, Y., Zhang, N., Sun, Q., Cao, X., Sun, L.. *Thermal properties enforcement of carbonate ternary via lithium fluoride: a heat transfer fluid for concentrating solar power systems*. *Renew Energy* 2017;111:523-31.
- [8] Ummadisingu, A., Soni, M.. *Concentrating solar power technology, potential and policy in India*. *Renew Sustain Energy Rev* 2011;15:5169 – 75.
- [9] Ahmed, S., Islam, M.T., Karim, M.A., Karim, N.M.. *Exploitation of renewable energy for sustainable development and overcoming power crisis in Bangladesh*. *Renew Energy* 2014;72:223-35.

- [10] Sims, R.E., Rogner, H.H., Gregory, K.. *Carbon emission and mitigation cost comparisons between fossil fuel, nuclear and renewable energy resources for electricity generation*. Energy Policy 2003;31:1315-26.
- [11] EIA. *U.S. Energy Information Administration international energy outlook*. Available from ([https://www.eia.gov/outlooks/ieo/pdf/0484\(2017\).pdf](https://www.eia.gov/outlooks/ieo/pdf/0484(2017).pdf)); 2017 [Last accessed on 22 January 2018].
- [12] IEA. *Energy Technology Perspectives 2015: Mobilising Innovation to Accelerate Climate Action*. Paris: IEA. Available from (https://www.iea.org/newsroomandevents/speeches/150504_ETP_slides.pdf); 2015 [Last accessed on 17 November 2015].
- [13] Sharma, A.. *A comprehensive study of solar power in India and World*. Renew Sustain Energy Rev 2011;15:1767 – 76.
- [14] Sun, J., Liu, Q., Hong, H.. *Numerical study of parabolic-trough direct steam generation loop in recirculation mode: characteristics, performance and general operation strategy*. Energy Convers Manag 2015;96:287 – 302.
- [15] Carrillo, A.J., et al., *Solar Energy on Demand: A Review on High Temperature Thermochemical Heat Storage Systems and Materials*. Chemical Reviews, 2019. **119**(7): p. 4777-4816.
- [16] Verma, V. and K. Murugesan, *Experimental study of solar energy storage and space heating using solar assisted ground source heat pump system for Indian climatic conditions*. Energy and Buildings, 2017. **139**: p. 569-577.
- [17] Kalogirou, S., *The potential of solar industrial process heat applications*. Applied Energy, 2003. **76**(4): p. 337-361.
- [18] Kumar, L., M. Hasanuzzaman, and N.A. Rahim, *Global advancement of solar thermal energy technologies for industrial process heat and its future prospects: A review*. Energy Conversion and Management, 2019. **195**: p. 885-908.

- [19] Otanicar, T., R.A. Taylor, and P.E. Phelan, *Prospects for solar cooling – An economic and environmental assessment*. Solar Energy, 2012. **86**(5): p. 1287-1299.
- [20] Chidambaram, L.A., et al., *Review of solar cooling methods and thermal storage options*. Renewable and Sustainable Energy Reviews, 2011. **15**(6): p. 3220-3228.
- [21] Sampaio, P.G.V. and M.O.A. González, *Photovoltaic solar energy: Conceptual framework*. Renewable and Sustainable Energy Reviews, 2017. **74**: p. 590-601.
- [22] Stropnik, R. and U. Stritih, *Increasing the efficiency of PV panel with the use of PCM*. Renewable Energy, 2016. **97**: p. 671-679.
- [23]. Kuravi, S., et al., *Thermal energy storage technologies and systems for concentrating solar power plants*. Progress in Energy and Combustion Science, 2013. **39**(4): p. 285-319.
- [24] SolarPACES. *Solar thermal electricity global outlook 2016*. Available from (http://www.solarpaces.org/images/GP-ESTELA-SolarPACES_Solar-Thermal-Electricity-Global-Outlook-2016_Executive-Summary.pdf); 2016 [Last accessed on 07 May2016].
- [25] Izquierdo, S., Montanes, C., Dopazo, C., Fueyo, N.. *Analysis of CSP plants for the definition of energy policies: the influence on electricity cost of solar multiples, capacity factors and energy storage*. Energy Policy 2010;38:6215-21.
- [26] Teske S, Leung J, Crespo L, Bial M, Dufour E, Richter C, et al. *Solar thermal electricity: Global outlook 2016*. Eur Sol Therm Electr Assoc 2016.
- [27] Yasinskiy A, Navas J, Aguilar T, Alcántara R, Gallardo JJ, Sánchez-Coronilla A, et al. *Dramatically enhanced thermal properties for TiO₂-based nanofluids for being used as heat transfer fluids in concentrating solar power plants*. Renew Energy 2017;119:809 – 19.
- [28] Franz Trieb, Christoph Schillings, Marlene O ‘Sullivan, Thomas Pregger, Hoyer-Klick C. *Global potential of concentrating solar power*. In: Proceedings of the SolarPACES. Berlin, Germany; 2009.

- [29] Brenna M, Foiadelli F, Roscia M, Zaninelli D. *Evaluation of solar collector plant to contribute climate change mitigation*. In: Proceedings of the IEEE international conference on sustainable energy technologies, ICSET. Singapore; 2008. p.198 - 202.
- [30] Philibert C. *Technology roadmap: concentrating solar power*: OECD/IEA; 2010.
- [31] FirstGreen. *Comparison of CSP technologies*. Available from <https://firstgreenconsulting.wordpress.com/2012/06/04/comparison-of-csptechnologies/comparison-of-csp-technologies/>; 2012 [Last accessed on 18October 2016].
- [32] CEC. *California Energy Commission solar power plant licensing projects*. Available from http://www.energy.ca.gov/maps/renewable/Solar_Power_Plant_Licensing_Projects.pdf; 2014 [Last accessed on 04 May 2017].
- [33] Richter C, Teske S, Nebrera J. *Concentrating solar power global outlook 09*. Greenpeace International/European Solar Thermal Electricity Association (ESTELA)/IEA SolarPACES, Report; 2009.
- [34] EU. European Commission, Energy Research Knowledge Centre (ERKC). *Thematic research summary-concentrating solar power*. Available from https://setis.ec.europa.eu/energy-research/sites/default/files/library/ERKC_TRS_Concentrating_solar_power.pdf; 2013 [Last accessed on 04 May 2017].
- [35] SolarPACES. *CSP projects around the world*. Available from <http://www.solarpaces.org/csp-technology/csp-projects-around-the-world>; 2016 [Last accessed on 07 May 2016].
- [36] EC. *European Commission TECHNICAL BACKGROUND: concentrated solar power*. Available from http://ec.europa.eu/research/energy/eu/index_en.cfm?pg=research-csp-background; 2015 [Last accessed on 07 May 2016].
- [37] Fernández-García, A., et al., *Parabolic-trough solar collectors and their applications*. 2010. **14**(7): p. 1695-1721.
- [38] Fuqiang, W., et al., *Progress in concentrated solar power technology with parabolic trough collector system: A comprehensive review*. 2017. **79**: p. 1314-1328.

- [39] Good, P., et al., *Towards a commercial parabolic trough CSP system using air as heat transfer fluid*. 2014. **49**: p. 381-385.
- [40] Turchi, C.S., M.J. Wagner, and C.F. Kutscher, *Water use in parabolic trough power plants: summary results from WorleyParsons' analyses*. 2010, National Renewable Energy Lab.(NREL), Golden, CO (United States).
- [41] Cheng, Z., et al., *Three-dimensional numerical study of heat transfer characteristics in the receiver tube of parabolic trough solar collector*. 2010. **37**(7): p. 782-787.
- [42] Hachicha, A., et al., *Heat transfer analysis and numerical simulation of a parabolic trough solar collector*. 2013. **111**: p. 581-592.
- [43] Lenzen, F., *Overview of Parabolic Troughs and Linear Fresnel Receivers, presentation at the IEA workshop on solar electricity roadmaps*. 2014, Paris.
- [44] Mwesigye, A. and J.P.J.A.E. Meyer, *Optimal thermal and thermodynamic performance of a solar parabolic trough receiver with different nanofluids and at different concentration ratios*. 2017. **193**: p. 393-413.
- [45] Zhu, G., et al., *History, current state, and future of linear Fresnel concentrating solar collectors*. 2014. **103**: p. 639-652.
- [46] Abbas, R., et al., *High concentration linear Fresnel reflectors*. 2013. **72**: p. 60-68.
- [47] Moghimi, M., K. Craig, and J.P.J.S.E. Meyer, *Optimization of a trapezoidal cavity absorber for the Linear Fresnel Reflector*. 2015. **119**: p. 343-361.
- [48] Baharoon, D.A., et al., *Historical development of concentrating solar power technologies to generate clean electricity efficiently—A review*. 2015. **41**: p. 996-1027.
- [49] Morin, G., et al., *Comparison of linear Fresnel and parabolic trough collector power plants*. 2012. **86**(1): p. 1-12.

- [50] DoE, U. *Concentrating solar power commercial application study: reducing water consumption of concentrating solar power electricity generation*. in *Report to Congress*. Washington, DC: USDOE. 2009.
- [51] Pheng, L.G., et al., *A review of Parabolic Dish-Stirling Engine System based on concentrating solar power*. 2014. **12**(4): p. 1142.
- [52] Giostri, A.J.E.P., *Preliminary analysis of solarized micro gas turbine application to CSP parabolic dish plants*. 2017. **142**: p. 768-773.
- [53] Schiel, W. and T. Keck, *9 - Parabolic dish concentrating solar power (CSP) systems*, in *Concentrating Solar Power Technology*, K. Lovegrove and W. Stein, Editors. 2012, Woodhead Publishing. p. 284-322.
- [54] Natarajan, S.K., et al., *Experimental analysis of a two-axis tracking system for solar parabolic dish collector*. 2019. **43**(2): p. 1012-1018.
- [55] Barker, L., M. Neber, and H.J.S.E. Lee, *Design of a low-profile two-axis solar tracker*. 2013. **97**: p. 569-576.
- [56] Coventry, J. and C.J.S.E. Andraka, *Dish systems for CSP*. 2017. **152**: p. 140-170.
- [57] Islam, M.T., et al., *A comprehensive review of state-of-the-art concentrating solar power (CSP) technologies: Current status and research trends*. 2018. **91**: p. 987-1018.
- [58] Cameron, M. and N.A. Ahmed. *A novel solar concentrating dish for reduced manufacturing cost*. in *Applied Mechanics and Materials*. 2014. Trans Tech Publ.
- [59] El Ouederni, A., et al., *Experimental study of a parabolic solar concentrator*. 2009. **12**(3): p. 395-404.
- [60] Li, Z., et al., *Study on the radiation flux and temperature distributions of the concentrator–receiver system in a solar dish/Stirling power facility*. 2011. **31**(10): p. 1780-1789.

- [61] Lovegrove, K., G. Burgess, and J.J.S.E. Pye, *A new 500 m² paraboloidal dish solar concentrator*. 2011. **85**(4): p. 620-626.
- [62] Peiyao, Y., et al. *Development of the Experimental Bench for a Research on Solar-Dish Power Generation*. in *Proceedings of ISES World Congress 2007 (Vol. I–Vol. V)*. 2008. Springer.
- [63] Poullikkas, A., et al., *Parametric analysis for the installation of solar dish technologies in Mediterranean regions*. 2010. **14**(9): p. 2772-2783.
- [64] Rafeeu, Y., M.J.R. Ab Kadir, and S.E. Reviews, *Thermal performance of parabolic concentrators under Malaysian environment: A case study*. 2012. **16**(6): p. 3826-3835.
- [65] Stine, W.B. and R.B. Diver, *A compendium of solar dish/Stirling technology*. 1994, Sandia National Labs., Albuquerque, NM (United States).
- [66] Thakkar, V., et al., *Performance analysis methodology for parabolic dish solar concentrators for process heating using thermic fluid*. 2015. **12**(1): p. 101-114.
- [67] Nuwayhid, R., F. Mrad, and R.J.R.E. Abu-Said, *The realization of a simple solar tracking concentrator for university research applications*. 2001. **24**(2): p. 207-222.
- [68] Kaushika, N., K.J.E.C. Reddy, and Management, *Performance of a low cost solar paraboloidal dish steam generating system*. 2000. **41**(7): p. 713-726.
- [69] Wei, X., et al., *Tracking and ray tracing equations for the target-aligned heliostat for solar tower power plants*. 2011. **36**(10): p. 2687-2693.
- [70] Guo, M., et al., *Tracking formulas and strategies for a receiver oriented dual-axis tracking toroidal heliostat*. 2010. **84**(6): p. 939-947.
- [71] Wei, X., et al., *A new method for the design of the heliostat field layout for solar tower power plant*. 2010. **35**(9): p. 1970-1975.

[72] Lipps, F. and L.L.J.S.E. Vant-Hull, *A cellwise method for the optimization of large central receiver systems*. 1978. **20**(6): p. 505-516.

[73] Gretz, J., *EURELIOS, the world's first thermomechanical helioelectric power plant*. Endeavour, 1982. **6**(1): p. 34-39.

[74] Gretz, J., *Concept and operating experiences with Eurelios 1 MW helioelectric power plant of the European Communities*. IEE Proceedings A - Physical Science, Measurement and Instrumentation, Management and Education - Reviews, 1987. **134**(5): p. 399-406.

[75] Barbaliscia, F. and A.J.I.N.C.C. Lavagnini, *Analysis of solar-radiation characteristics at the EURELIOS power plant of Adrano*. 1983. **6**(1): p. 83-95.

[76] Faas, S., *10-mwe solar-thermal central-receiver pilot plant: thermal-storage-subsystem evaluation-subsystem activation and controls testing phase*. 1983, Sandia National Labs., Livermore, CA (USA).

[77] Tyner, C.E., J.P. Sutherland, and W.R. Gould Jr, *Solar two: A molten salt power tower demonstration*. 1995, Sandia National Labs., Albuquerque, NM (United States).

[78] NREL. *Solar Two Demonstrates Clean Power for the Future*. Available from: <https://www.nrel.gov/docs/legosti/fy97/22835.pdf>.

[79] Williams, G., *Solar Thermal Energy at the Ivanpah Power Facility*.

[80] Whitaker, M.B., et al., *Life cycle assessment of a power tower concentrating solar plant and the impacts of key design alternatives*. 2013. **47**(11): p. 5896-5903.

[81] NREL. *Ivanpah Solar Electric Generating System*. Available from: https://web.archive.org/web/20151012092620/http://www.nrel.gov/csp/solarpaces/project_detail.cfm/projectID=62#.

[82] Sullivan, R. and J.M. Abplanalp, *Visibility and Visual Characteristics of the Ivanpah Solar Electric Generating System Power Tower Facility*. 2015, Argonne National Lab.(ANL), Argonne, IL (United States).

[83] Okoroigwe, E., A.J.R. Madhlopa, and S.E. Reviews, *An integrated combined cycle system driven by a solar tower: A review*. 2016. **57**: p. 337-350.

[84] Collado, F.J., J.J.R. Guallar, and S.E. Reviews, *A review of optimized design layouts for solar power tower plants with campo code*. 2013. **20**: p. 142-154.

[85] Mendelsohn, M., T. Lowder, and B. Canavan, *Utility-scale concentrating solar power and photovoltaic projects: A technology and market overview*. 2012, National Renewable Energy Lab.(NREL), Golden, CO (United States).

[86] Romero, M., J.J.W.I.R.E. González-Aguilar, and Environment, *Solar thermal CSP technology*. 2014. **3**(1): p. 42-59.

[87] [Divya KC, Østergaard J., *Battery energy storage technology for power systems —an overview*. 2009, *Electr Power Syst Res*, 79: p. 511–20.](#)

[88] Maytorena, V. and J.J.S.E. Hinojosa, *Effect of non-uniform concentrated solar flux on direct steam generation in vertical pipes of solar tower receivers*. 2019. **183**: p. 665-676.

[89] Birnbaum, J., et al., *A direct steam generation solar power plant with integrated thermal storage*. 2010. **132**(3).

[90] Joseph Stekli, Levi Irwin, Ranga Pitchumani, *Technical challenges and opportunities for concentrating solar power with thermal energy storage*, ASME J. of Thermal Science and Engineering Applications, JUNE 2013, Vol. 5 / 021011-1.

[91] Jon T. Van Lew, Peiwen Li, Cho Lik Chan, Wafaa Karaki, Jake Stephens, *Analysis of Heat Storage and Delivery of a Thermocline Tank Having Solid Filler Material general on thermal storage*, Journal of Solar Energy Engineering, MAY 2011, Vol. 133 / 021003-1.

[92] Gil, A., Medrano, M., Martorell, I., La´zaro, A., Dolado, P., Zalba, B., and Cabeza, L. F., 2010, *State of the Art on High Temperature Thermal Energy Storage for Power Generation. Part 1—Concepts, Materials and Modellization*, Renewable Sustainable Energy Rev., 14(1), p. 31–55.

- [93] Medrano, M., Gil, A., Martorell, I., Potau, X., and Cabeza, L. F., 2010, *State of the Art on High-Temperature Thermal Energy Storage for Power Generation. Part 2—Case Studies*, *Renewable Sustainable Energy Rev.*, 14(1), p. 56–72.
- [94] Yu-ting Wu, Nan Ren, Tao Wang, Chong-fang Ma, *Experimental study on optimized composition of mixed carbonate salt for sensible heat storage in solar thermal power plant*, *Solar Energy* 85 (2011) 1957–1966.
- [95] Canada, S., Brosseau, D. A., and Price, H., 2006, *Design and Construction of the APS 1 MWe Parabolic Trough Power Plant*, ASME Conference Proceedings, p. 91–98.
- [96] XCEL THERM® 600 Engineering Properties, Radco Industries, (<http://www.radcoind.com/>).
- [97] C. Lang, B. Lee, *Heat transfer fluid life time analysis of diphenyl oxide/biphenyl grades for concentrated solar power plants*, International Conference on Concentrating Solar Power and Chemical Energy Systems, SolarPACES 2014, *Energy Procedia* 69 (2015) 672 – 680.
- [98] Therminol VP-1, <http://www.solutia.com> last accessed Set. 28th, 2015.
- [99] Manohar S. Sohal, Matthias A. Ebner, Piyush Sabharwall, Phil Sharpe, *Engineering Database of Liquid Salt Thermophysical and Thermochemical Properties*, March 2010, Report # INL/EXT-10-18297, by Idaho National Laboratory Idaho Falls, Idaho 83415.
- [100] R. W. Bradshaw and N. P. Siegel (2008). *Molten nitrate salt development for thermal energy storage in parabolic trough solar power systems*, Proceedings of ES2008, Energy Sustainability 2008, August, 10-14, 2008, Jacksonville, FL, p 1-7.
- [101] A. Baraka, A. I. Abdel-Rohman, and A. A. El Hosary, (1976). *Corrosion of Mild Steel in Molten Sodium Nitrate-Potassium Nitrate Eutectic*, *British Corrosion Journal*, 11(1), p. 43-46.
- [102] Chao-Jen Li, Peiwen Li, Kai Wang, Edgar Emir Molina, *Survey of Properties of Key Single and Mixture Halide Salts for Potential Application as High Temperature Heat Transfer Fluids for Concentrated Solar Thermal Power Systems*, AIMS (American Institute of Mathematical Science) Journal Energy, Volume 2, Issue 2, p. 133-157, DOI: 10.3934/energy.2014.1.133.

- [103] K. Vignarooban, P. Pugazhendhi, C. Tucker, D. Gervasio and A.M. Kannan, *Corrosion Resistance of Hastelloys in Molten Metal-Chloride Heat-Transfer Fluids for Concentrating Solar Power Applications*, Solar Energy 103 (2014), p. 62-69.
- [104] Thermophysical and Electric Properties, Chapter 2, *Handbook on Lead-bismuth Eutectic Alloy and Lead Properties, Materials Compatibility, Thermal-hydraulics and Technologies*, published by the OECD/NEA.
- [105] Low Prandtl number thermal-hydraulics, Chapter 10, *Handbook on Lead-bismuth Eutectic Alloy and Lead Properties, Materials Compatibility, Thermal-hydraulics and Technologies*, published by the OECD/NEA, p. 48-57.
- [106] Nicholas Boerema, Graham Morrison, Robert Taylor, Gary Rosengarten, *Liquid sodium versus Hitec as a heat transfer fluid in solar thermal central receiver systems*, Solar Energy, Vol. 86, Issue 9, 2012, p. 2293–2305.
- [107] Ouagued, M., A. Khellaf, and L. Loukarfi, *Estimation of the temperature, heat gain and heat loss by solar parabolic trough collector under Algerian climate using different thermal oils*. Energy Conversion and Management, 2013. **75**: p. 191-201.
- [108] Cabaleiro, D., et al., *Thermophysical properties of (diphenyl ether+biphenyl) mixtures for their use as heat transfer fluids*. The Journal of Chemical Thermodynamics, 2012. **50**: p. 80-88.
- [109] Modi, A. and F.J.A.T.E. Haglind, *Performance analysis of a Kalina cycle for a central receiver solar thermal power plant with direct steam generation*. 2014. **65**(1-2): p. 201-208.
- [110] Jalili Jamshidian, F., S. Gorjian, and M. Shafiee Far, *An Overview of Solar Thermal Power Generation Systems*. Journal of Solar Energy Research, 2018. **3**(4): p. 301-312.
- [111] Nunes, V.M.B., et al., *Molten salts as engineering fluids – A review: Part I. Molten alkali nitrates*. Applied Energy, 2016. **183**: p. 603-611.
- [112] Weinberg, A.M., *A REVIEW OF MOLTEN SALT REACTOR TECHNOLOGY. PREFACE. MOLTEN-SALT REACTORS*. 1970.
- [113] Kearney, D., et al., *Assessment of a molten salt heat transfer fluid in a parabolic trough solar field*. 2003. **125**(2): p. 170-176.

[114] Bauer, T., et al., *Material aspects of Solar Salt for sensible heat storage*. Applied Energy, 2013. **111**: p. 1114-1119.

[115] Corp, B.E., *Design, handling, operation and maintenance procedures for Hitec molten salt*. 1981, Sandia National Laboratories.

[116] Boerema, N., et al., *Liquid sodium versus Hitec as a heat transfer fluid in solar thermal central receiver systems*. Solar Energy, 2012. **86**(9): p. 2293-2305.

[117] Vignarooban, K., et al., *Heat transfer fluids for concentrating solar power systems – A review*. Applied Energy, 2015. **146**: p. 383-396.

[118] Blake, D.M., et al. *New heat transfer and storage fluids for parabolic trough solar thermal electric plants*. in *Proceedings of the 11th SolarPACES international symposium on concentrating solar power and chemical energy technologies*. 2002.

[119] Bradshaw, R. and R.J.R.S.-. Carling, *A review of the chemical and physical properties of molten alkali nitrate salts and their effect on materials used for solar central receivers*. 1987.

[120] Fernández, A.G., M.I. Lasanta, and F.J. Pérez, *Molten Salt Corrosion of Stainless Steels and Low-Cr Steel in CSP Plants*. Oxidation of Metals, 2012. **78**(5): p. 329-348.

[121] Fernández, A.G., et al., *Corrosion properties of a ternary nitrate/nitrite molten salt in concentrated solar technology*. Renewable Energy, 2015. **80**: p. 177-183.

[122] Fernández, A.G., et al., *Corrosion of stainless steels and low-Cr steel in molten $\text{Ca}(\text{NO}_3)_2\text{-NaNO}_3\text{-KNO}_3$ eutectic salt for direct energy storage in CSP plants*. Solar Energy Materials and Solar Cells, 2015. **141**: p. 7-13.

[123] Ferrara, A., R. Haslett, and J. Joyce. *Molten salt thermal energy storage for utility peaking loads*. in *iecc*. 1977.

[124] Myers, P.D. and D.Y. Goswami, *Thermal energy storage using chloride salts and their eutectics*. Applied Thermal Engineering, 2016. **109**: p. 889-900.

- [125] Robelin, C. and P. Chartrand, *Thermodynamic evaluation and optimization of the (NaCl+KCl+MgCl₂+CaCl₂+ZnCl₂) system*. The Journal of Chemical Thermodynamics, 2011. **43**(3): p. 377-391.
- [126] Robelin, C., P. Chartrand, and A.D. Pelton, *Thermodynamic evaluation and optimization of the (NaCl+KCl+MgCl₂+CaCl₂+MnCl₂+FeCl₂+CoCl₂+NiCl₂) system*. The Journal of Chemical Thermodynamics, 2004. **36**(9): p. 809-828.
- [127] Chartrand, P. and A.D. Pelton, *Thermodynamic evaluation and optimization of the LiCl-NaCl-KCl-RbCl-CsCl-MgCl₂-CaCl₂ system using the modified quasi-chemical model*. Metallurgical and Materials Transactions a-Physical Metallurgy and Materials Science, 2001. **32**(6): p. 1361-1383.
- [128] Armijo, K.M., et al., *Operational Modes of a 2.0 MWth Chloride Molten-Salt Pilot-Scale System*. 2019, Sandia National Lab.(SNL-NM), Albuquerque, NM (United States).
- [129] Vignarooban, K., et al., *Vapor pressure and corrosivity of ternary metal-chloride molten-salt based heat transfer fluids for use in concentrating solar power systems*. Applied Energy, 2015. **159**: p. 206-213.
- [130] Xu, X., et al., *Entropy generation and Carnot efficiency comparisons of high temperature heat transfer fluid candidates for CSP plants*. International Journal of Hydrogen Energy, 2017. **42**(31): p. 20316-20323.
- [131] Du, L., et al., *Thermal properties and thermal stability of the ternary eutectic salt NaCl-CaCl₂-MgCl₂ used in high-temperature thermal energy storage process*. Applied Energy, 2017. **204**: p. 1225-1230.
- [132] Du, L., et al., *Thermal Stability of the Eutectic Composition in NaCl-CaCl₂-MgCl₂ Ternary System Used for Thermal Energy Storage Applications*. Energy Procedia, 2017. **105**: p. 4185-4191.
- [133] Wei, X., et al., *A New Ternary Chloride Eutectic Mixture and its Thermo-physical Properties for Solar Thermal Energy Storage*. Energy Procedia, 2014. **61**: p. 1314-1317.

- [134] Wei, X., et al., *Quaternary Chloride Eutectic Mixture for Thermal Energy Storage at High Temperature*. Energy Procedia, 2015. **75**: p. 417-422.
- [135] Wei, X., et al., *Design and thermal properties of a novel ternary chloride eutectics for high-temperature solar energy storage*. Applied Energy, 2015. **156**: p. 306-310.
- [136] Lorenzin, N. and A. Abánades, *A review on the application of liquid metals as heat transfer fluid in Concentrated Solar Power technologies*. International Journal of Hydrogen Energy, 2016. **41**(17): p. 6990-6995.
- [137] Pacio, J. and T. Wetzel, *Assessment of liquid metal technology status and research paths for their use as efficient heat transfer fluids in solar central receiver systems*. Solar Energy, 2013. **93**: p. 11-22.
- [138] Frazer, D., et al., *Liquid metal as a heat transport fluid for thermal solar power applications*. 2014. **49**(Supplement C): p. 627-636.
- [139] Marocco, L., et al., *Numerical analysis of a solar tower receiver tube operated with liquid metals*. International Journal of Thermal Sciences, 2016. **105**: p. 22-35.
- [140] Subbotin, V., et al., *Liquid-metal coolants for nuclear power*. 2002. **92**(1): p. 29-40.
- [141] Yuan, C., et al., *A new solar fuels reactor concept based on a liquid metal heat transfer fluid: Reactor design and efficiency estimation*. Solar Energy, 2015. **122**: p. 547-561.
- [142] Yuan, C. and Y.J.J.T.E. Kawajiri, *A new solar fuels reactor using a liquid metal heat transfer fluid: modeling and sensitivity analysis*. 2015.
- [143] Bachelier, C. and W. Jäger, *Thermal and hydraulic evaluation of a linear Fresnel solar collector loop operated with molten salt and liquid metal*. Applied Energy, 2019. **248**: p. 207-216.
- [144] Prabu, T. and C.J.J.o.S.E.E. Ajay Sekar, *Improving heat transfer in hybrid solar systems using liquid metal alloys as a coolant*. 2017. **139**(6).

- [145] Wang, Xiaoxin, *Investigation of the Thermal and Transport Properties of NaCl-KCl-MgCl₂-CaCl₂ Molten Salt for Application as HTF and TES Media in CSP Systems*. 2020. University of Arizona, PhD dissertation.
- [146] Hoffman, H. W., Cohen, S. I., 1960, *Fused salt heat transfer: Part III: Forced-convection heat transfer in circular tubes containing the salt mixture NaNO₂-NaNO₃-KNO₃*,” Oak Ridge National Laboratory, Report No. ORNL-2433.
- [147] Kirst, W., Nagle, W., Castner, J., 1940, *A new heat transfer medium for high temperatures*, Transactions of the AIChE, 36, p. 371-394.
- [148] Wu, Y. T., Chen, C., Liu, B., Ma, C. F., 2012, *Investigation on forced convective heat transfer of molten salts in circular tubes*, Int. Communication of Heat Mass, 39(10), p. 1550-1555. <https://doi.org/10.1016/j.icheatmasstransfer.2012.09.002>.
- [149] Gnielinski, V., 1976, *New equations for heat and mass transfer in turbulent pipe and channel flow*. Int. Chemical Engineering, 16(2), p. 359-368.
- [150] Hausen, H., 1959, *Neue Gleichungen für die Wärmeübertragung bei freier oder erzwungener Stromung (New equations for heat transfer in free or forced flow)*, Allgemeine Wärmetechnik, 9, p. 75-79.
- [151] Xu, Xiankun, Wang, Xiaoxin, Li, Peiwen, Li, Yuanyuan, Hao, Qing, Xiao, Bo, Elsentriecy, Hassan, Gervasio, Dominic, 2018, *Experimental Test of Properties of KCl-MgCl₂ Eutectic Molten Salt for Heat Transfer and Thermal Storage Fluid in Concentrated Solar Power Systems*, ASME J Sol Energy Eng, 140(5), p. 051011. <https://doi.org/10.1115/1.4040065>.
- [152] Li, Peiwen, Molina, Edgar, Wang, Kai, Xu, Xiankun, Dehghani, Ghazal, Kohli, Amit, Hao, Qing, Kassae, Mohamad H., Jeter, Sheldon M., Teja, A.S., 2016, *Thermal and transport properties of NaCl-KCl-ZnCl₂ eutectic salts for new generation high temperature heat transfer fluids*, ASME J Sol Energy Eng, 138(5), p. 054501. <https://doi.org/10.1115/1.4033793>.
- [153] Wang, Xiaoxin, Rincon, Jesus Del, Li, Peiwen, Zhao, Youyang, Vidal, Judith, 2021, *Thermophysical properties experimentally tested for NaCl-KCl-MgCl₂ eutectic molten salt as next generation high temperature HTF in CSP systems*, ASME J Sol Energy Eng, 143(4), p.041005. <https://doi.org/10.1115/1.4049253>.
- [154] Dunn RI, Hearps PJ, Wright MN. *Molten-salt power towers: newly commercial concentrating solar storage*. Proc IEEE 100 (2012): p. 504–515.

[155] Zhao Youyang, Vidal Judith, *Potential Scalability of a Cost-Effective Purification Method for MgCl₂-Containing Salts for Next-Generation Concentrating Solar Power Technologies*, Solar Energy Mater. Sol. Cells 215 (2020): p. 110663.

[156] J. Pacio, Cs. Singer, Th. Wetzel, R. Uhlig, *Thermodynamic evaluation of liquid metals as heat transfer fluids in concentrated solar power plants*, Applied Thermal Engineering, Volume 60, Issues 1–2, 2 October 2013, p. 295–302.

[157] J. Pacio, Th. Wetzel, *Assessment of liquid metal technology status and research paths for their use as efficient heat transfer fluids in solar central receiver systems*, Solar Energy, Vol. 93, July 2013, p. 11–22.

[158] Manfred Becker, *Comparison of heat transfer fluids for use in solar thermal power stations*, Electric Power Systems Research, Volume 3, Issues 3–4, 1980, p. 139–150.

[159] Zappa, William, Junginger, Martin, Broek, Machteld van den, 2019, *Is a 100% renewable European power system feasible by 2050, ?* Applied Energy, Volumes 233–234, p. 1027-1050.
<https://doi.org/10.1016/j.apenergy.2018.08.109>.

[160] Zou, Peng, Chen, Qixin, Yu, Yang, Xia, Qing, Kang, Chongqing, 2017, *Electricity markets evolution with the changing generation mix: An empirical analysis based on China 2050 High Renewable Energy Penetration Roadmap*, Applied Energy, 185(1), p. 56-67.
<https://doi.org/10.1016/j.apenergy.2016.10.061>.

[161] Hand, M. M, Baldwin, S., DeMeo, E., Reilly, J., Mai, T., Arent, D., et al, 2012, *Renewable Electricity Futures Study*. National Renewable Energy Lab, Golden, CO, Report No. NREL/TP-6A20-52409.

[162] Stekli, J., Irwin, L., and Pitchumani, R., 2013, *Technical Challenges and Opportunities for Concentrating Solar Power with Thermal Energy Storage*, ASME. J. Thermal Sci. Eng. Appl., 5(2), p. 021011. <https://doi.org/10.1115/1.4024143>.

[163] Mehos, M., Turchi, C.S., Denholm, Jorgensen, P., Ho, C., and Armijo, K., 2016, *On the Path to SunShot: Advancing Concentrating Solar Power Technology, Performance, and Dispatchability*, National Renewable Energy Laboratory, Golden, CO, NREL/TP- 5500- 65668.

[164] Shahabuddin, M., Alim, M.A., Alam, Tanvir, Mofijur, M., Ahmed, S.F., Perkins, Greg, 2021, *A critical review on the development and challenges of concentrated solar power*

technologies, Sustainable Energy Technologies and Assessments, 47(2), p. 101434.
<https://doi.org/10.1016/j.seta.2021.101434>.

[165] Turchi, C. S., Ma, Z., Neises, T. W., and Wagner, M. J., 2013, *Thermodynamic Study of Advanced Supercritical Carbon Dioxide Power Cycles for Concentrating Solar Power Systems*, ASME Journal of Solar Energy Engineering, 135(4), p. 041007.
<https://doi.org/10.1115/1.4024030>.

[166] He, Yaling, Qiu, Yu, Wang, Kun, Yuan, Fan, Wang, Wenqi, Li, Mingjia, Guo, Jiaqi, 2020, *Perspective of concentrating solar power*, Energy, 198(1), p. 117373.
<https://doi.org/10.1016/j.energy.2020.117373>.

[167] Qiu, Yu, Li, Mingjia, Li, Mengjie, Zhang, Honghu, Ning, Bo, 2019, *Numerical and experimental study on heat transfer and flow features of representative molten salts for energy applications in turbulent tube flow*, *Int. J. of Heat and Mass Transfer*, 135, p. 732-745.
<https://doi.org/10.1016/j.ijheatmasstransfer.2019.02.004>.

[168] Li, M.J., Jin, B., Yan, J.J., Ma, Z., Li, M.J., 2018, *Numerical and experimental study on the performance of a new two-layered high-temperature packed-bed thermal energy storage system with changed-diameter macro-encapsulation capsule*, *Appl. Therm. Eng.*, 142, p. 830–845.
<https://doi.org/10.1016/j.applthermaleng.2018.07.026>.

[169] Lake, J. A., 2002, *The fourth generation of nuclear power*, *Progress in Nuclear Energy*, 40(3), p. 301-307. [https://doi.org/10.1016/S0149-1970\(02\)00023-9](https://doi.org/10.1016/S0149-1970(02)00023-9).

[170] Romatoski, R. R., Hu, L.W., 2017, *Fluoride salt coolant properties for nuclear reactor applications: A review*, *Annals of Nuclear Energy*, 109(2), p. 635-647.
<https://doi.org/10.1016/j.anucene.2017.05.036>.

[171] He, Yaling, Zheng, Z.J., Du, B.C., Wang, Kang, Qiu, Yu, 2016, *Experimental investigation on turbulent heat transfer characteristics of molten salt in a shell-and-tube heat exchanger*, *Applied Thermal Engineering*, 108, p. 1206-1213.
<https://doi.org/10.1016/j.applthermaleng.2016.08.023>.

[172] Qiu, Yu, Li, M.J., Wang, W.Q., Du, B.C., Wang, Kang, 2018, *An experimental study on the heat transfer performance of a prototype molten-salt rod baffle heat exchanger for concentrated solar power*, *Energy*, 156, p. 63-72. <https://doi.org/10.1016/j.energy.2018.05.040>.

[173] Silverman, M.D., Huntley, W.R., Robertson, H. E., 1976, *Heat transfer measurements in a forced convection loop with two molten fluoride salts LiF-BeF₂-ThF₂-UF₄ and eutectic NaBF₄-NaF*, Oak Ridge National Laboratory, Report No. ORNL-TM-5335.

[174] Cooke, J. W., Cox, B. W., 1973, *Forced-convection heat transfer measurements with a molten fluoride salt mixture flowing in a smooth tube*, Oak Ridge National Laboratory, Report No. ORNL-TM-4079.

[175] Hoffman, H. W., Lones, J., 1955, *Fused salt heat transfer. Part II. Forced convection heat transfer in circular tubes containing NaF-KF-LiF eutectic*, Oak Ridge National Laboratory, Report No. ORNL-1777.

[176] Grele, M. D., Gedeon, L., 1954, *Forced-convection heat-transfer characteristics of molten FLiNaK flowing in an inconel X system*, U.S. National Advisory Committee for Aeronautics (NACA) Research Memorandum No. E53L18.

[177] Vriesema, B., 1979, *Aspects of molten fluorides as heat transfer agents for power generation*, Ph.D. dissertation, Delft University of Technology, Delft, Netherlands.

[178] Hoffman, H. W., Cohen, S. I., 1960, *Fused salt heat transfer: Part III: Forced-convection heat transfer in circular tubes containing the salt mixture NaNO₂-NaNO₃-KNO₃*, Oak Ridge National Laboratory, Report No. ORNL-2433.

[179] Ferná'ndez, A.G., Gomez-Vidal, J., Oro', E., Kruizenga, A., Sole', A., Cabeza, L.F., *Mainstreaming commercial CSP systems: a technology review*, *Renewable Energy* 140 (2019): p. 152-176.

[180] Hand, M. M, Baldwin, S., DeMeo, E., Reilly, J., Mai, T., Arent, D., et al, 2012, *Renewable Electricity Futures Study*, National Renewable Energy Lab, Golden, CO, Report No. NREL/TP-6A20-52409.

[181] Stekli, J., Irwin, L., and Pitchumani, R., 2013, *Technical Challenges and Opportunities for Concentrating Solar Power With Thermal Energy Storage*, *ASME. J. Thermal Sci. Eng. Appl.*, 5(2), p. 021011.

[182] Tian Y, Zhao CY. *A review of solar collectors and thermal energy storage in solar thermal applications*, *Applied Energy* 104 (2013): p. 538–553.

[183] Lake J. A., 2002, *The fourth generation of nuclear power*, Progress in Nuclear Energy, Vol. 40, p. 301-307.

[184] Peiwen Li, Ben Xu, Jingxiao Han, Yongping Yang, *Verification of a Model of Thermal Storage Incorporated with an Extended Lumped Capacitance Method for Various Solid-fluid Structural Combinations*, Journal Solar Energy, Vol. 105, July 2014, p. 71–81.

[185] Xu Ben, Li Peiwen, Chan Cholik. *Extending the validity of lumped capacitance method for large Biot number in thermal storage application*. Solar Energy 86 (2012): p. 1709-1724.

[186] Lew Jon T Van, Li Peiwen, Chan Cholik. *Analysis of Heat Storage and Delivery of a Thermocline Tank Having Solid Filler Material*, Journal of Solar Energy Engineering 133(2011): p. 021003.

[187] F. Dittus, L. Boelter, *Heat transfer in automobile radiators of the tubular type*. Int. Commun. Heat Mass Transfer 12 (1985): p. 3–22.

[188] Kays, W. M., Crawford, M. E., and Weigand, B., *Convective Heat and Mass Transfer*, McGraw Hill, 2005, fourth ed.

[189] Incropera, F. P., and DeWitt, D. P., *Introduction to Heat Transfer*, John Wiley and Sons, Inc, 2002, fourth ed.

[190] Li Peiwen, Lew Jon T Van, Chan Cholik, Karaki Wafaa, Stephens Jake, O'Brien J.E. *Similarity and generalized analysis of efficiencies of thermal energy storage systems*, Renewable Energy 39 (2012): p. 388-402.

[191] Adrian Bejan, *Entropy Generation Minimization –The method of thermodynamic optimization of finite-size systems and finite-time processes*, 1995, CRC Press.

[192] Adrian Bejan, *Advanced Engineering Thermodynamics*, 3rd Edition, 2006, Wiley.

[193] Incropera, F. P., and DeWitt, D. P., 2002, *Introduction to Heat Transfer*, 4th Ed., Wiley, New York.

[194] Gnielinski, V., *New equations for heat and mass transfer in the turbulent flow in pipes and channels*, Int. Chem. Eng., Vol. 16, p. 359, 1976.

[195] Kays, W. M., and M. E. Crawford, *Convective heat and mass transfer*, McGraw-Hill, New York, 1980.

[196] Petukhov, B.S., in T.F. Irvine and J.P. Hartnett, Eds., *Advances in Heat Transfer*, Vol. 6, Academic Press, New York, 1970.

[197] Kai Wang, Edgar Molina, Ghazal Dehghani, Ben Xu, Peiwen Li, Qing Hao, Pierre Lucas, Mohamad H. Kassaee, Sheldon M. Jeter, Aryn S. Teja, *Experimental Investigation to the Properties of Eutectic Salts by NaCl-KCl-ZnCl₂ for Application as High Temperature Heat Transfer Fluids*, ES-FuelCell2014-6578, Proceedings of the ASME 2014, 8th International Conference on Energy Sustainability, June 30-July 2, 2014, Boston, MA, USA.

[198] R. H. Notter, C.H. Sleicher, *A Solution to the Turbulent Graetz-Problem III Fully Developed and Entrance Region Heat Transfer Rates*, Chem. Eng. Sci., Vol. 27 (1972) p. 2073-2093.